Design, Fabrication and Characterization of Passive and Active Polymer Photonic Devices

Geetha K

International School of Photonics
Cochin University of Science and Technology
Cochin – 682 022, India

Ph D Thesis submitted to
Cochin University of Science and Technology
In partial fulfillment of the requirements for the
Degree of Doctor of Philosophy

June, 2006

Design, Fabrication and Characterization of Passive and Active Polymer Photonic Devices

Ph D Thesis in the filed of Photonics

Author
Geetha K
Research Fellow
International School of Photonics
Cochin University of Science & Technology
Cochin – 682 022, India
Email : geetha@cusat.ac.in; geethadas@gmail.com

Research Advisors
Dr. P Radhakrishnan
Professor, International School of Photonics
Cochin University of Science & Technology
Cochin – 682 022, India
Email : radhak@cusat.ac.in

Dr. V P N Nampoori
Professor, International School of Photonics
Cochin University of Science & Technology
Cochin – 682 022, India
Email : vpnnampoori@cusat.ac.in

International School of Photonics,
Cochin University of Science & Technology
Cochin – 682 022, INDIA

www.photonics.cusat.edu

June 2006

Front cover : Multimode laser emission from a 50 μm thick polymer planar waveguide doped with Rhodamine 6G

Dedicated to

My beloved father

CERTIFICATE

Certified that the research work presented in the thesis entitled "***Design, fabrication and characterization of passive and active polymer photonic devices"*** is based on the original work done by Mrs. **Geetha K** under my guidance and supervision at the International School of Photonics, Cochin University of Science and Technology, Cochin – 22, India and has not been included in any other thesis submitted previously for the award of any degree.

Cochin 682 022
1 June, 2006

Dr. P Radhakrishnan
(Supervising Guide)

DECLARATION

Certified that the work presented in the thesis entitled "***Design, fabrication and characterization of passive and active polymer photonic devices***" is based on the original work done by me under the guidance and supervision of Dr. P Radhakrishnan, Professor, International School of Photonics, Cochin University of Science and Technology, Cochin – 22, India and co-guidance of Dr. V P N Nampoori, Professor, International School of Photonics, Cochin University of Science and Technology, Cochin – 22, India and has not been included in any other thesis submitted previously for the award of any degree.

Cochin 682 022

1 June, 2006 Geetha K

Preface

The rapid developments in fields such as fibre optic communication engineering and integrated optical electronics have expanded the interest and have increased the expectations about guided wave optics, in which optical waveguides and optical fibres play a central role. The technology of guided wave photonics now plays a role in generating information (guided-wave sensors) and processing information (spectral analysis, analog-to-digital conversion and other optical communication schemes) in addition to its original application of transmitting information (fibre optic communication).

Passive and active polymer devices have generated much research interest recently because of the versatility of the fabrication techniques and the potential applications in two important areas – short distant communication network and special functionality optical devices such as amplifiers, switches and sensors. Polymer optical waveguides and fibres are often designed to have large cores with 10-1000 micrometer diameter to facilitate easy connection and splicing.

Large diameter polymer optical fibres being less fragile and vastly easier to work with than glass fibres, are attractive in sensing applications. Sensors using commercial plastic optical fibres are based on ideas already used in silica glass sensors, but exploiting the flexible and cost effective nature of the plastic optical fibre for harsh environments and throw-away sensors.

In the field of Photonics, considerable attention is centering on the use of polymer waveguides and fibres, as they have a great potential to create all-optical devices. By attaching organic dyes to the polymer system we can incorporate a variety of optical functions. Organic dye doped polymer waveguides and fibres are potential candidates for solid state gain media.

High power and high gain optical amplification in organic dye-doped polymer waveguide amplifier is possible due to extremely large emission cross sections of dyes. Also, an extensive choice of organic dye dopants is possible resulting in amplification covering a wide range in the visible region.

The thesis presented in seven chapters deals with the work carried out on polymer optical fibre sensors and dye doped polymer waveguide gain media.

Chapter 1 gives an overview of guided wave polymer photonic devices. Historical development of polymer waveguides/fibres and commonly used polymer materials together with their applications have been covered. An overview of passive components with emphasis on polymer fibre optic sensors and different sensing techniques is given. The potential of polymer waveguides and fibres as optically active media is also discussed. Recent developments in the related fields such as conjugated polymer devices and polymer photonic band gap materials have also been mentioned.

Chapter 2 discusses the design, fabrication and characterization of a refractometer using a side polished polymer fibre, which has got a wide dynamic range. Following a ray optics approach to multimode fibres, a theoretical model was developed for understanding the sensor performance for various launching angles to the fibre. Based on the theoretical observations, the experiment was designed. The sensing element was fabricated by encapsulating a slightly bent polymer optical fibre in a block of resin. Maximum sensitivity and sensing range was obtained for a launching angle of 30^0. The experimental results are explained on the basis of theoretical calculations.

Chapter 3 presents an evanescent wave absorption sensor for chemical reaction rate measurements. General theory of evanescent wave absorption in fibres is overviewed. A theoretical study of the effect of a high refractive index overlay on the exposed core region of the fibre, on the evanescent wave absorption is presented. Details of the modeling related to the evanescent wave absorption for different overlay refractive indices and overlay thicknesses are also included in this chapter. It was observed that the evanescent wave absorption coefficient increases with increase in overlay refractive index and overlay thickness. Experiments were also performed for studying the reaction kinetics of a standard chemical reaction. Experimental results for bare fibre as well as fibres with different overlay thickness are also presented in this chapter .

Chapter 4 gives the details of the fabrication and characterization of dye doped polymer planar waveguide structures. Rhodamine 6G doped polymethyl methacrylate (PMMA) planar film waveguides with various dye concentrations and thicknesses were prepared by tape casting technique. The optical attenuation in the waveguides is an important parameter of interest. The loss characterization was done by a non-destructive side illumination fluorescence technique, the details of which are presented in this chapter. The experimental results for waveguides with various dye concentration and thickness are discussed in this chapter. The studies showed that the attenuation mechanisms in a dye doped waveguide – especially for the dyes having an overlap between the absorption and emission spectra – can be explained only with a space dependent attenuation coefficient. In such cases, the transmitted light will not strictly obey the conventional Beer-Lambert's law.

In **Chapter 5**, the observation of Amplified Spontaneous Emission (ASE) from the dye doped planar waveguide structures of various thicknesses and dye concentrations has been presented. Optical gain characterization was done by a variable stripe length method widely used for both organic and inorganic materials prepared in slab geometry. The cross-section of the pump beam was in the form of a stripe. The variation of gain with dye concentration as well as film thickness has been studied. The propagation characteristics of ASE through the waveguide are also discussed. This was done by shifting the position of the excitation stripe in such a way that the ASE from the end of the pump stripe was guided along different lengths of the waveguide. With increase in propagation length through the waveguide, the emission peak showed a red-shift due to self-absorption and re-emission by the dye molecules. As the radiation was propagated through the amplifying medium, a spectrally narrow output at longer wavelengths was obtained due to the gain achieved at these wavelengths. Thus we could tune the ASE wavelength.

Chapter 6 describes the details of our work on multimode laser emission from a transversely pumped free standing polymer film of Rh6G doped PMMA . Since the film was freestanding – surrounded by air on both sides – the reflections from the lateral faces of the sample provided the optical feedback for laser action. This was evident from the lasing mode-spacing dependence on the film thickness. The leaky mode emission from the film waveguide showed a planar microcavity-like behaviour due to Fabry-Perot effects. Selective mode excitation was also observed with an increase in pump energy.

Summary and conclusions of the work carried out are given in **Chapter 7.** Future prospects are also discussed in this chapter.

List of Publications

International Journals

1. **K. Geetha**, M. Rajesh, V.P.N. Nampoori, C.P.G. Vallabhan and P.Radhakrishnan, "Propagation characteristics and wavelength tuning of amplified spontaneous emission from dye doped polymer", *Appl. Opt.* **45**, 764-769 (2006)

2. **K. Geetha**, M. Rajesh, V.P.N. Nampoori, C.P.G. Vallabhan and P.Radhakrishnan, "Laser emission from transversely pumped dye-doped free-standing polymer film", *J.Opt. A: Pure Appl. Opt.* **8**,189-193 (2006)

3. **K. Geetha**, M. Rajesh, V.P.N. Nampoori, C.P.G. Vallabhan and P.Radhakrishnan, "Loss characterization in rhodamine 6G doped polymer film waveguide by side illumination fluorescence", *J.Opt. A: Pure Appl. Opt.* **6**, 379-383 (2004).

4. **K. Geetha**, Pramod Gopinath, K P Unnikrishnan, S Thomas Lee ,C. P. G. Vallabhan,V. P. N. Nampoori and P. Radhakrishnan, "Studies on optical loss coefficient in plastic waveguides", Proceedings of SPIE – International Society of optical Engineering, No. 4904, 382-390 (2002).

5. M Rajesh, **K Geetha**, M. Sheeba, P Radhakrishnan, C P G Vallabhan and V P N Nampoori, "Characterization of Rhodamine 6G doped polymer optical fiber by side illumination fluorescence", *Optical Engg* (In Press)

6. M. Rajesh, **K. Geetha**, M. Sheeba, P. Radhakrishnan, C. P. G Vallabhan and V. P. N Nampoori, "A fiber optic smart sensor for studying the setting characteristics of various grades of cement", *Optics and lasers in Engineering* **44,** 486-493 (2006)

7. S. Thomas Lee, **K. Geetha**, V.P.N. Nampoori, C.P.G. Vallabhan and P. Radhakrishnan, " Microbent Optical fibers as evanescent wave sensors", *Opt. Engg.* **41**, 3260-3264 (2002).

8. **K. Geetha**, M. Rajesh, V. P. N. Nampoori and P. Radhakrishnan, "A modified design of refractometer using side polished polymer fibre". (Communicated to Optical and Quantum Electronics)

International Conferences

1. **K. Geetha**, M. Rajesh, C.P.G. Vallabhan , V.P.N. Nampoori and P.Radhakrishnan, "Design of a refractometer with wide dynamic range using side polished polymer optical fibre", Proceedings of Seventh International Conference on Optoelectronics, Fiber Optics and Photonics (PHOTONICS 2004) Dec 9-11, Kochi (2004)

2. **K. Geetha**, T. Anto Johny, V. Kumar, C.P.G. Vallabhan, V.P.N. Nampoori and P.Radhakrishnan, "Modes in planar waveguides based on sol-gel derived thin films of nano ZnO", Proceedings of Sixth International Conference on Optoelectronics, Fiber Optics and Photonics (PHOTONICS 2002), Dec 14-16,Mumbai(2002)

3. M. Rajesh, M. Sheeba, **K. Geetha**, P. Radhakrishnan, C.P.G. Vallabhan and V.P.N. Nampoori, "A Fiber optic distributed sensor to characterize the properties of concrete mix", Proceedings of Seventh International Conference on Optoelectronics, Fiber Optics and Photonics (PHOTONICS 2004) Dec 9-11, Kochi (2004)

4. M. Rajesh, M. Sheeba, **K. Geetha**, P. Radhakrishnan, C.P.G. Vallabhan and V.P.N. Nampoori, "Fiber optic sensor for the detection of paraffin oil traces in coconut oil", Proceedings of Seventh International Conference on Optoelectronics, Fiber Optics and Photonics (PHOTONICS 2004) Dec 9-11, Kochi (2004)

National Conferences

1. **K. Geetha**, M. Rajesh,V. P. N. Nampoori, C.P.G. Vallabhan and P. Radhakrishnan, "Side Illumination Fluorescence Technique for the characterisation of optical loss in Dye doped planar waveguides", National Laser Symposium 2003, Kharagpur

1. **K. Geetha**, Pramod Gopinath, K. P. Unnikrishnan, S. Thomas Lee, C. P. G. Vallabhan,V. P. N. Nampoori and P. Radhakrishnan, "Side Illumination Fluorescence Studies in Dye doped Polymer Waveguide", Proceedings of National Laser Symposium 2001, December 19-21, CAT Indore, pp141-142. (2001)

ACKNOWLEDGEMENTS

With deep sense of gratitude, I express my heartfelt thanks to Prof. P. Radhakrishnan for the guidance, support and encouragement given through out my research work.

I am extremely thankful to Prof. V. P. N. Nampoori for the inspiration, guidance and encouragement without which this work would not have materialized.

I sincerely thank Prof. C.P.Girijavallabhan for his help and support. His valuable suggestions have helped me a lot in my research work. I am equally thankful to Prof. V.M. Nandakumaran for the timely help and encouragement. I also acknowledge Mr. M. Kailasnath.

I am very much indebted to Dr. Reghu Natarajan, C-MET, Thrissur and Mr. Denny Alapatt, for providing me with the samples.

I am also grateful to Dr. Rani Joseph, Dept. of Polymer Science and Rubber Technology, Cusat, who devoted her precious time for meaningful discussions.

I owe much to Dr. A. Deepthy for the moral support and timely advices.

I am thankful to all research scholars of ISP for their constant support and priceless help. I am extremely thankful to Rajesh M whose timely support helped me a lot in completing my work. The help rendered by Manoj Mathew is also worth mentioning .

I remember the wonderful moments with Pramod, Sajan, Binoy, Unni, Prasanth, Pravitha, Jyotsna, Bindu, Aneesh ,Thomas Lee, Rajesh S, Rekha, Santhi, Dilna, Sreeja and Suresh Sir. I have also enjoyed the motherly affection from Achamma teacher. The love and support from Sr. Ritty is greatly acknowledged.

I am thankful to all my friends - Sheeba, Thomas, Litty, Lyjo, Dann, Manu, Vinu, Sajeev, Parvathy, Saritha, Jayasree teacher and Bindu Krishnan. I am extremely thankful to Jijo, who helped me a lot in designing the cover page.

.

I extend my sincere thanks to the non-teaching staff of ISP for all the help and assistance.

The financial assistance from CSIR, India is greatly acknowledged.

In this moment, I would like to remember all my friends especially Deepa Chandran, Grace, Vinod, Majo, Binu, Saritha and Jalaja who always encouraged me and supported me.

I am extremely grateful to my brother and all my relatives. Their love and support have always been there. I also remember with gratitude the help and concern from my in-laws who have always shown keen interest in my studies.

There are no words to express gratitude to my parents who have always guided me, believed in me and strived for my achievements. It is only because of them, I have reached here. I bow my head to them.

I don't know how to thank properly my husband Devidas and my little Kunjunni. Without their constant support, patience, co-operation and encouragement I would not have accomplished this task.

Last, but most important of all, I thank *Almighty God*.

Geetha. K

Contents

Polymer based guided wave photonics - An overview

This chapter gives an overview of guided wave polymer photonic devices. Commonly used polymer materials together with their applications have been covered in this chapter. An overview of passive components and active components with emphasis on polymer optical fibre sensors and polymer waveguide lasers is presented.

1.1 Introduction

The rapid developments in fields such as fibre optic communication engineering and integrated optical electronics have expanded the interest and increased expectations about guided wave optics, in which optical waveguides and optical fibres play a central role. The recent surge in demand for photonic components that meet economic criteria as well as technical requirements in the telecom and datacom industries has opened the door for novel technologies that enable unique functions and/or unconventional high-yield manufacturing without sacrificing high performance. Advanced polymer technologies can fit the bill in every aspect. Polymer waveguide technology has a great potential for economic mass production of complex planar photonic circuits and polymer optical fibres. The low cost prospect arises from the availability of a wide range of inexpensive optical polymers and the simplicity of fabricating waveguides from them. A significant subset of optical polymer materials has shown excellent optical, chemical and mechanical characteristics that are very attractive for wide range of applications such as optical communication devices, physical and chemical sensors, memories and illuminators.

1.2 Towards polymer based optical components

Polymers can be used to develop both passive and active optical components. Polymer optical fibres (POFs) have attracted much attention in past decades because they have some unique characteristics, such as flexibility, ease of handling, relative low cost, high geometrical versatility and relatively high resistance to fracture. Their large diameter (typically 1 mm) enables easy

coupling. These characteristics make them especially suitable to be a transmission medium in local area networks (LANs) and short-haul optical communications.

Polymer fibres were first developed in 1968 by the US Company Dupont, who sold the patents to Mitsubishi Rayon in Japan. Thereafter, NTT and Keio University in Japan achieved several important developments in material techniques. Worldwide research and development have been predominantly focused on poly methyl methacrylate (PMMA) based fibres. The low absorption windows for PMMA based fibres lie in the visible region of the electromagnetic spectrum [1-3].

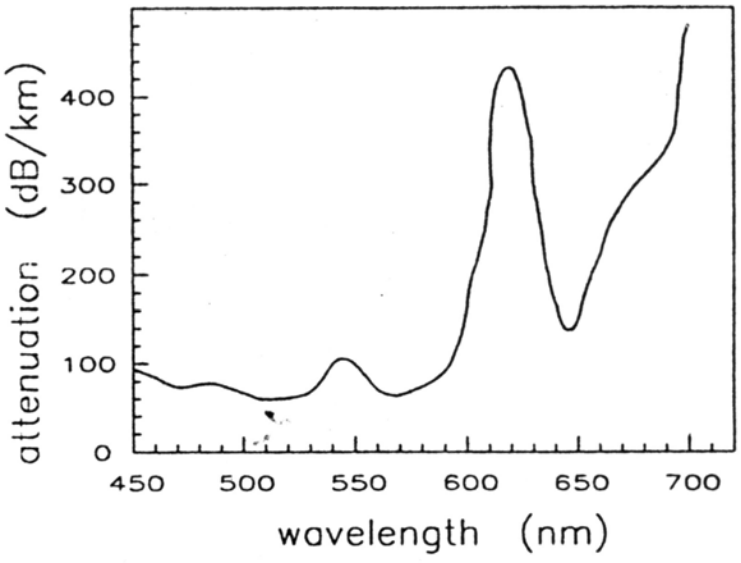

Fig 1.1 Attenuation spectrum of POF based on poly methyl methacrylate [1]

In 1995, Koike developed a perfluorinated graded-index (GI) polymer optical fibre using a teflon-type fluoropolymer called CYTOP, with low absorption from visible wavelengths to 1300nm (50 dB/km), enabling light sources and detectors developed for silica fibre to be used with perfluorinated POF [4]. The anticipated bandwidth was 1 GHz. In 2000, a GI POF with an attenuation of 16 dB at 1300nm and 569 GHz over 1 km was fabricated by Asahi Glass. Such improvements in POF performance in the telecommunications sector enhance sales and reduce the cost of POF components and enable it to be commercially viable for sensing applications as well.

The low processing temperature of polymer fibres (200-300^{0}C) allows to introduce required nonlinearity by doping with organic dyes. For this reason, increasing research activities have also been carried out in the field of active polymer optical fibres, most of which aim at making polymer optical fibre amplifiers or lasers.

Multimode fibre technology and, increasingly, also multimode planar waveguide devices are largely employed in short-distance communication applications such as LAN and interconnects. The revival of the use of multimode optical technologies in this area is driven and stimulated by the need for higher bit rates and the prospective low cost of these technologies. The last few years have seen a revival of industrial and academic research in the field of integrated optics, in general, and also in the field of polymer technology. Due to the material property restriction of $LiNbO_3$ and III-V compound material systems, a sizable portion of the research work on guided wave devices has been shifted to polymer-based materials. Polymer-based waveguide technology has emerged as the most suitable candidate for the fabrication of large-cross-section multimode integrated optical waveguides. The mechanical and chemical properties of

polymers open new frontiers for optical-device technology. Low material dispersion, unlimited device size and cost effectiveness are the major factors that cannot be provided using conventional inorganic materials. The most appealing characteristic of polymer waveguide technology is the simplicity and flexibility of waveguide fabrication methods. Polymer thin films can be deposited in a wide thickness range by spin or dip coating using relatively simple equipment. Large cross section channel waveguides have been fabricated using reactive ion etching, photopatterning, molding and hot and soft embossing [5-7]. Several multimode integrated optical elements have been successfully realized in polymer waveguide technology [8-10], including complete transceiver modules that comprise light sources, power splitters, (de)multiplexers and detectors [11].

1.3 Materials and applications

Optical polymer materials can exist in a broad refractive index range from n=1.296 to 1.7. Note that no optical polymer material exists that has a refractive index as high as that offered by inorganic materials like Si (n=3.5) or Si_3N_4 (n=2) that could allow the design of ultra-compact photonic structures like photonic band gap materials do. The refractive indices of a variety of polymer materials can be tailored and precisely controlled to suit a specific design purpose. This additional characteristic is rarely found in other waveguide technologies - with the exception of SiO_xN_y technology [12]. Each of the polymer systems available today has a unique set of properties that make it suitable for specific applications.

Teflon® AF polymers have the lowest index of refraction of any known polymers. The amorphous copolymer of 2,2-bis(trifluoromethyl)-4,5-difluoro-

1,3-dioxole, trade named Teflon-AF 2400 has got the refractive index 1.296 and has been investigated as an aqueous-core optical waveguide. This polymer is physically and optically stable and is transparent in the spectral range from 200 to 2000 nm [13]. This polymer is used as the cladding of liquid core waveguides used for absorption spectroscopy[14], water analysis[15] and Raman spectroscopy [16].

For a polymer to be transparent, it has to be fully amorphous. Polymers which meet this requirement and applied for the fabrication of optical fibres are poly methyl methacrylate (PMMA), polystyrene (PS) and polycarbonate (PC). The refractive indices of these polymers are 1.492, 1.59 and 1.58 respectively. Most PMMA-based or PS-based polymer fibres cannot withstand temperatures higher than 90^0C. However, it is desirable to increase the temperature working range of polymer fibres. Polymer fibres based on polycarbonates show high thermal resistance and can be used at temperatures as high as 150^0C. But they have large attenuation. Commercially available POFs mainly have PMMA core and fluorinated polymer with refractive index around 1.417 as the cladding. In recent years, perfluorinated materials have been used for the POF's core. These materials have much lower losses and GI POFs based on these materials present a dispersion comparable to that of a silica GI optical fibre [17].

The commonly used polymers for waveguide fabrication are, poly methyl methacrylate, polystyrene, poly vinyl alcohol (PVA), poly acrylic acid(PA), poly carbonates. As noted earlier, polymer waveguides have a great potential to create all-optical devices, which can be realized by the incorporation of various functional materials such as organic dyes in the polymer host matrix. The basic requirements imposed on a polymeric host for lasing dye molecules are good optical transparency at both pump and lasing wavelengths, good solubility

of the dye in the material and resistance to pump laser radiation. PMMA has been the most frequently used host for lasing dyes due to its excellent optical transparency in the visible and its relatively high laser-damage resistance. The matrix viscoelastic properties of polymers determine the optical damage resistance. The external plasticization of the polymer, by adding low molecular weight dopants, improves significantly the laser resistance. For example, by the copolymerization of methyl methacrylate (MMA) with 2-hydroxyethyl methacrylate (HEMA) , the plasticity of the material can be internally increased. The presence of HEMA as comonomer not only increases the plasticity of the material while maintaining the good transparency in the near-ultraviolet and visible spectral ranges, but also ensures good solubility of dyes such as Rhodamine 6G due to the polar character of HEMA [18].

Polymers synthesised from deuterated methacrylate and deuterated fluoromethacrylate monomers achieve high transparency from the visible to infra-red region by eliminating C-H vibrational bond absorption. In general polymers exhibit high absorption loss in the IR region due to the vibrational excitation of the C-H bonds. Absorption bands caused by vibration transitions and their overtones can be shifted to the longer wavelength regions outside the telecommunication-spectral windows by replacing the lighter hydrogen atom in the C-H bonds with heavier ones such as deuterium and halogens. The wavelength shift takes place because the transition energy is inversely proportional to the square root of the mass of the atoms in the bond and hence by increasing the mass, the transition energy decreases. This method has been successfully implemented by many workers to reduce polymer absorption losses in the IR region [5,6,19]. The refractive index of deuterated poly(fluoromethacrylate) (d-PFMA) can be controlled by changing the fluorine

content. An increase in the fluorine content causes a decrease in the refractive index of d-PFMA. The refractive index can be controlled in the range from 1.363-1.484 at a wavelength of 1300 nm [20].

Optical polymers that are thermally stable up to very high temperatures (up to 400^0C) have been reported. These include polyimides, deuterated polysiloxane and nonhalogenated acrylic polymers [5,21].

The emergence of semiconducting polymers has evoked great research activities in the field of conjugated polymer waveguide devices . Conjugated materials with high-photoluminescence quantum yields attract very wide interest of fundamental research and technological application. Within every class of conjugated polymers the spectral luminescence characteristic can be tailored by varying the effective conjugation length (the average number of chemical repeat units in the undisturbed sequence of the polymer). In this way, the energetic position of the highest occupied molecular orbital and the lowest unoccupied molecular orbital can be tuned. Such a tuning parameter to modify the energy gap, is generally, besides the band gap tuning by composition, not available for classical inorganic semiconductor materials with fixed types of atoms and set of lattice parameters. In this sense, conjugated polymers are very versatile and constitute a novel class of semiconductor laser materials. A variety of optoelectronic devices have been demonstrated in which conjugated polymers are used as the active semiconducting materials, including diodes, light emitting diodes, photodiodes, field-effect transistors and light-emitting electrochemical cells [22-26]. With the improvements of organic chemistry, conjugated polymeric materials with quantum yields equivalent to laser dyes are now available [27]. In particular, there is now significant interest for those stemming

from the poly(paraphenylene) (PPP) and poly(phenylene-vinylene) (PPV) family [28,29].

1.4 Guided wave polymer photonic devices

This section gives an overview of important passive and active optical devices based on polymer fibres as well as planar waveguides.

1.4.1 Couplers

A directional coupler is one of the most important elements in optical integrated circuits. It is used for constructing many components, such as multi/demultiplexers, optical switches and power splitters. Low loss single mode directional couplers were successfully fabricated on acrylic substrates with polymers synthesised from deuterated methacrylate and deuterated fluoromethacrylate monomers[30]. The coupling ratio was tuned by bending the couplers on the flexible substrates. Polyimides which have high thermal stability over 300^0 C are attractive materials for fabricating optical waveguides. Using fluorinated copolyimides with high transparency at optical telecommunication wavelengths of 1.3 and 1.55 μm, Kobayashi et al fabricated channel optical waveguides by photolithography and conventional reactive ion etching, and made directional couplers out of them [31]. Light coupling between dual-core squarylium dye (ISQ) doped POFs was also reported [32].

1.4.2 Filters

Tunable filters can be based on Bragg gratings. Gratings in planar polymers can be produced by a variety of techniques such as casting, molding, embossing, e-beam writing, and photochemical processes. The first three techniques produce surface-relief gratings while the last two typically produce

bulk index gratings. Photochemical fabrication processes induce an index modulation through two-beam interference. This effect can be achieved through the use of either interference of split laser beams or a phase mask in which two beams corresponding to the +1 and –1 diffracted orders interfere. Tunable wavelength filters based on the thermo-optic refractive index change of the polymer waveguide with Bragg reflection grating has been reported [33]. Fluorinated polymers are incorporated for low-loss waveguide operating around 1.55 μm. Bragg reflection gratings are fabricated using a phase mask and a high-index polymer resole. The phase mask technique, owing to its simplicity and superior stability, is the popular one and used for the fabrication of Bragg gratings on polymer fibres as well. The Optical Communications Group at the University of South Wales (Sydney, Australia), first announced the creation of Bragg gratings in polymer fibres [34] and the applications of Bragg gratings for Wavelength Division Multiplexing (WDM) devices [35].

1.4.3 Optical switching and logic gates

The first reports on planar thermo-optic polymer devices appeared at the end of 1980's [36]. The thermooptic (TO) effect of polymers is ten times larger than that of silica. This means that the refractive indices of polymers are highly dependent on temperature. Therefore, the use of polymers instead of silica can significantly reduce the electrical power needed for switching. Polymer optical waveguides have been produced from several types of polymers and have been applied to several types of TO switches such as the Mach–Zehnder (MZ) interferometer, directional coupler, and Y-branching-types. For example, MZ-type TO switches, where electrical power consumption is as low as 5 mW, have been fabricated using a deuterated fluoromethacrylate polymer (d-PFMA) optical waveguides[37]. 4x4 directional coupler TO switches, which operate at a

wavelength of 1.55 μm, have been fabricated using polymethyl methacrylate optical waveguides [38].Fluorinated polyimide waveguides with low polarization dependent loss (PDL) and TO switches made from them were also demonstrated [39]. The Y-branching type switches showed a switching speed faster than 8 ms.

Thermo optic switches have rather limited speed. For faster operation, other material effects should be applied. The electro-optic effect in a polymer is used to change the refractive index of the material. Digital optical switches based on electro-optic polymers have been reported recently [40].

Dye doped polymers can be applied for ultra-high-speed optical switching waveguide devices. In this case, third-order optical nonlinearity is used where switching speed faster than picoseconds can be obtained. The dc Kerr effect, which is based on third order nonlinearity, has an enormous technological potential, because it allows the realisation of high-speed all-optical functions like switching, amplification and optical logic gate. Kuzyk et al have demonstrated all-optical switching using a squarylium doped PMMA single mode fibre, in a Sagnac interferometer set up [41].

1.4.4 Optical Sensors

The availability of high performance optical waveguiding components has been of essential significance to the progress in optical sensing made during the last 20 years. In general these components modify one or more characteristic parameters of the guided light : intensity (amplitude), wavelength (spectral distribution), optical phase, polarization (state and/or degree) and frequency or time dependencies.

The most popular sensing technique is based on intensity modulation, in which the magnitude to be measured produces a detectable change in the intensity of the light.

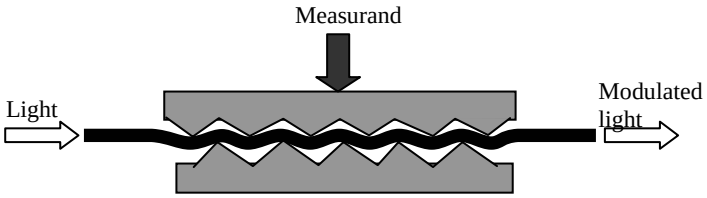

(a) Intensity modulation using microbends

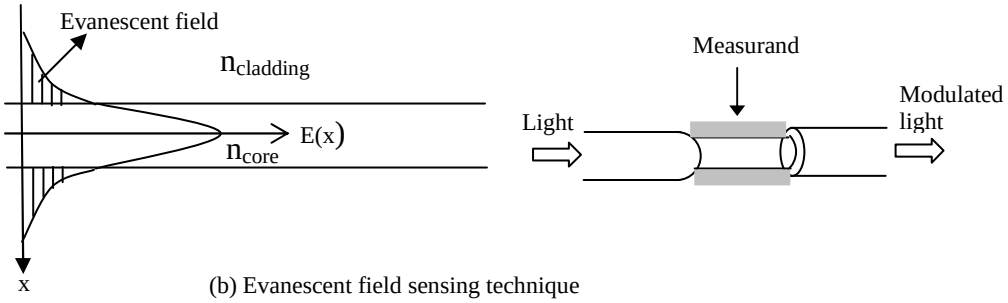

(b) Evanescent field sensing technique

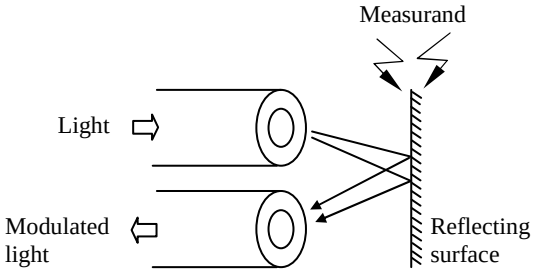

(c) Reflective configuration of coupling based sensor

Fig 1.2 Various schemes of intensity modulated sensors

This approach provides simple and potentially low-cost devices because it is easier to measure the optical power than the phase or the state-of-

polarisation of an optical radiation. In addition, this is the most suitable approach with multimode fibres because the phase and state of polarization information is lost when light is propagated through this kind of fibre.

The most significant techniques on which intensity-modulated fibre optic sensors are based are micro and macro bending, evanescent field absorption and coupling between fibres in an extrinsic configuration .

When the highest measurand sensitivity is required, interferometric techniques are appropriate.

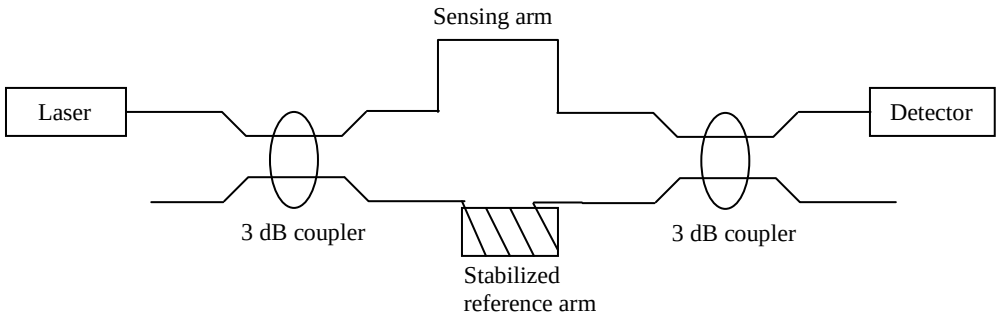

Fig 1.3 Fibre optic Mach-Zehnder interferometer

Large diameter polymer optical fibres are attractive in sensing applications since they are less fragile and vastly easier to work with than glass fibres. Sensors using commercial polymer optical fibres are based on ideas already used in silica glass sensors, but exploiting the flexible and inexpensive nature of the polymer optical fibre for harsh environments and throw-away sensors. An example of this technology transfer is a displacement sensor developed by Ioannides et al [42], based on an array of three POFs, with the centre fibre emitting light that is reflected from a mirror surface and captured by two outer fibres, the ends of which are positioned at different distances from the

mirror. The unique features of POFs make them attractive in medical environments in addition to the usual advantages of immunity to electromagnetic interference, intrinsic safety and chemical immunity.

There are several techniques of simply altering the optical properties of commercially available POF, so as to tailor them for specific applications. Removing the cladding from an optical fibre and replacing with the measurand is a well known technique used to fabricate evanescent field sensors. Among the works reported are biofilm sensors where the stripped fibre was exposed to biofouling and scaling conditions in a closed loop water supply [43,44]. Tapering the fibres increases the penetration of the evanescent field. Silica fibres are traditionally tapered using heat and pull techniques, but for POF tapers, an alternative technique of chemical etching using organic solvents has been developed by Merchant et al. [45].

The refractive index profile of the POFs can be easily tailored for sensing requirements. Refractive index profiling is obtained by dip coating the stripped or clad fibres with optical epoxies, sol gels or polymers of defined refractive indices. This technique was employed for the fabrication of sensors for humidity monitoring [46] and vapour phase alcohol detection [47]. These sensors were based on the swelling phenomenon in the cladding polymer layer. The unclad portion of the fibres were coated with swelling polymers, which swell due to the attachment of water molecules or alcohol molecules thereby changing the refractive index of the cladding layer.

Fibre Bragg grating (FBG) is a very important and potential optical device in optical telecommunication and sensing fields. Due to smaller Young's modulus and larger thermo-optic coefficient than silica, polymer FBGs might be advantageous over silica FBGs in sensing applications. Useful photosensitivity

has been found in PMMA based POFs [34,48,49]. A grating with 28 dB transmission rejection has also been reported [50]. Polymer FBG sensors have proved to exhibit more than 10 times sensitivity than silica FBGs [51].

Sensors based on dye doped polymer fibres have also been reported. Muto et al have fabricated moisture sensitive fibres using PMMA doped with phenol red dye [52]. The propagation loss of this fibre at 530 nm increased with increasing water vapour in air, thus operating as an excellent humidity sensor with a fast response time. This sensor was equally good in detecting moisture equivalent in the soil.

POFs are also successfully employed in structural health monitoring in the form of strain sensors [53,54].

Another attractive research area is using side polished fibre components. In a side polished fibre, the cylindrical symmetry of the fibre is altered by polishing it in a longitudinal plane, so that the sensing region takes the form of a planar structure.

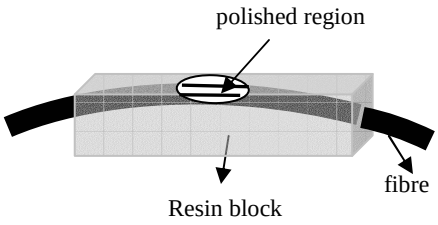

Fig 1.4 Side polished fibre component

To make the cladding removal process easier, the fibre is often secured in a supporting medium with epoxy or other means. Side polished silica fibres have long been used for the fabrication of fibre sensors and other devices such as

couplers, polarisers, filters etc [55-59]. When interacting with a deposited waveguide or metallic layer on the coupling region, small shift in wavelength or change in polarization or intensity of the output signal can be analyzed revealing the chemical composition, pressure, temperature etc. of the medium surrounding the sensing region. The main advantage of the side- polished fibre sensor is that it requires only a very small amount of the analyte . The compact nature of these fibres have been exploited in developing sensors for measuring various physical and chemical parameters such as pressure, temperature, humidity, refractive index and pH [56,60-62]. The device fabrication becomes much easier with POFs in comparison with glass fibres. Moreover, the use of polymer fibre make the device more economic too, especially in situations where throw-away sensors are to be used. In literature only a few reports are available on the application of side polished POF sensors [63, 64].

In recent years several planar optical waveguide sensors have been suggested for biological applications. Typically, the sensors are used for measuring the refractive index of liquids or various aqueous solutions of biological substances, such as mammalian cells, bacterial cells, and proteins. Recently, a new class of optical waveguide biosensors has been introduced with the so-called reverse symmetry design [65,66]. In this technique, the waveguide substrate has a refractive index less than the refractive index of the aqueous cover medium (~1.33). This design offers deeply penetrating evanescent optical fields into the analyzed cover sample. A possibility of realizing reverse symmetry is using nanoporous materials with a refractive index ~1.2 as a substrate. Using polystyrene (PS) films on nanoporous silica, such a waveguide has been demonstrated for refractometry [66], bacteria detection [67] and living cell detection [68].

1.4.5 Lasers and Amplifiers

Motivated by the enormous impact of lasers on modern technology, there is an ongoing search for advanced laser materials, in particular for novel solid-state lasing media which open up new possibilities for applications and technologies. Supplied with the toolbox of modern organic chemistry, new materials can be constructed and designed with specific properties. One of the objectives is to design advanced materials with an improved laser performance and an extended wavelength range. Furthermore, it is of important interest to develop new designs of compact laser sources attractive to the widespread field of photophysical and photochemical applications. In this scenario, one can either utilize dilute systems of organic dyes embedded in host matrices or alternatively employ films of highly luminescent conjugated polymers.

In the dye-doped matrix systems, the dye molecules – rhodamines, coumarins, pyrromethenes etc – are dispersed in solid host media which are either chosen to be sol-gel materials or polymers. Polymeric matrices offer several advantages such as wide spectral coverage by chemical tailoring of structure, processability that permits fabrication of devices of virtually any shape and potentially very low cost. They show better optical transparency, homogeneity of refractive index and good compatibility with the organic dye.

Waveguide structures provide long gain length and optical confinement, which offer reduction of lasing threshold, a requirement for efficient lasing. Polymer fibres are especially attractive as waveguide structures because of their symmetric output beam profile and adaptability to optical-fibre-based communication systems. Work on polymer optical amplifiers (POFA) was started in Keio University. Graded-index (GI) type rhodamine B doped POFA were successfully prepared which gave a maximum gain of 27 dB at 591 nm [69,70].

Efforts were taken to prevent degradation of dyes and to enhance their solubility in PMMA, and high gain of 33 dB was achieved with rhodamine B doped GI POFA [71]. Amplifiers based on step index polymer fibres were also demonstrated. Peng et al developed a simple technique to fabricate dye doped step index fibre and achieved an optical gain of 23 dB and a broad gain band width [72]. Liang et al demonstrated 23 dB gain from a 60 cm long rhodamine B doped step index polymer fibre, at 630 nm which is closer to the low loss window of PMMA based optical fibres [73]. Although optical fibres have many advantages over bulk optics as a laser medium, there have been only a few reports on polymer fibre lasers. The pioneering work by Muto et al showed lasing from step-index polymer fibres with 2 cm length [74]. Kobayashi et al demonstrated efficient and photostable lasing from graded-index polymer optical fibres with 5 cm length [75]. Both studies were based on commercial dye doped polymer fibres. Transversely pumped laser based on rhodamine 6G doped GI POF was demonstrated by Kuriki et al [76]. Blue lasing from a step-index glass-clad polymer fibre doped with a fluorescent stilbenoid compound was also reported recently[77]. Lasing was observed at 489 nm, when a 1.4 cm long fibre was photopumped with nanosecond pulses at 355 nm .

The demand for compact visible lasers has accelerated the research in the field of planar waveguide lasers. Polymer optical waveguides and fibres are often designed to have large cores with 10-1000 micrometer thickness to facilitate easy connection and splicing, and hence waveguide amplifiers and lasers compatible with these multimoded passive components should be developed. So the host polymer has to allow the formation of thick films and also give facets with high optical qualities. Two photon pumped upconverted lasing in 4-Dicyanmethylene-2-methyl-6-(p-dimethylaminostyryl)-4-H-pyran

(DCM) dye doped PMMA waveguide was observed by Mukherjee in 1993 [78]. Wide range tunable laser emission have been reported from polymer thin film waveguides in optically pumped distributed feedback scheme [79,80]. The samples used were PMMA and poly-vinyl carbazole (PVK) films doped with rhodamine 6G, DCM and coumarine laser dyes.

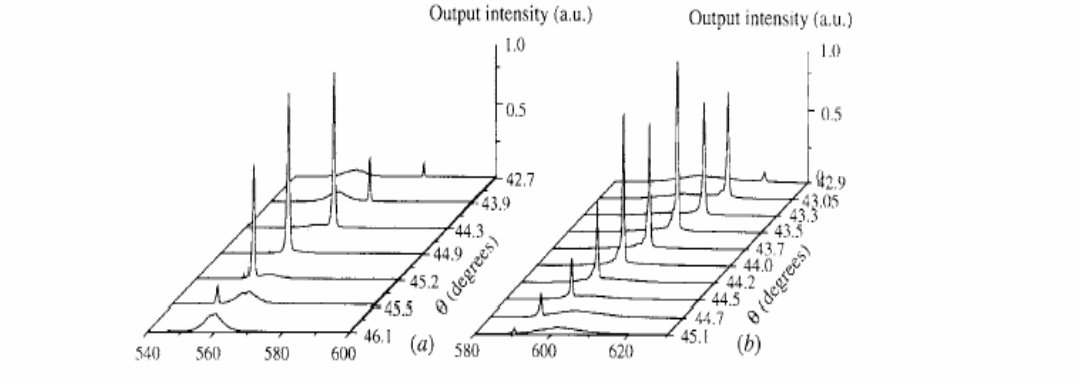

Fig 1.5 DFB laser action of Rh6G in PMMA (a) and DCM in PVK (b) [79]

Multimode laser emission from a transversely pumped free standing PMMA film doped with rhodamine 6G was also reported recently[81]. Polymer waveguide lasers operating in the near-infrared region is another notable work. Lasing at around 820 nm in a simple low-finesse cavity was observed from multimode waveguides based on poly(1-vinyl-2-pyrrolidone) doped with a near-IR-emitting compound, 2-(6-(4-dimethylaminophenyl)-2,4-neopentylene-1,3,5-hexatrienyl)-3-methyl-benzothiazolium perchlorat which is commercially known as LDS821 (Exciton) [82]. The room temperature fabrication of all the above mentioned dye doped polymer waveguides offer full integrability with optical circuits regarding its material, structure and processing.

During the past few years, conjugated polymers have attracted intensive interest for applications of light emitting diodes, solid state lasers, solar cells and displays. In addition to their semiconducting behaviour, the intrinsic emissive properties of this class of materials in films are comparable to that of organic laser dyes in dilute solutions. In contrast to other organic chromophores, they suffer little concentration quenching. Several groups have photopumped thin films of conjugated polymers and studied the amplified spontaneous emission from them [83,84]. Laser action from the conjugated polymer Poly(2,5-bis(2'-ethyl-hexyl-oxy)-1,4-phenylenevenylene) (BEH:PPV) in a cavity made with 2 dielectric mirrors providing a high finess planar cavity has been demonstrated in the late 90's[85]. Stimulated emission in blue green region was observed from optically pumped waveguides of methyl substituted conjugated ladder type poly(paraphenylene) [86]. Frolov et al have studied stimulated emission in various scattering media containing π-conjugated polymers and organic laser dyes with high optical gain [87]. Amplified spontaneous emission and distributed feedback lasing from conjugated compound 1,4-Bis[2-[4-[N,N-di(p-tolyl)amino]phenyl] vinyl] benzene (BTAPVB) in polymeric waveguides have also been reported [88].

Microcavity lasers is a novel approach to lasing action in optically pumped organic solids. The design of a microcavity provides a possibility for a compact light-emitting device structure. The microcavity devices consist of luminescent material placed within a Fabry-Perot resonator with a length of the order of the wavelength of the emitted light. In this way, the light emission is coupled to the cavity mode(s) and characteristically the light output is spectrally narrowed and directed [89]. Lasing from a conjugated polymer microcavity was the first report of laser emission from a solid-state homopolymer[90]. Here one

of the cavity mirrors was formed by a distributed Bragg reflector. The DBR is a chirped mirror so that longer wavelengths are reflected deeper inside the stack and therefore several discrete modes are supported within the visible range. Becker et al built a planar microcavity structure whose resonance wavelengths can be tuned by application of external control voltage [91]. The device comprised of a thin film of a fluorescent semiconducting polymer combined with an electrically switchable liquid crystal layer, which are sandwiched between the two cavity mirrors. A tunability of 56 nm was obtained with this structure.

Spherical designs of microstructure resonators too can be implemented for compact miniature laser devices. This combines effective coupling of the emission to the resonator modes within a microstructure and with the resonant modes being ring modes along the characteristic circumference. It is an alternative concept to the planar microcavities – Fabry-Perot cavities – and can be employed for different spherical geometries. These ring microlasers are also called whispering-gallery-mode lasers and can be fabricated as rings, discs or spheres with characteristic dimensions of 1-100μm. Lasing at low-power thresholds can be achieved by virtue of the strong optical confinement due to the high contrast of the refractive index between the active medium and the surrounding. This provides light guiding into closed optical paths (ring modes) and coupling of these high refractive modes. Laser action will then occur along these circumferences for which the gain exceeds the round trip losses.

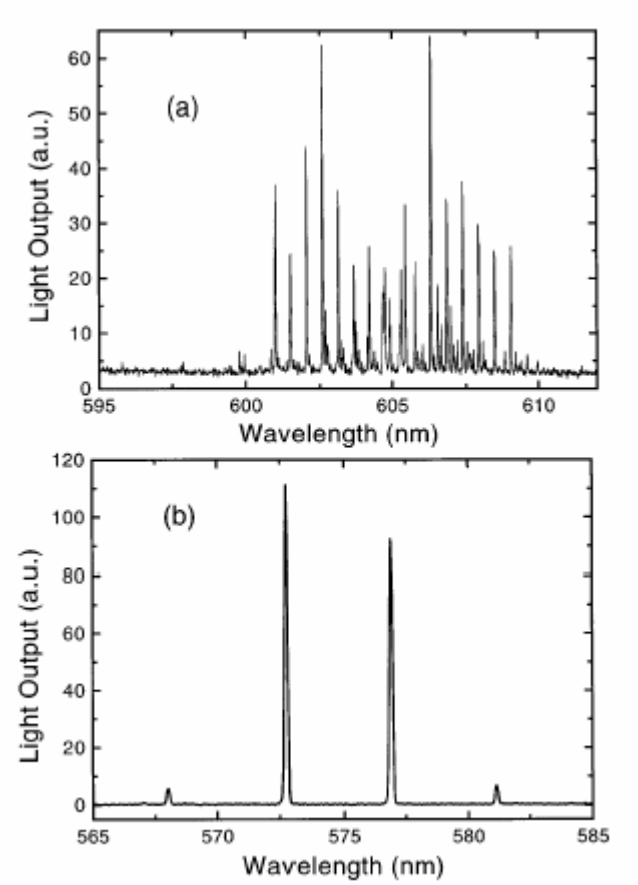

Fig 1.6. Laser emission from polymer microring lasers for (a) a 125 μm diameter glass fibre core and (b) a 17 μm diameter glass fibre core [93]

Devices of thin fibres coated with films of dye doped polymers [92,93] or conjugated polymers [94] and flat polymer microdiscs [93] have been demonstrated as whispering-gallery microlasers.

1.5 Polymers in Photonic band gap structures

Since the invention of the laser, the field of photonics has progressed through the development of engineered materials which manipulate the flow of light. Photonic band gap (PBG) materials are a new class of dielectrics which are the photonic analogues of semiconductors. The photonic band gap is a frequency interval over which the linear electromagnetic propagation effects have been turned off. The presence of a defect in a PBG structure generally results in a "localized state", that is, a tightly confined region of light energy which must stay within the defect, since it cannot propagate in the structure, and since its energy is not being absorbed. Defects, appropriately designed and arranged, can create waveguides with unprecedented directional control (eg. one micron radius, 90 degree bends with 98 percent transmission efficiency), drop/add filters, multiplexers/demultiplexers, resonators, extremely fast laser cavities, etc. All of this can be achieved on a very small length scale (on the order of tens of microns), so that an astounding level of integration is feasible. Ever since this idea was introduced by John [95] and Yablonovitch [96], various structure designs and device applications from microwave to optical frequencies have been proposed and realized [97–99].

Photonic crystals (PCs) have attractive optical properties that can be tuned by their geometry. Variables such as lattice parameter, hole diameters, and other geometrical parameters directly impact the transmission spectra and dispersion of light propagating through the PC structure. The choice of materials is made based on the ultimate function desired for the device, such as light emission or nonlinear behaviour for active devices. Polymers have recently been demonstrated to achieve very high-speed optical modulation, higher than that

expected to be achieved using semiconductors [100] and hence, it is natural to try to develop polymer-based photonic crystals. Other passive applications, such as small turning radius in highly integrated waveguides, filtering, and dispersion devices are less dependent on the material properties and can also be implemented in polymers.

Recently, direct lithography in electron-beam sensitive polymers was investigated to fabricate 2D-slab polymer-based photonic crystal structures [101]. PMMA doped with azo dye Disperse Red 1 (DR1) chromophores was used as a test material to produce optimized low-index contrast photonic crystals presenting a photonic band gap for TE polarization. Air-clad polymer photonic crystals were fabricated that used a thin supporting membrane of Si_3N_4 to enhance physical stability of the polymer layer, and to enable integration with ridge waveguides for simplified testing. Earlier, fabrication and transmission measurements for finite two-dimensional polymer photonic crystal slab waveguides fabricated from a benzocyclobutene polymer on a low refractive index substrate from teflon, was reported [102]. A square air hole lattice (500 nm lattice constant, 300 nm hole diameter) was realized by electron beam lithography and reactive ion etching. Polarization and wavelength dependent transmission results showed TE-like and TM-like stop gaps at 1.3 μm excitation wavelengths.

The idea of guiding light using microstructure has been reported in silica fibres [103]. Researchers from the University of Sydney, Australia have fabricated photonic crystal fibre based on POF. As with the silica counterpart, these ‘holey’ fibres have periodic air holes running along its entire length [104]. These air holes confine the light to a central core by a modified form of total internal reflection, rather than the refractive index step of a standard fibre.

However, microstructured POFs (MPOF) offer many advantages over the silica ones. The fabrication is much easier due to much more favourable balance between surface tension and viscosity at the draw temperature which reduces the chance of holes collapsing. The MPOF structure is not restricted to close-packed arrangements of circular holes, as is the case for the microstructure silica fibres fabricated by the capillary stacking technique. More material modifications are possible owing to the much lower processing temperatures and intrinsic tailorability of polymers. The base materials and fibre processing is cheaper while the fibres remain flexible even at large diameters. Microstructured POFs are an exciting new development, offering opportunities to develop fibres for a wide range of applications in telecommunications and optical sensing [105]. In 2004, microstructures POF doped with Rhodamine 6G was fabricated and demonstrated as an optical amplifier and a fibre laser [106].

1.6 Scope of the thesis

The main objective of the research work is the design of compact polymer based devices for various photonic applications. Polymer optical fibres and dye doped polymer planar waveguide structures were chosen to be the suitable candidates for the realization of the same. This thesis focuses on the design, fabrication and characterization of polymer optical fibre sensors and polymer waveguide lasing media. The second and third chapters describe the fabrication of side polished polymer fibre sensors for refractive index measurement and chemical reaction rate measurement Theoretical modeling was done wherever necessary. Fabrication and optical characterization of dye doped polymer film waveguide is given in the fourth chapter. Observation of amplified

spontaneous emission (ASE), optical gain measurements and wavelength tuning of ASE are presented in the fifth chapter. Sixth chapter discusses the multimode laser emission from free standing dye doped film waveguides. Conclusions and future prospects are discussed in the last chapter.

References

1. T. Kaino, K. Jinguji, S. Nara, *Appl. Phys. Lett.* **42** (7), 567-569 (1983).
2. C. Koeppen, R.F. Shi, W.D. Chen, A.F. Garito, *J. Opt. Soc. Am. B* **15**(2), 727-739 (1998).
3. G. D. Peng, P.L. Chu, SMIREE, X. Lou, R.A. Chaplin, *J. Electrical and Electron. Engg, Australia-IE Aust & The IREE Society* **15**(3), 289-296 (1995).
4. Y. Koike, *7th International Plastic Optical Fibres Conference, Berlin*, 1-8(1998)
5. L. Eldada, L.W. Shacklette, *IEEE J. Select. Topics Quantum Electron*. **16**, 54 (2000).
6. R. Yoshimura, M. Hikita, S. Tomaru, S. Imamura, *J. Lightwave Technol*. **16**, 1030 (1998).
7. R. T. Chen, S. Tang, T. Jannson, *Appl. Phys. Lett* **63**, 1032 (1993).
8. D. Israel, R. Baets, M.J. goodwin, N. Shaw, M.D. Salik, C.J. Groves-Kirkby, *J. Lightwave Technol.* **13**, 1057 (1995).
9. I. Ilic, R. Scarmozzino, R.M. Osgood, J.T. Yardley, K.W. Beeson, M.J. MacFarland, K.M.T. Stengel, *IEICE Trans. Commun*. **E80-B**, 135(1997).
10. S. Musa, N.S. Lagali, B. Docter, G. Sengo, G.J.M. Krijnen, A. Driessen, *Proc. Of the 13th IEEE/LEOS Conference, Puerto Rico*, 468 (2000).
11. L. Aronson, B.E. Lemoff, L.A. Buckman, D.W. Dolfi, *IEEE Photon. Technol. Lett.* **10**, 1489 (1998).
12. K. Wörhoff, A. Driessen, P.V. Lambeck, L.T.H. Hilderink, P.W.C. Linders, T.J.A. Popma, Sens. Actuat. **74**, 9-12 (1999).
13. http://www2.dupont.com/Teflon_Industrial/en_US/products/product_by_name/teflon_af/properties.html
14. P. Dress,H. Franke, *Appl. Phys. B* **63**, 12-19 (1996).
15. P. Dress, M. Belz, K.F. Klein, K.T.V. Grattan, H. Franke, *Appl. Opt*., **37**(21), 4991-4997 (1998).
16. M. Holtz, P.K. Dasgupta, G. Zhang, *Anal. Chem*. **71**, 2934 (1999).
17. Y. Koike, T. Ishigure, E. Nihei, *J. of Lightwave Technol*. **13**, 1475-1489 (1995).
18. A. Costela, I. Garcia-Moreno, J.M. Figuera, F. Amat-Guerri, R. Sastre, *Laser Chem* **18**, 63-84(1998).
19. S. Imamura, R. Yoshimura, T. Izawa, *Electron Lett* **27**, 1342 (1991).
20. Polymer Optical Fibers, Ed. Hari Singh Nalga, American Scientific Publishers, California, 2004.

21. M. Usui, M. Hikita, T. Watanabe, M. Amano, S. Sugawara, S. Hayashida, S. Imamura, *J. Lightwave Technol*. **14**, 2338 (1996).
22. H. Tomozawa, D. Braun, S. Philips, A. J. Heeger, H. Kroemer, *Synth. Met* **22**, 63 (1987).
23. D. Braun, A.J. Heeger, *Appl. Phys. Lett* **58**, 1982-1984 (1991).
24. G. Yu, A.J. Heeger, *J. Appl. Phys*. **78**, 4510 (1995).
25. J.H. Burroughes, C. A. Jones, R.H. Friend, *Nature* **335**, 137 (1988).
26. Y. Yang, A.J. Heeger, *Nature* **372**, 344 (1994).
27. G. Kranzelbinder, G. Leising, *Rep. Prog. Phys*. **63**, 729-762 (2000).
28. C. Zenz, W. Graupner, S. Tasch, G. Leising, K. Müllen, U. Scherf, *Appl. Phys. Lett* **71**(18), 2566-2568 (1997).
29. M. D. McGehee, R.Gupta, S. Veenstra, E. K. Miller, M. A. Diaz-Garcia, A. J. Heeger, *Phys. Rev. B* **58** (11), 7035-7039 (1998).
30. R. Yoshimura, H. Nakagome, S. Imamura, T. Izawa, *Electron. Lett* **28**, 2135-2136(1992)
31. J. Kobayashi, T. Matsuura, S. Sasaki, and T. Maruno, *J.Lightwave Technol* **6**(4), 610-614 (1998).
32. S.R. Vigil, Z. Zhou, B.K. Canfield, J. Tostenrude, M.G. Kuzyk, *J.Opt. Soc. Am. B* **15**(2), 895-900 (1998).
33. M.C. Oh, H.J Lee, M.H Lee, J.H. Ahn, S. G. Han, H.G. Kim, *Appl. Phys. Lett* **73**, 2543-2545 (1998).
34. Z. Xiong, G. D. Peng, B. Whu, P.L. Chu, *IEEE Photon. Technol. Lett* **11**, 352-354 (1999).
35. P.L. Chu, G. D. Peng, H.Y. Liu, *Proceedings of the Asia-Pacific Polymer Optical fibre Workshop, Sydney*, 76-94 (2001).
36. B.L. Booth, *J. Lightwave Technol* **7**, 1445 (1989).
37. Y. Hida, H. Onose, S. Imamura, *IEEE Photon. Technol. Lett* **5**, 782–784 (1993).
38. N. Keil, H. H. Yao, C. Zawadzki, B. Strebel, *Electron. Lett.* **30**, 639–640 (1994).
39. J. Kobayashi, T. Matsuura, Y. Hida, S. Sasaki, T. Maruno, *J. Lightwave Technol* **16**, 1024-1029 (1998).
40. W. Yuan, S. Kim, G. Sadowy, C. Zhang, C. Wang,W.H. Steier, H.R. Fetterman, *Electron. Lett* **40** (3) (2004).
41. M. G. Kuzyk, D. W. Garvey, S.R. Vigil, D.J. Welker, *Chem. Phys*. **245**, 533-544 (1999).
42. N. Ioannides, D. Kalymnios, I. W. Rogers, *POF'96, Fifth International Conference on Plastic Optical Fibres and Applications, France,251-55 (1996).*
43. R. Philip Chandy, P.J. Scully, P. Eldridge, H.J. Kadim, M. Gérard Grapin, M.G. Jonca, M. Gérard D'Ambrosio and F. Colin, *IEEE J. on Selected topics in Quantum Electronics*, **6**(5), 764-772 (2000) .
44. R. Philip Chandy, P.J. Scully and D. Thomas, *Sensors and Actuators B* **71,** 19-23 (2000).

45. D. F. Merchant, P.J. Scully, N.F. Schmitt, *Sensors and Actuators* **76**, 365-371 (1999).
46. Shinzo Muto, Osamu Suzuki, Takashi Amano, Masayuki Morisawa, *Meas. Sci. Technol*.**14,** 746–750 (2003)
47. Masayuki Morisawa, Yumiko Amemiya, Hidenori Kohzu, Chuan Xin Liang, Shinzo Muto, *Meas. Sci. Technol*. **12,** 877–881(2001).
48. G.D. Peng, Z. Xiong, P.L. Chu, *Opt. Fibre Techn*. **5**, 242-251 (1999)
49. H.B. Liu, H.Y. Liu, G.D. Peng, T.W. Whitbread, *IEEE Photon. Technol. Lett* **17**(2),411-413 (2005).
50. H.Y. Liu, G.D. Peng, P.L. Chu, *IEEE Photon. Technol. Lett* **14**, 935-937 (2002).
51. H. B. Liu, H.Y. Liu, G. D. Peng, P.L. Chu, *Opt Commun* **219**, 139-142 (2003).
52. Shinzo Muto, Akihiko Fukasawa, Takayuki Ogawa, Masayuki Morisawa, Hiroshi Ito, *Jap. J. Appl. Phys* **29**(6), L 1023-L 1025 (1990).
53. K. S. C. Kuang, W.J. Cantwell, P.J. Scully, *Meas. Sci. Technol*. **13**, 1523-1534 (2002).
54. K. S. C. Kuang, S. T Quek, M. Maalej, *Meas. Sci. Technol*. **15,** 2133–2141 (2004).
55. S. M.Tseng and C.L.Chen, *Appl. Opt*. **31**(18), 3438-47(1992).
56. Ainhoa Gaston, Ibon Lozano, Fatima Perez, Fernando Auza, Joaquin Sevilla, *IEEE Sensors Journal* **3**(6), 806-810 (2003)
57. Kyung-Rak Sohn, Kwang-Taek Kim, Jae-Won Song, *Sensors and Actuators A* **101**, 137-142 (2002).
58. S. Lee, J. Sokoloff, B. McGinnis, and H. Sasabe, *Appl. Opt*. **37**, 453-462 (1998).
59. N. Chen, S. Chi, and S. Tseng, *Opt. Lett*. **29**, 2219-2221 (2004).
60. Javier Senosiain, Idoya Diaz, Ainhoa Gaston and Joaquin Sevilla, *IEEE Trans. On Instrumentation and Measurement*, **50**(6), 1656-1660(2001).
61. Radan Slavik, Jiří Homola, Jiří Čtyroký, *Sensors and Actuators B* **51** , 311-315 (1998).
62. Navneet K. Sharma, B.D. Gupta, *Optics Communications* 216, p299-303 (2003).
63. Joseba Zubia, G. Garitaonaindiá and Jon Arrúe, *Appl. Optics* **39**(6), 941-946 (2000).
64. R.M. Ribeiro, João L.P. Canedo, Marcelo M. Werneck, Liliana R. Kawase, *Sensors and Actuators A* **101,** 69-76(2002).
65. Horvath R, Lindvold L R ,Larsen N B , *Appl. Phys.* B **74,** 383–93 (2002).
66. Horvath R, Pedersen H C , Larsen N B , *Appl. Phys. Lett.* **81,** 2166–2168 (2002)
67. Horvath R, Pedersen H C, Skivesen N, Selmeczi D, Larsen N B, *Opt. Lett.* **28,** 1233–1235 (2003)
68. Horvath R, Pedersen H C, Skivesen N, Selmeczi D, Larsen N B, *Appl. Phys. Lett.* **86,** 071101 (2005)
69. A. Tagaya, Y. Koike, T. Kinoshita, E. Nihei, T. Yamamoto, K. Sasaki, *Appl. Phys. Lett* **63**, 883-884 (1993)

70. A. Tagaya, Y. Koike, E. Nihei, S. Teramoto, K. Fujii, T. Yamamoto, K. Sasaki, *Appl. Opt.* **34,** 988-992 (1995).
71. A. Tagaya, S. Teramoto, E. Nihei, K. Sasaki, Y. Koike, *Appl. Opt.* **36**(3)**,** 572-578 (1997).
72. G. D. Peng, P.L. Chu, Z. Xiong, T. W. Whitbread, R. P. Chaplin, *J. Ligthwave. Techn* **14**(10), 2215-2223 (1996)
73. Hao Liang, Zhiqiang Zheng, Zengchang Li, Jie Xu, Biao Chen, Hui Zhao, Qijin Zhang, Hai Ming, *J. of Appl. Polym. Science*. **93**, 681–685 (2004)
74. S. Muto, A. Ando, O. Yoda, T. Hanawa, H. Ito, *Trans. Inst. Electron. Commun. Eng. Jpn. Sect*. **E 70**, 317(1987).
75. T. Kobayashi, K. Kuriki, N. Imai, T. Tamura, K. Sasaki, Y. Koike, Y. Okamoto, *Proc. SPIE* **3623**, 206-214 (1999).
76. K. Kuriki, T. Kobayashi, N. Imai, T. Tamura, S. Nishihara, Y. Nishizawa, A. Tagaya, Y. Koike, Y. Okamoto, *Appl. Phys. Lett* **77**(3), 331-333 (2000).
77. T. Kobayashi, W. J. Blau, H. Tillmann, H. Horhold, *J.Opt. A : Pure Appl. Opt* **4**, L1-L3 (2002).
78. A. Mukherjee, *Appl. Phys. Lett* **62** (26),3423-3425(1993).
79. Vincent Dumarcher, Licinio Rocha, Christine Denis, Celine Fiorini, Jean-Michel Nunzi, Frank Sobel, Bouchta Sahraoui, Denis Gindre, *J.Opt. A: Pure Appl. Opt* **2,** 279-283 (2000).
80. F. Sobel, D. Gindre, J.M. Nunzi, C. Denis, V. Dumarcher, C. Fiorini-Debuisschert, K.P. Kretsch, L. Rocha, *Opt. Mat* **27**, 199-201(2004).
81. K. Geetha, M. Rajesh, V.P.N. Nampoori, C.P.G. Vallabhan, P. Radhakrishnan, *J.Opt. A : Pure Appl. Opt* **8**,189-193 (2006)
82. T. Kobayashi, J. Savatier, G. Jordan, W.J. Blau, Y. Suzuki, T. Kaino, *Appl. Phys. Lett* **85** (2), 185-187 (2004).
83. Michael D. McGehee, Rahul Gupta, Siegfried Veenstra, E. Kirk Miller, Maria A. Diaz-Garcia, Alan J. Heeger, *Phys. Rev. B* **58** (11), 7035-7039 (1998).
84. A. K. Sheridan, G.A. Turnbull, A.N. Safonov, I.D.W. Samuel, *Phys. Rev. B* **62**(18), R11 929-R11 932 (2000).
85. A. Schülzgen, Ch. Spiegelberg, M.M. Morrell, S.B. Mendes, B. Kippelen, N. Peyghambarian, M.F. Nabor, E.A. Mash, P.M. Allemand, *Appl. Phys. Lett* **72**(3), 269-271 (1998).
86. C. Zenz, W. Graupner, S. Tasch, G. Leising, K. Müllen, U. Scherf, *Appl. Phys. Lett* **71**(18), 2566-2568 (1997).
87. S.V. Frolov, Z.V. Vardeny, K. Yoshino, A. Zakhidov, R.H. Baughman, *Phys. Rev. B* **59** (8), R5284-R5287 (1999).
88. N. Tsutsumi, T. Kawahira, W. Sakai, *Appl. Phys. Lett* **83**(13), 2533-2535 (2003).
89. T. Tsutsui, N. Takada, S. Saito, *Appl. Phys. Lett* **65**, 1869-1871 (1994).
90. N. Tessler, G.J. Denton, R.H. Friend, *Nature* **382**(22), 695-697(1996).
91. H. Becker, R.H. Friend, T. D. Wilkinson, *Appl. Phys. Lett* **72**(11), 1266-1268(1998).

92. H.P. Weber, R. Ulrich, *Appl. Phys. Lett* **19**, 38-40 (1971).
93. M. Kuwata-Gonokami, R.H. Jordan, A. Dobalapur, H.E. Katz, M.L.Schilling, R.E. Slusher, S. Ozawa, *Opt. Lett* **20**(20), 2093-2095(1995).
94. S.V. Frolov, Z.V. Vardeny, K. Yoshino, *Appl. Phys. Lett* **72**(15), 1802-1804 (1998).
95. S. John, *Phys. Rev. Lett*. **58**, 2486 (1987).
96. E. Yablonovitch, *Phys. Rev. Lett*. **58**, 2059 (1987).
97. S. Fan, P. R. Villeneuve, J. D. Joannopoulos, H. A. Haus, *Phys. Rev. Lett*. **80**, 960 (1998).
98. A. Yariv, Y. Xu, R. K. Lee, and A. Scherer, *Opt. Lett*. **24**, 711 (1999).
99. K. Busch and S. John, *Phys. Rev. Lett*. **83**, 967 (1999).
100. S. S. Lee *et al.*, *IEEE J. Quantum Electron*. **36**, 527 (2000).
101. R. R. Panepucci, B. H. Kim, V. R. Almeida, M. D. Jones, *J. Vac. Sci. Technol. B* **22**(6), 3348-3351(2004).
102. C. Liguda, G. Böttger, A. Kuligk, R. Blum,M. Eich, H. Roth, J. Kunert, W. Morgenroth, H. Elsner, H. G. Meyer, *Appl. Phys. Lett* **78**(17), 2434-2436(2001)
103. R.F. Cregan, B.J. Mangan, J.C. Knight, T.A. Birks, P.St. J. Russel, P.J. Roberts, D.C. Allan, *Science* **285,** 1537-1539 (1999).
104. M. A. van Eijkelenborg, M.C.J. Large, A. Argyros, J. Zagari, S. Manos, N.A. Issa, I. Bassett, S. Fleming, R.C. McPhedran, C.M. de Sterke, N.A.P. Nicorovici, *Opt. Express* **9**(7), 319-327 (2001).
105. M. A. van Eijkelenborg, A. Argyros, G. Barton, I.M. Bassett, M. Fellew, G. Henry, N.A. Issa, M.C.J. Large, S. Manos, W. Padden, L.Poladian, J. Zagari, *Opt. Fiber Technol*. **9**, 199-209 (2003).
106. A. Argyros, M. A. van Eijkelenborg, S. D. Jackson, R.P. Mildren, *Opt. Lett* **29**(16), 1882-1884 (2004).

2

Development of a side polished polymer optical fibre refractometer

The design, fabrication and characterization of a fibre refractometer using a side polished polymer fibre which has got a wide dynamic range are discussed. Following a ray optics approach to multimode fibres, a theoretical model was developed for understanding the sensor performance for various launching angles to the fibre. Experimental details are given in the second section. The experimental results are explained on the basis of theoretical calculations.

2.1 Introduction

Precise measurement of refractive index of transparent liquids is very important in modern industry. Bio-sensing, testing adulteration in food, medicines, fuels, oil and beverages are some of the areas where refractometers find application. Traditional methods for determining the refractive index of liquids include spectrometry (using hollow prism), Abbe refractometer, prism coupling technique etc.[1-3]. All the above mentioned techniques involve bulk components which make them inconvenient in remote sensing as well as in situations where the quantity of the test sample is small.

Fibre optic sensors offer many advantages over the conventional sensing mechanisms. Their miniature size, low cost, ease of installation, high immunity to electromagnetic interference and high sensitivity make fibre based sensors promising candidates for remote sensing. Due to these reasons, considerable interest has been directed towards the development of various fibre optic sensors among which fiber optic refractive index sensors find importance in sensor technology. Takeo et al [4] had proposed a refractive index sensor in which a plastic clad silica fibre bent in the form of a U-shape with a section of cladding removed acts as the sensing region. Sensitive refractometers based on tapered fibres and microbent fibres have also been reported [5-7]. Fiber grating sensors [8] and fibre optic surface plasmon resonance sensors have been evolved as highly sensitive refractometric devices, which find great deal of application as bio-sensors [9-12].

Side polished optical fibres have long been used for the fabrication of fibre sensors and other devices such as couplers, polarisers, filters etc [13-17]. The main advantage of the side-polished fibre sensor is that it requires only a

very small amount of the analyte .The device fabrication becomes much easier with polymer optical fibers(POF) in comparison with glass fibres. Moreover, the use of plastic fibre make the device more economic too, especially in situations where throw-away sensors are to be used. Recently, sensors based on large diameter plastic fibres for bio-film growth measurement [18,19] humidity monitoring [20], alcohol detection [21] and strain measurements [22] have been reported. In literature only a few reports are available on the application of POF as refractive index sensors, where the sensing element is a side-polished polymer fibre[23-25]. The previously reported side-polished POF sensors had response for the refractive indices of only a narrow range lying between that of cladding and core. Moreover, for low refractive indices, these sensors showed poor response.

We aimed at the design and fabrication of a side polished POF refractive index sensor with a wide dynamic measuring range and the details are given in this chapter. This chapter has two sections. The first section has the details of the simulation and experimental details are given in the second section.

2.2 Theoretical Modeling

2.2.1 Light transmission loss through side polished POF – Ray approach

In order to study the transmission losses in the sensing region, we followed a simple intuitive approach similar to the one developed by Yi-Zhen Lin et al [26] to analyze the light transmission in leaky and absorbing planar waveguides.

For a multimode fibre, the transmission losses can be analyzed by applying ray theory. The general principle of waveguide refractive index sensor is

based on the Fresnel's reflection and transmission coefficients at the interface between two media.

In a side polished fibre (SPF), the cylindrical symmetry is altered by polishing it in a longitudinal plane, thereby proportioning a very sensitive region within the fibre. Due to such side polished geometry, the sensing region takes the form of a planar structure. The intensity of the propagating electro magnetic field can be perturbed by the external medium lying close to the polished surface.

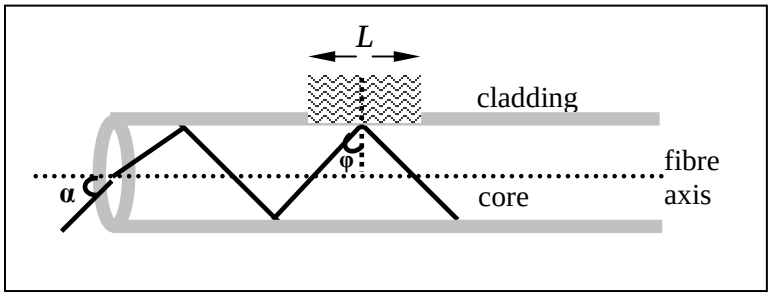

Fig 2.1. Schematic of the relevant section of the refractive index sensor

To obtain the net power transmission of the incident ray in the sensing region, we have to find the number of reflections at the core-external medium interface. The number of bouncings m of the ray at the interface within the distance L is given as

$$m \approx \frac{L}{d \tan \varphi} \qquad \ldots\ldots(2.1)$$

where d is the core diameter and φ is the angle that the incident ray makes with the normal at the core-cladding interface. (see Figure 2.1)

If I_0 is the power launched into the fiber, then the output power after propagation through the sensing region is ,

$$I \approx I_0 R^m \qquad \text{……(2.2)}$$

where $R = |r|^2$ and r is the Fresnel's coefficient of reflection.

In our model, we do not consider any specific polarization state of the incident light beam and 'r' is the coefficient of reflection for an arbitrary polarization. From Fresnel's reflection, the general behaviour of the sensor can be explained as follows. Liquids having refractive indices much lower than that of the core, yield the same maximum output power since all the rays undergo total internal reflection. As the refractive index of the liquid approaches the core refractive index, the output power decreases sharply. For refractive indices larger than the core, the output intensity shows only slow increase. The problem with this design is that the sensitivity is very poor for refractive indices which are much smaller than the core refractive index[23,24] and this sets a limit to the operating range of the sensor.

In order to improve the performance at the low refractive index region, we studied the effect of the launching angle and fibre geometry. The theoretical analysis on how these parameters could improve the sensor performance is discussed in the following sections.

2.2.2. Performance of the sensor with launching angle as the varying parameter

2.2.2.1 *Case (i): Straight fibre*

As inferred from equation (2.2), we see that the sensor response to the refractive index of the cladding material depends on both reflectance at the core-cladding interface and the number of reflections in the sensing region. These two parameters depend on φ - the angle which the ray incident at the core-cladding interface makes with the normal, which in turn is determined by the launching angle α (fig 2.1). Applying Snell's law and Fresnel's reflection coefficients in

equation(2.2), we can simulate the dependence of sensor response on the launching angle.

Figure 2.2 shows the power loss through the fibre for different cladding refractive indices at different launching angles. The simulated results are for the fibre parameters, n_{core} = 1.49, d =0.980 mm, and L = 2 cm .

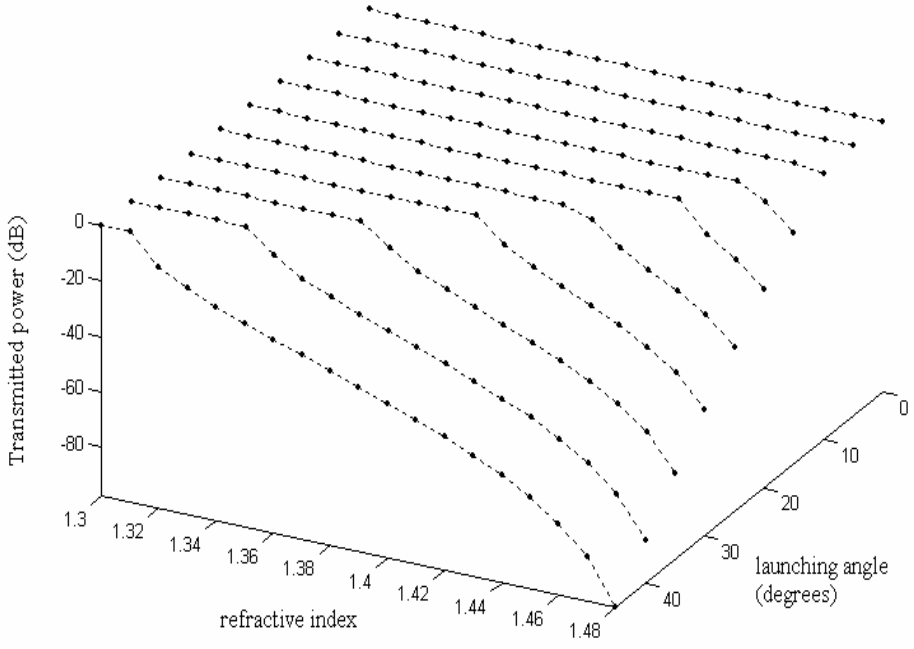

Fig 2.2 Simulation of transmission characteristics in straight fibre for different launching angles α varying between 0^0 to 30^0

We observe that the sensing range of refractive index strongly depends on the launching angle α. At smaller launching angles, the sensor has no response in the low-refractive index region. As α increases, the sensitivity at the low refractive index region increases, thereby increasing the sensing range. From fig 2.2, we can infer that for a fibre with numerical aperture (NA) 0.5,

maximum sensing range is obtained for $\alpha=30^0$, which corresponds to the acceptance angle of this fibre. Increasing the launching angle (α), further will enhance the sensing range which implies that POFs with larger numerical aperture can be employed for a wide dynamic range of refractive index measurement. For large values of α, the corresponding angle φ will be less than the critical angle for the core-liquid interface, even for lower values of n_{liq}. This simply means that higher order modes (those corresponding to larger α) fail to satisfy the guiding condition , even for small values of n_{liq} and leak to the cladding liquid, while lower order modes will satisfy the guiding condition for all values of $n_{liq} < n_{core}$.

2.2.2.2 ***Case (ii): Bent fibre***

In the case of a straight fiber, the incident angle (at the core-cladding interface) of a guided ray launched into the fiber remains the same in the sensing region. Thus for a given launching angle, the value of φ remains the same for the whole probe region and hence gives fixed values for the number of reflections at the core-cladding interface (m) and reflection coefficient (r) for a particular value of the refractive index of the cladding. Therefore for a given fibre with a specific launching angle, a decrease in the value of φ causes increase in m and decrease in r, thereby increasing the transmission loss through the sensor. In the case of a bent fibre, as the ray enters the bent region , the angle that the ray makes with the normal to the core-cladding interface at the outer surface of the bent region decreases [27] as seen in fig(2.3).

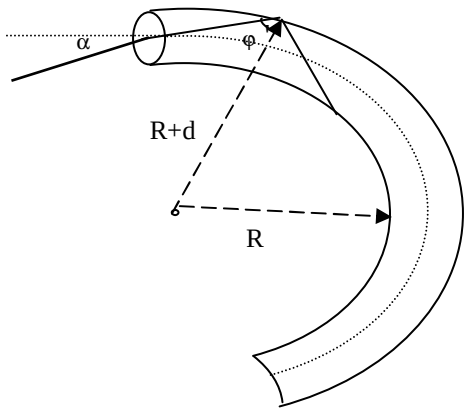

Fig 2.3 Propagation of meridional ray along a curved fibre showing the relevant parameters

Considering only meridional rays, the angle φ' for the bent region is given by

$$\varphi' = \sin^{-1}(K\sin\varphi) \qquad \ldots\ldots(2.3)$$

with $K = \dfrac{(R+h)}{(R+d)}$ where d is the core diameter, R is the bending radius, h is the distance at which the ray is incident on the entrance of the bent section of the fibre from the core-cladding boundary ($0 \le h \le d$) . [27]

When K=1, equation (2.3) reduces to that for a straight fibre. The sensitivity of the device for a particular cladding refractive index depends on the value of K and φ. A decrease in the value of K and φ increases the power loss through the sensing region. The value of K can be lowered by decreasing the bend radius R.

We have already seen in the case of straight fibres with NA=0.5 that the sensing range is maximum for a launching angle of 30^0. Keeping α as 30^0 , the transmission loss for bent fibres for different values of K can be simulated. (fig 2.4)

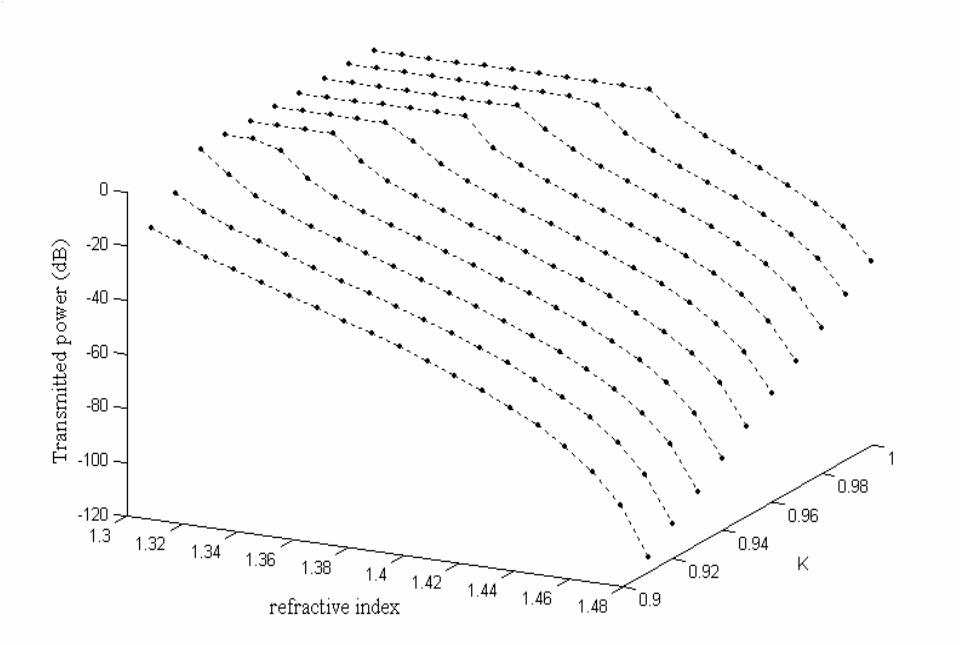

Fig 2.4 Simulation of transmission characterisitics for bent fibres with launching angle 30^0

As is clear from fig 2.4, by decreasing K, sensor response at lower refractive index region gets improved. We see that with a suitable combination of launching angle and bent radius, the operating range can be tuned as per our requirements.

2.3 Fabrication of sensor head

The optical fibre used in the experiment was a standard commercial step index polymer optical fibre (POF) with a polymethylmethacrylate (PMMA) core of diameter 0.980mm surrounded by a thin cladding layer of fluorinated polymer. The core refractive index (n_{core}) was 1.49 and the numerical aperture was 0.5. For side polishing, fibres are usually held in a host-block as protection which allows polishing and prevents the fibre from breaking. The host materials commonly used for this purpose are fused silica, etched silicon V-grooves and epoxy resins [13,28,29]. A small length (about 10 cm) of the fibre was inserted into a curved metallic frame bent to a radius of 2 cm and the whole piece was encapsulated in a block of resin. From the top side, the sheath was removed from a small length (2 cm) of the fibre and was polished until the core region was exposed. Polishing was done using silicon carbide powder and alumina powder of two different grades (0.3μ and 0.05μ) . A small cuvette was also attached to the resin block (Fig 2.5)

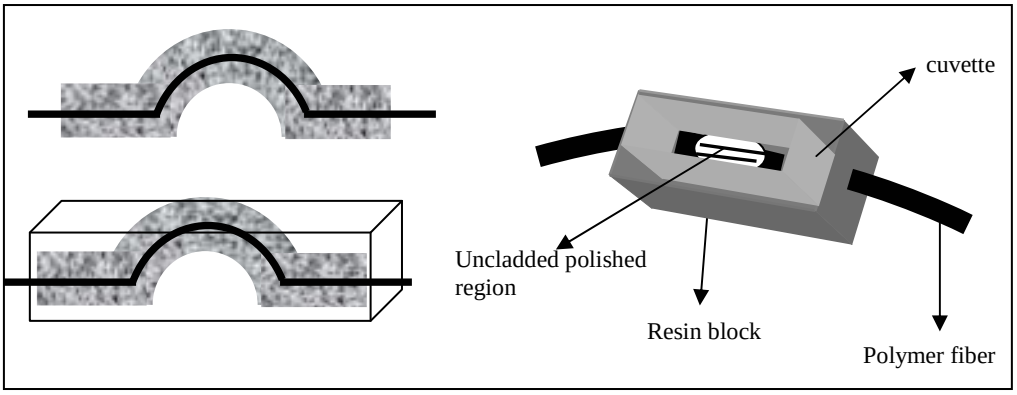

Fig 2.5 Side Polished POF sensing element

2.4 Experimental Results and Discussion

We have seen that bent fibres are more sensitive than straight ones, so experiments were conducted with bent fibre sensor head. Freshly prepared sucrose solutions with known refractive indices were poured into the cuvette so as to cover the unclad portion. The height of the liquid level is an important parameter which affects the power loss in the sensing region. When a very thin layer of liquid is taken, the rays reflected at the liquid-air interface will go back to the core. However, when the thickness of the liquid layer is increased to a certain level, the reflected rays at the liquid-air interface no longer enter the core, thereby causing greater power loss than in the case with thin cladding layer. Beyond this level, the output power remains constant even with further increase in the liquid layer thickness.

The device can be developed by either forming a very thin layer of liquid cladding (by adding a few drops of liquid on the polished section) or by forming a thick layer of liquid cladding over the polished section. When working with very thin liquid layers, the level height should be accurately measured and should be maintained for all sets of measurements, which make the device more complicated. Therefore the latter method was used for the present studies. We have carried out the experiments with liquid layer thickness of 1mm. The analyte volume required for this arrangement was only less than 0.5 ml. The temperature of the sample solutions were maintained at 20^0C.

As inferred from our theoretical model sensing range increases for higher launching angles to the fibre. In order to tune the range of the sensor to our requirements a selective excitation at higher launching angles was done. For this, the laser source was mounted on a precision rotation stage so as to change

the launching angle into the fibre. Schematic of the experimental setup is given in fig (2.6).

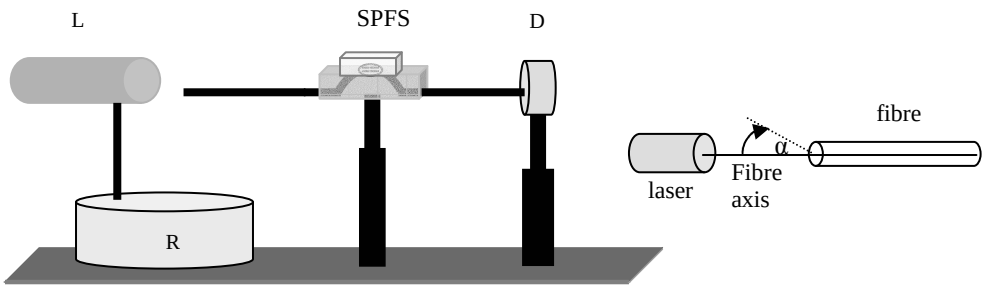

Fig 2.6 Experimental setup for refractive index measurements L – He-Ne laser(632.8 nm), R- rotation stage, SPFS- side polished fibre sensor, D-detector (Newport -818-SL)

A parallel beam of light from a He-Ne laser (632.8 nm) was incident on the fibre tip which is positioned to be always at the centre of the precision rotator so as to facilitate accurate angle measurement. The light transmitted through the sensor was coupled to a Si detector(New Port 818-SL) with a power meter (Newport 1815C). The transmission output of the sensor was normalized to that in air.

The sensor output for different launching angles is shown in fig(2.7). There is fairly good agreement between the theory and experimentally obtained results, especially in the tuning of the sensing range by varying launching angle.

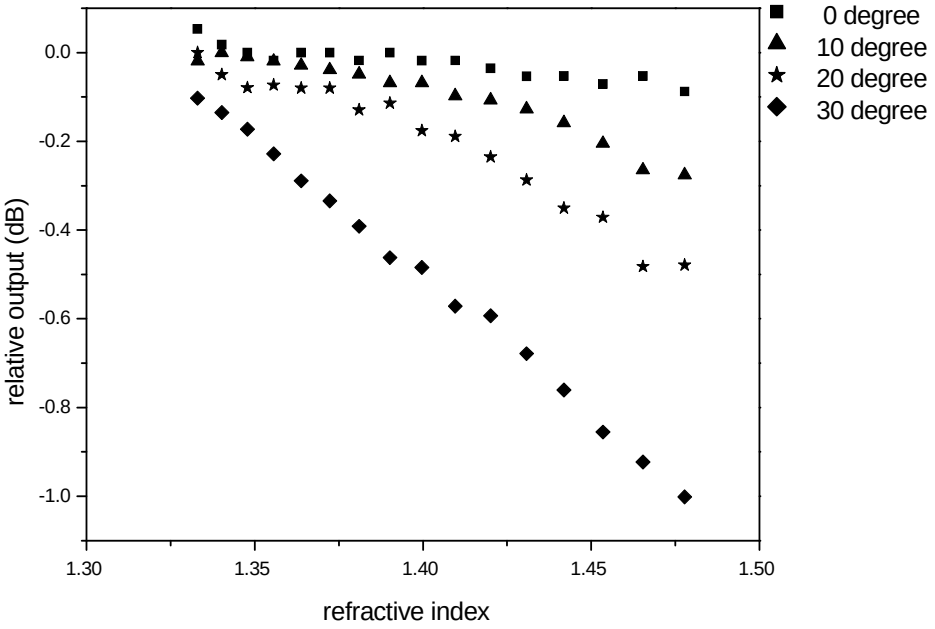

Fig 2.7 Sensor response for various launching angles. Accuracy of data points are better than 0.4%

We can see that the operating range of the sensor increases with the launching angle (see Table 2.1) which can be well explained on the basis of our theoretical model described in the previous sections. For $\alpha=30^0$, we get the maximum sensing range 1.333 – 1.477 refractive index units(RIU) and maximum sensitivity -6.219 dB/RIU.

Launching angle (α)	Sensing range	Sensitivity dB/RIU
0^0	1.390-1.477	-0.876(1)
10^0	1.390-1.477	-2.587(2)
20^0	1.372-1.477	-4.044(2)
30^0	1.333-1.477	-6.219(2)

Table 2.1 Sensitivity and measuring range of the sensor for various launching angles

Experimentally observed results show an increase in sensitivity in the whole sensing range with increasing α, unlike in the case of theoretically obtained results (see fig 2.4 and fig 2.7). This deviation of experimental results from the theoretically predicted behaviour may be attributed to the fact that , we have considered only meridional rays in our theoretical model. In practice, a multimode fibre supports a large number of skew rays also. When a parallel beam of light is incident on the fibre, a large number of skew rays will be propagated through the fibre. The number of reflections they undergo at the sensing region is greater than that of the meridional rays [11]. The path length, number of reflections and effective numerical aperture of skew rays can be significantly different from those of the meridional rays even in a straight fibre [30]. In curved and conical fibres, skew ray propagation is even more complex and predominant. As the angle of launching increases, the fibre supports more skew rays than the meridional rays. Therefore, the contribution to the reflection loss from skew rays increases with the launching angle, thereby increasing the sensitivity.

The temporal response of the sensor for various analyte refractive indices is given in fig 2.8.

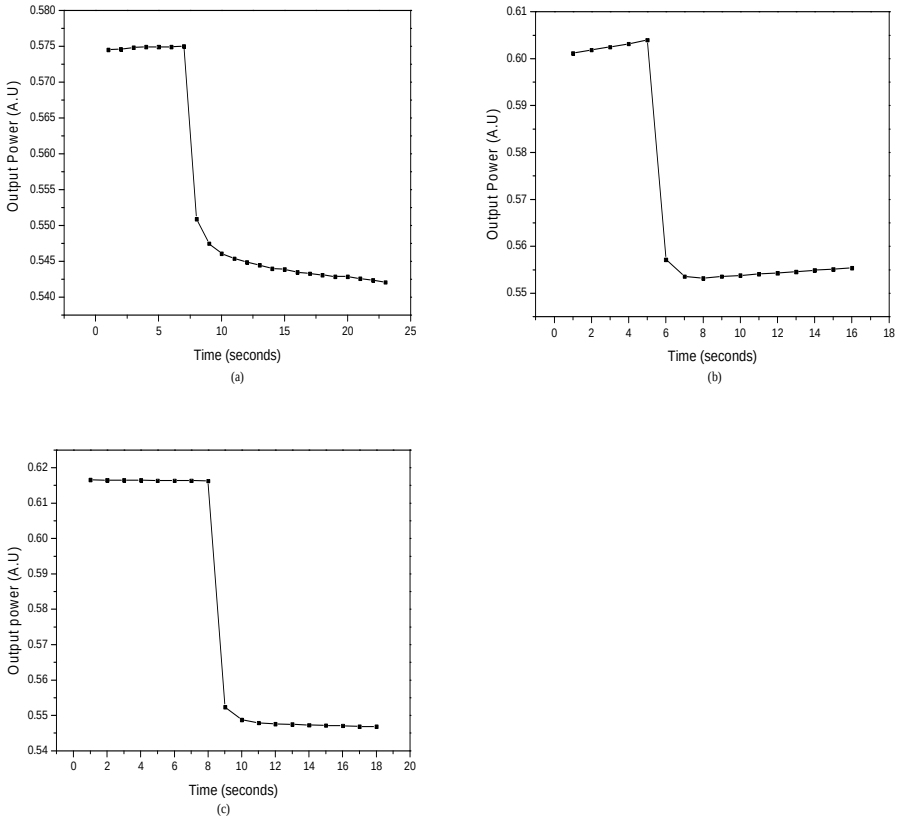

Fig 2.8 Temporal response of the sensor for cladding liquid refractive indices (a) 1.333 (b) 1.420 (c) 1.465

The data acquisition was done by interfacing the detector with a PC using Labview 7.0. The temporal response of the sensor was found to be less than 1 second, which is limited by the sampling rate of the detecting scheme. The response time for the refractive indices within the operating range was found to be almost the same.

The proposed sensor can be made cost effective by using LED as the light source. The low cost, simplicity, miniature size and compact nature make the present refractometer more attractive for various industrial applications. The sensitivity and sensing range can be tuned to our requirements by appropriately adjusting the launching angle and curvature of the fibre. With this device, only less than 0.5 ml sample is required for sensing and hence it is suitable for measurements when the available quantity of the analyte is very small.

2.5 Conclusions

We have presented a refractive-index sensor exhibiting a wide dynamic range using side polished polymer optical fibres. A novel method for tuning the sensitivity and sensing range by selective excitation at higher launching angles in a bent fibre has been discussed. For a slightly bent polymer optical fibre with numerical aperture 0.5, maximum sensitivity and sensing range was obtained for the excitation with a parallel beam of light, launched at an angle 30^0 with respect to the fibre axis. The response time of the sensor was found to be less than 1 second. Since the quantity of sample required for the present sensing mechanism is very less (about 0.5 ml), one can effectively employ this sensor for bio-sensing applications and other cases where the amount of the samples available is very small.

References

1. Hiroshi Yoshimura, *J. Phys .E : Sci. Instrum,* **21,** 571-578 (1988).
2. G. H. Meeten, A. N. North , *Meas. Sci. Technol,* **2**, 441-447 (1991).
3. G. H. Meeten, A.N. North, *Meas. Sci. Technol* **6**, 214-221(1995) .
4. T. Takeo, H. Hattori, *Jpn.J.Appl.Phys* **21**(10), 1509-1512 (1982).

5. A. Kumar, T.V.B. Subrahmoniam, A.D. Sharma, K. Thyagarajan, B.P. Pal, I.C. Goyal, *Electron. Letts* **20,** 534-35 (1984).
6. J. Villatoro, D. Monzon-Hernandez and D. Talavera, *Electron.Lett* **40**(2), 106-07(2004).
7. Thomas Lee S, P. Sureshkumar, K. Geetha, P. Radhakrishnan, C.P.G. Vallabhan and V.P.N. Nampoori, *Proceedings of SPIE- International Society for Optical Engineering*, **4920** (2002).
8. Kerstin Schroeder, Wolfgang Ecke, Rudolf Mueller, Reinhardt Willsch and Andrey Andreev, *Meas. Sci. Technol* **12,** 757-764(2001) .
9. C. Ronot-Trioli, A. Trouillet, C. Veillas, H. Gagnaire, *Sensors and Actuators A* **54,** 589-593 (1996) .
10. Radan Slavik, Jiří Homola, Jiří Čtyroký, *Sensors and Actuators B* **54** , 74-79 (1999).
11. A. Trouillet, C. Ronot-Trioli, C.Veillas and H. Gagnaire, *Pure Appl.Opt* **5**, 227-237 (1996) .
12. M. Mitsushio, S. Higashi, M.Higo, *Sensors and Actuators A* **111,** 252-259 (2004).
13. S. M.Tseng and C.L.Chen, *Appl. Opt.* **31**(18), 3438-47(1992).
14. Ainhoa Gaston, Ibon Lozano, Fatima Perez, Fernando Auza, Joaquin Sevilla, *IEEE Sensors Journal* **3**(6), 806-810 (2003)
15. Kyung-Rak Sohn, Kwang-Taek Kim, Jae-Won Song, *Sensors and Actuators A* **101**, 137-142 (2002).
16. S. Lee, J. Sokoloff, B. McGinnis, and H. Sasabe, *Appl. Opt.* **37**, 453-462 (1998).
17. N. Chen, S. Chi, and S. Tseng, *Opt. Lett.* **29**, 2219-2221 (2004).
18. R. Philip Chandy, P.J. Scully, P. Eldridge, H.J. Kadim, M. Gérard Grapin, M.G. Jonca, M. Gérard D'Ambrosio and F. Colin, *IEEE J. on Selected topics in Quantum Electronics*, **6**(5), 764-772 (2000) .
19. R. Philip Chandy, P.J. Scully and D. Thomas, *Sensors and Actuators B* **71,** 19-23 (2000).
20. Shinzo Muto, Osamu Suzuki, Takashi Amano, Masayuki Morisawa, *Meas. Sci. Technol.* **14**, 746-750(2003).
21. M. Morisawa, Y. Amemiya, H. Kohzn, C. Xin Liang and S. Muto, *Meas. Sci. Technol* **12**, 877-881(2001) .
22. K.S.C. Kuang, W.J. Cantwell, P.J. Scully, *Meas. Sci. Technol.* **13**, 1523-1534 (2002).
23. Joseba Zubia, G. Garitaonaindiá and Jon Arrúe, *Appl. Optics* **39**(6), 941-946 (2000).
24. R.M. Ribeiro, João L.P. Canedo, Marcelo M. Werneck, Liliana R. Kawase, *Sensors and Actuators A* **101,** 69-76(2002)
25. M. Sheeba, M. Rajesh, C.P.G. Vallabhan, V.P.N. Nampoori , P. Radhakrishnan, *Meas. Sci. Technol* **16**, 2247-2250 (2005).
26. Yi-Zhen Lin, Jing-Hong Zhan, Shiao-Min Tseng, *IEEE Photonics Tech. Lett.* **9**(9), 1241-1243 (1997)

27. B. D. Gupta, H. Dodeja, A.K. Tomar, *Opt. Quantum Electron* **28**, 1629-39, (1996) .
28. R. Alonso, F. Villuendas, J. Tomos and J.Pelayo, *Sens and Actuators A* **37-38**, 87-192 (1993).
29. Javier Senosiain, Idoya Diaz, Ainhoa Gaston and Joaquin Sevilla, *IEEE Trans on Instrumentation and Measurement* **50**(6), 1656-1660 (2001).
30. N.S. Kapany, Fibre Optics – Principles and Applications, Academic Press, NewYork (1967)

Side polished polymer optical fibre based chemical sensor

An evanescent wave absorption sensor for chemical reaction rate measurements is discussed. A theoretical study of the effect of a high refractive index overlay on the exposed core region of the fibre, on the evanescent wave absorption is presented. Experiments were also performed for studying the reaction kinetics of a standard chemical reaction.

3.1 Introduction

During the past two decades, there has been a rapid growth in research and development activities of fibre optic chemical sensors employing a number of different strategies. The most popular among them are the absorption-based and fluorescence based systems. In the absorption based system, the sensing fibre uses the evanescent field extending from the core so as to interact with the chemical species [1-5]. This technique is of particular interest for it allows the development of distributed sensor systems. Fluorescence based systems also rely on absorption, but the sensing is performed by monitoring changes in the intensity or lifetime of the fluorescent light generated by the species or an intermediate dye [6,7]. It should be noted that the waveguide design plays a crucial role in optimizing the sensor performance.

One of the new techniques in the design of fibre optic sensors is the usage of side polished fibres. Compact side polished fibre sensors are being deployed in various industrial and medical markets. Sensors based on side polished fibres for measuring various physical and chemical parameters such as pressure, temperature, humidity, refractive index and pH have been reported in the recent years[8-12]. Side polished fibres have also been used to develop devices such as couplers, power monitors, filters and polarisers.[13,14].

Advantages of fibre optic sensors over commercially available conventional sensors are many. However, from the applicability viewpoint, more attention should be paid over certain key parameters such as cost, size and sensitivity. In order to compete with the existing devices, novel fabrication techniques, well suited for industrialization, have to be developed. The successful design of such a device requires a thorough knowledge of the transmission loss

characteristics through the sensor. Designing and optimizing the functions of these devices can be made through numerical modeling as well as analytical techniques.

This chapter deals with a theoretical study on the effect of a high refractive index overlay on the sensitivity of an absorption sensor based on side polished polymer optical fibre. Experimental verification was also performed, by applying this sensor to study the reaction rate of a standard chemical reaction.

3.2 Complex refractive index and absorption

In order to model waveguide sensors, the absorption of a chemical species at a given wavelength must be expressed in terms of a complex refractive index. The relation between the quantities $\in$ (molar extinction coefficient) or α_m (molar absorption coefficient) and the complex refractive index $n - jk$ are [15],

$$k = 0.183 \in C\lambda = \frac{\alpha_m C\lambda}{4\pi} \qquad \ldots\ldots (3.1)$$

where C is the concentration of the chemical species and λ is the wavelength .

For a chemical species with large extinction coefficients or in high concentrations, the real part of the refractive index (n) will also vary with the solute concentration. In an optical waveguide or fibre sensor, changes in k produce changes in the attenuation of the guided modes, that can be taken as a measure of the sensitivity of the sensor. Small changes in the real part of the index of the chemical species with concentration will affect the real part of the propagation constant of the modes, but since this change is generally small

compared to the real component itself, it has negligible effect on the attenuation measurement.

3.3 Total internal reflection and Evanescent field

According to geometrical optics, as a light ray get total internally reflected, the transmittance in the second medium is zero, implying that there is no penetration of light in the second medium.

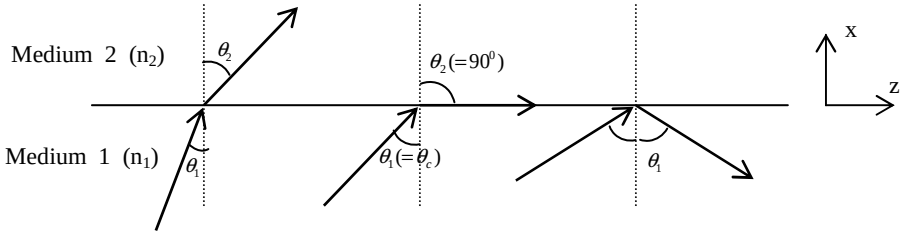

Fig 3.1 Light incident on an interface between two media – refraction and total internal reflection

In order to fully understand the phenomenon taking place at the dielectric interface we should follow an electromagnetic treatment of the interface problem[16].

For a uniform dielectric, the time independent wave equation is

$$\nabla^2 \mathbf{E} + n^2 k_0^2 \mathbf{E} = 0 \qquad \text{..... (3.2)}$$

For TE incidence at angle θ_1, the above equation becomes

$$\frac{\partial^2 E_y}{\partial x^2} + \frac{\partial^2 E_y}{\partial z^2} + n^2 k_0^2 E_y = 0 \qquad \text{.....(3.3)}$$

First considering the case of ordinary refraction, the field in each medium is written as

$$E_{y1} = E_1 \exp\left[-jk_0 n_1 \left(z\sin\theta_1 - x\cos\theta_1\right)\right] + E_R \exp\left[-jk_0 n_1 \left(z\sin\theta_1 + x\cos\theta_1\right)\right] \quad \text{.....(3.4.a)}$$

$$E_{y2} = E_T \exp\left[-jk_0 n_2 \left(z\sin\theta_2 - x\cos\theta_2\right)\right] \quad \text{.....(3.4.b)}$$

Now consider the case when the input beam is incident at an angle greater than critical angle. i.e., $\theta_1 > \theta_c$. When total internal reflection occurs, a propagating wave cannot arise in medium 2. The Snell's law $n_1 \sin\theta_1 = n_2 \sin\theta_2$ cannot be satisfied or rather cannot be satisfied with a real value of θ_2 . We can satisfy it only with a complex value of θ_2 such that

$$\cos\theta_2 = \pm j\sqrt{\left(\frac{n_1}{n_2}\right)^2 \sin^2\theta_1 - 1} \quad \text{.....(3.5)}$$

Using equation (3.5) in (3.4.b)

$$E_{y2} = E_T \exp\left[\pm k_0 n_2 x\sqrt{\left(\frac{n_1}{n_2}\right)^2 \sin^2\theta_1 - 1}\right] \exp\left(-jk_0 n_1 z\sin\theta_1\right) \quad \text{.....(3.6)}$$

Defining new parameters

$$\beta = k_0 n_1 \sin\theta_1, \kappa = \sqrt{n_1^2 k_0^2 - \beta^2}, \gamma = \sqrt{\beta^2 - n_2^2 k_0^2} \quad \text{.....(3.7)}$$

We write,

$$E_{y2} = E_T \exp\left(-\gamma x\right)\exp\left(-j\beta z\right) \quad \text{.....(3.8)}$$

The solution no longer has the form of a plane wave propagating at an angle θ_2, because its x dependence is not a complex exponential. Instead it is a wave whose amplitude distribution varies exponentially in the x-direction and that propagates along the interface in the z-direction. This is called ***evanescent wave***.

A field of this type stores energy and transports it in the direction of propagation (z) but does not transport energy in the transverse direction (Fig 3.2).

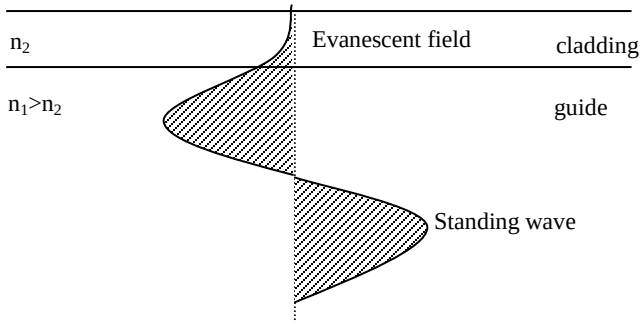

Fig 3.2 The exponentially decaying evanescent field in the cladding of the optical waveguide

The phase shift occurring on total internal reflection is given by $\tan\Phi = \frac{\gamma}{\kappa}$ for TE incidence and $\tan\Phi = \left(\frac{n_1^2}{n_2^2}\right)\frac{\gamma}{\kappa}$ for TM incidence.

This phase change is physically understood by the lateral shift of the reflected beam from the trajectory predicted by simple ray theory analysis (Fig 3.3). This lateral displacement is called ***Goos-Haenchen shift***.

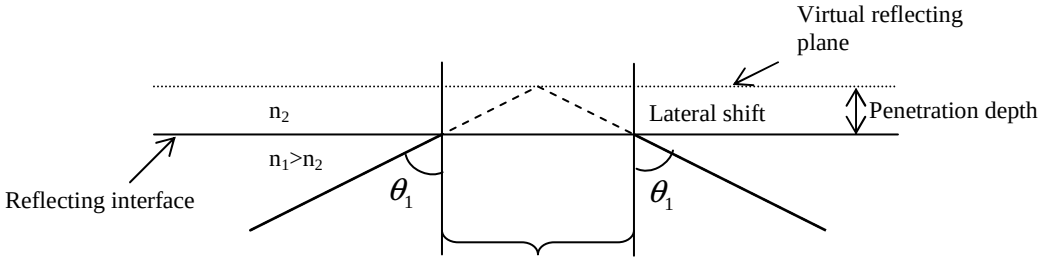

Fig 3.3 The lateral displacement of a light beam on reflection at a dielectric interface (Goos-Haenchen shift)

The geometric reflection appears to take place at a virtual reflecting plane, which is parallel to the dielectric interface, in the lower index medium.

If the lower-index region contains an absorbing chemical species ($n_2 = n - jk$), then the reflection coefficient of the ray is less than unity owing to *evanescent wave absorption.* In a waveguide/fiber, the evanescent wave interacts with the chemical species surrounding the core region where the cladding is being removed, giving rise to a phenomenon called *Attenuated Total Reflection (ATR).* The amount of the absorption depends on both the amplitude of the evanescent field in the low index medium and the number of reflections at the interface. The former increases dramatically for incident angles approaching the critical angle and the latter is inversely proportional to the waveguide thickness.

3.4 Ray optics approach to side polished fibre absorption sensor

The ray optics approach is the simplest way of calculating the attenuation of a guided wave caused by an absorbing species in the cladding region [15,17]. Consider a side polished fibre with core refractive index n_1 and cladding index n_2. In a side polished fibre (SPF), the cylindrical symmetry of the fibre is altered via polishing in a longitudinal plane and the sensing region takes the form of a planar structure. The intensity of the propagating electro magnetic field can be perturbed by the external medium lying onto the polished surface. Light transmission through the sensing region can be studied using ray optics approach for a multimode planar waveguide.

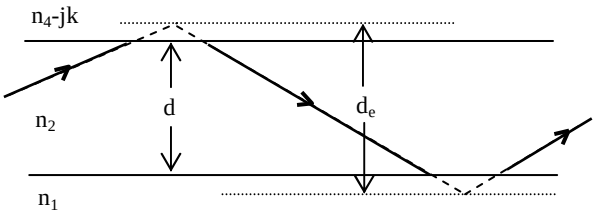

Fig 3.4 Side polished fibre with an absorbing liquid at the unclad portion

Let the lossy liquid be of a refractive index $n_4 - jk$. If the ray trajectory incident at an angle θ_1 makes n reflections per unit length at the guiding layer - lossy liquid boundary, then the attenuation of the guided wave due to the chemical absorption is given by [15,17]

$$\frac{P_0}{P_1} = \left(|r|^2\right)^n \qquad \ldots\ldots(3.9)$$

where P_0 and P_1 are the output and input powers and r is the reflection coefficient of the ray at the guide-liquid interface.

The sensing region shown in fig 3.4 has got an asymmetric planar waveguide structure. For such a structure, with the absorbing liquid on one side only, the number of reflections per unit length is given by [15,17]

$$n = \frac{1}{2d_e \tan\theta_1} \qquad \ldots\ldots(3.10)$$

where the parameter d_e is the effective thickness corresponding to the mode.

$d_e = d + d' + d''$ where d' and d'' are evanescent field penetration depths in the cladding and the absorbing liquid respectively.

The power loss in dB is then given by [15,17]

$$\text{Loss} = -4.343n(\ln|r|^2) \qquad \ldots\ldots..(3.11)$$

Fig 3.5 shows the attenuation curve at wavelength 632.8 nm for a side-polished fibre surrounded by an absorbing liquid with $n_4 = 1.33$ and $k = 2.161x10^{-6}$. The fibre has a core diameter 0.980 mm and refractive index 1.49. The curve is plotted against the effective index $\beta = n_2 \sin\theta_1$.

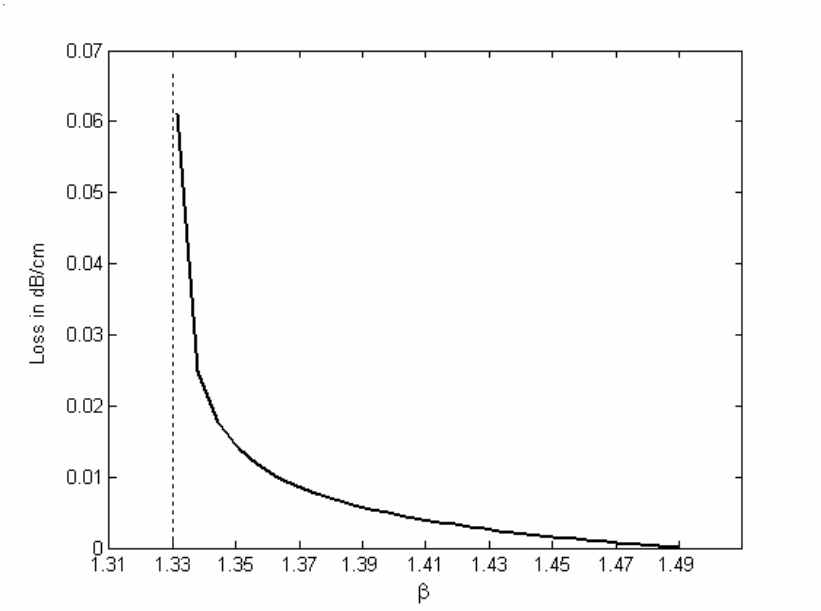

Fig 3.5 Attenuation versus effective index for side polished fibre surrounded with an absorbing liquid with refractive index 1.33-j2.161x10^{-6}

The highest sensitivity occurs for rays near cutoff ($\beta \approx n_4$) where the evanescent field is very large. A particular problem associated with achieving significant evanescent field penetration in the sensing region is that the lead fibre numerical aperture is considerably less than that in the core-liquid region. Consequently it is impossible to launch bound rays which would be incident on the core-liquid interface at angles close to the critical angle. By virtue of its cylindrical geometry a fibre will sustain nonbound or tunneling modes which are

launched into the fibre at angles greater than that the meridional numerical aperture permits [18]. Higher order modes can be generated at the sensing region by tapering the fiber at this location [19,20] or by bending [2,21]. A selective excitation of higher order modes can also be done by changing the launching angle to the fibre. Low order modes can be blocked using an annular beam mask at launch [1].

3.5 Effect of a high index overlay on the sensitivity

One method to enhance the sensitivity of a side polished fiber sensor is to give a high refractive index coating in the sensing region. This technique has already been used in D-fibers for methane gas sensing [22]. It is necessary to evaluate theoretically the attenuation properties of the waveguide sensor, for optimizing the device for maximum sensitivity. The matrix method [23] is a powerful tool for analyzing multilayer waveguides containing absorptive layers, but the processes are rather complicated for the complex manipulations. Stewart et al [22,24] evaluated the sensitivity enhancement of D-fiber sensors with high index overlay using a 4 layer waveguide model, perturbation method and matrix method . De-Kui Qing et al has done a group index method for the theoretical evaluation of absorption coefficient of waveguide sensors, for various designs of the sensing region [25].

The fibre chosen for our experimental work is a large core polymer fibre with N.A = 0.5. The core diameter is 980 microns. Owing to the large diameter of the fibre core, we followed a ray optics approach to our problem.

The sensing region can be considered as a planar leaky structure. In this region, light is partially confined to the core by reflection mechanisms other than

total internal reflection. The light transmission in the sensing region was evaluated by the reflection in a 3-layered structure [26].

The reflection coefficient $r^i(\theta)$ is given by [27]

$$r^i(\theta) = \frac{r_{23}^i + r_{34}^i \exp(-i2k_3 d_0)}{1 + r_{23}^i r_{34}^i \exp(-i2k_3 d_0)} \quad \ldots\ldots (3.12)$$

Where θ - the angle the ray makes with the normal to the core-overlay interface

And $i = s$ for s-polarised light & $i = p$ for p-polarised light.

Other terms are

r_{23} - Fresnel's reflection coefficients at the core-overlay interface

r_{34} - Fresnel's reflection coefficients at the overlay-liquid interface

d_0 - overlay thickness

d - core diameter

θ_1 - the angle of incidence at the core-overlay interface

θ_2 - the angle of incidence at the overlay-liquid interface

k_3 - transverse wave number in medium 3,

$$k_3 = k_0 n_3 \cos\theta_2 \quad \ldots\ldots (3.13)$$

case (i) No overlay

Only the reflections at the core-liquid boundary need to be considered in this case so that,

Fresnel's reflection coefficient

$$r_{24} = \frac{\left[(n_4 - i\alpha)^2 - n_2^2 \sin^2\theta_1\right]^{1/2} - n_2 \cos\theta_1}{\left[(n_4 - i\alpha)^2 - n_2^2 \sin^2\theta_1\right]^{1/2} + n_3 \cos\theta_1} \quad \ldots\ldots (3.14)$$

Reflectance $R = |r_{24}|^2$ ….. (3.15)

No. of reflections per unit length at the core-liquid boundary

$$N = \frac{1}{2d \tan\theta_1} \quad \text{..…. (3.16)}$$

where d - core diameter

Loss in dB , $L = -4.343N \ln|r_{24}|^2$ ……..(3.17)

case (ii) In presence of overlay

The reflection coefficient for the 3-layer structure should be applied.

$$r = \frac{r_{23} + r_{34} \exp(-i2k_3 d_0)}{1 + r_{23} r_{34} \exp(-i2k_3 d_0)} \quad \text{..…. (3.18)}$$

$$R_{ov} = |r|^2 \quad \text{..….. (3.19)}$$

No. of reflections per unit length at the overlay-liquid boundary

$$N_1 = \frac{1}{d \tan\theta_1 + d_0 \tan\theta_2} \quad \text{……..(3.20)}$$

Loss in dB , $L_{ov} = -4.343N_1 \ln|r|^2$ …… (3.21)

We define the sensitivity Enhancement factor

$$S = \frac{L_{ov}}{L} \quad \text{……. (3.22)}$$

For a given fibre, S depends on various parameters like,

(i) refractive index of the overlay (n_3)

(ii) overlay thickness (d_0)

(iii) angles θ_1 and θ_2 , which again depend on the launching angle to the fibre.

3.6 Results and discussion

The sensor performance is simulated for various overlay refractive indices and thicknesses. Figure 3.6 shows the attenuation for an overlay coated SPF for different launching angles. The overlay refractive index $n_3 = 1.59$, core refractive index $n_2 = 1.49$, and $\lambda = 670nm$. The loss experienced by the modes depends on the effective mode index. We can roughly say that each mode corresponds to a particular launching angle to the fibre. (Launching angle is the angle between the fibre axis and the ray incident on the fibre end).

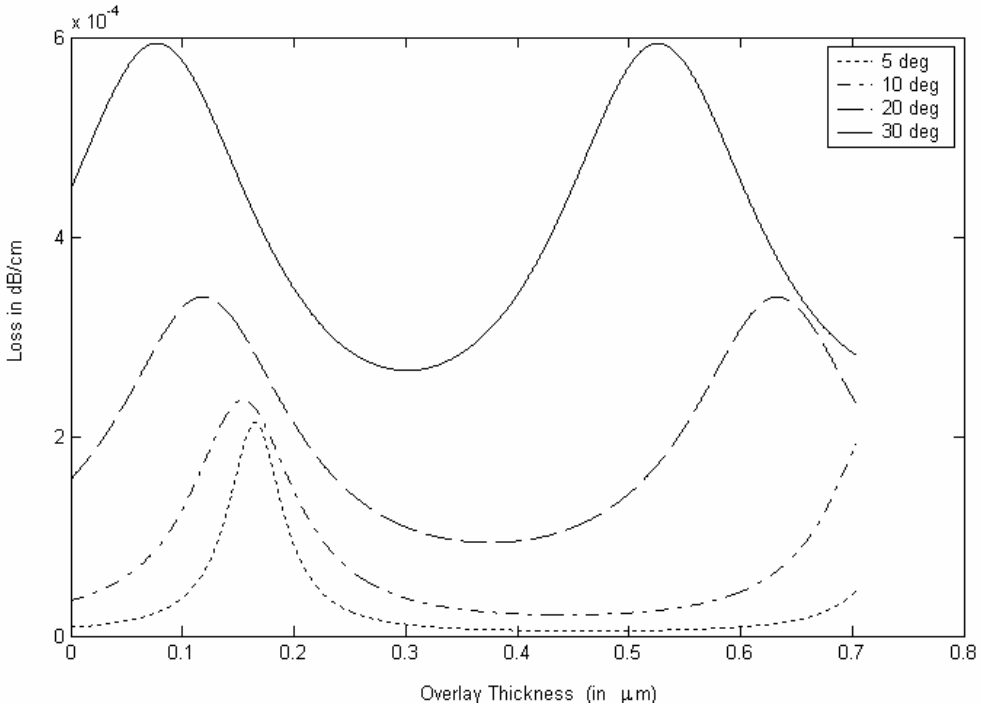

Fig 3.6 Attenuation vs overlay thickness plot for a side polished fibre with overlay refractive index 1.59, for launching angles 5^0, 10^0, 20^0 and 30^0.

We see that for higher order modes, corresponding to larger launching angles, there is considerable loss even without overlay. When the overlay thickness is increased, the loss is increased . There is an optimum overlay thickness for each mode for which the loss is maximum. We also note that the factor by which the loss gets enhanced with the overaly, is also different for different modes. Though the maximum attenuation is attained with the highest order modes, the factor by which the attenuation is increased is greater for lower order modes. Figures 3.7 (a) and 3.7(b) show the sensitivity enhancement factor vs overlay thickness plots, for a given overlay index 1.59, and for various launching angles.

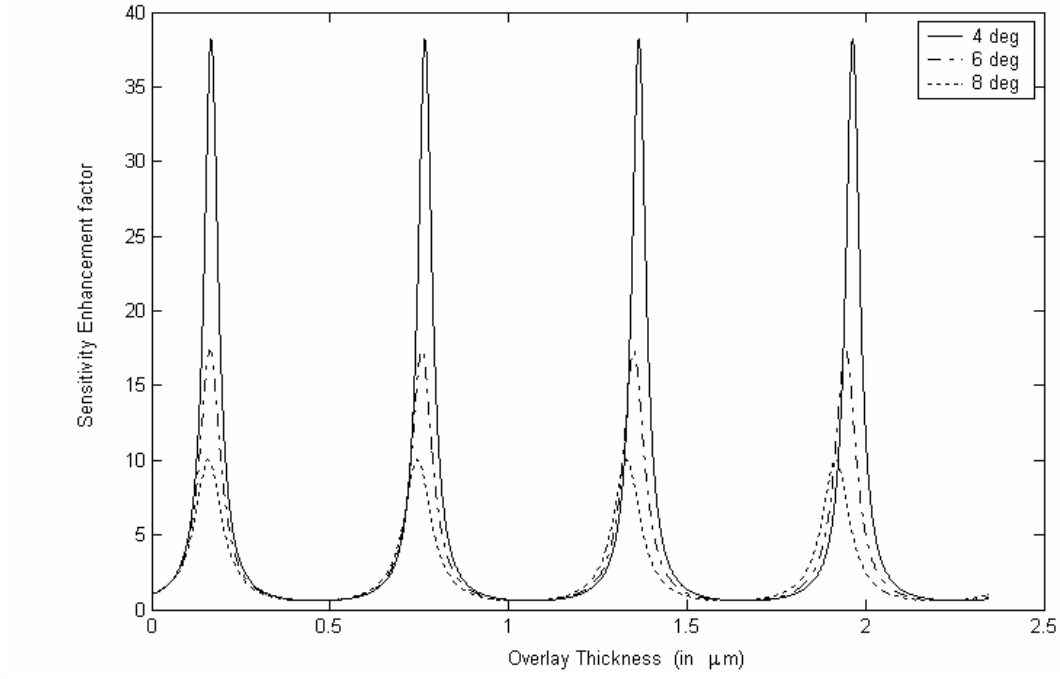

(a)

Fig 3.7 a Sensitivity enhancement vs overlay thickness plot for a side polished fibre with overlay index 1.59, for launching angles 4^0, 6^0 and 8^0.

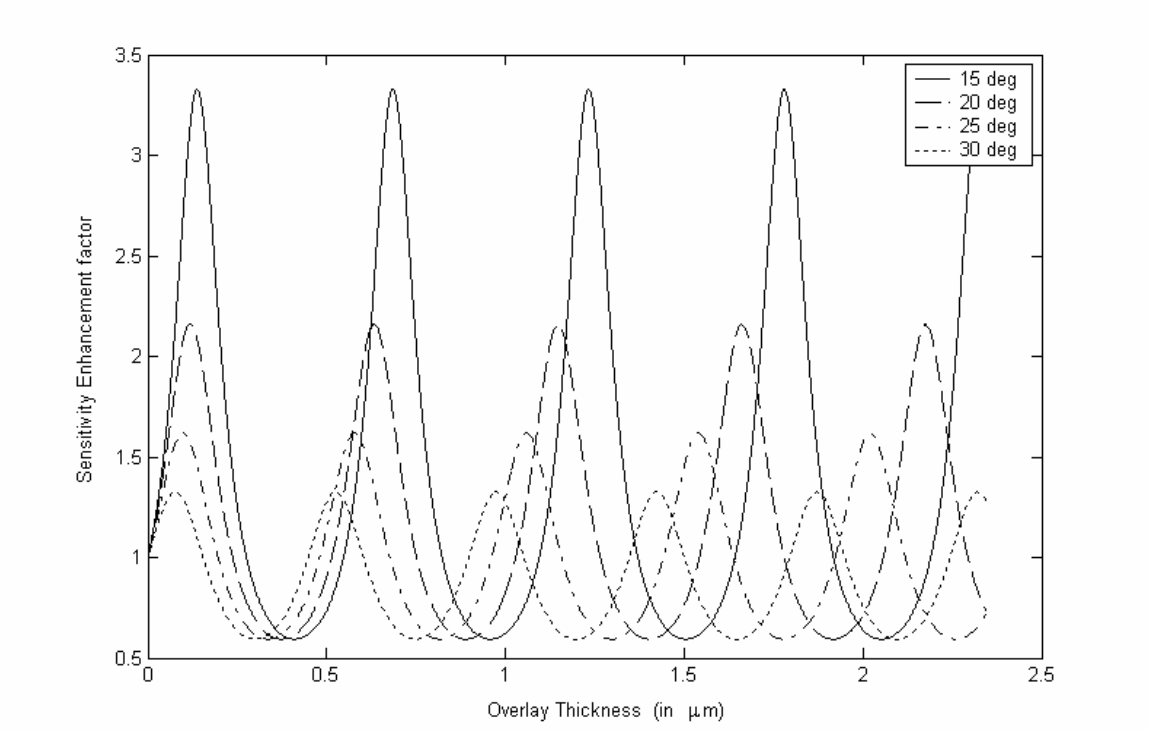

(b)

Fig 3.7 b Sensitivity enhancement vs overlay thickness plot for a side polished fibre with overlay index 1.59, for launching angles 15^0, 20^0, 25^0 and 30^0.

In a multimode fibre, the overall attenuation will be a weighted average over the modal distribution. In general, a single mode fibre is better in terms of sensitivity and stability since it can be designed for optimum sensing by employing its fundamental mode.

Figure 3.8 shows the effect of overlay refractive index on the sensitivity of the device. We see that by increasing the overlay refractive index, the sensitivity gets improved .

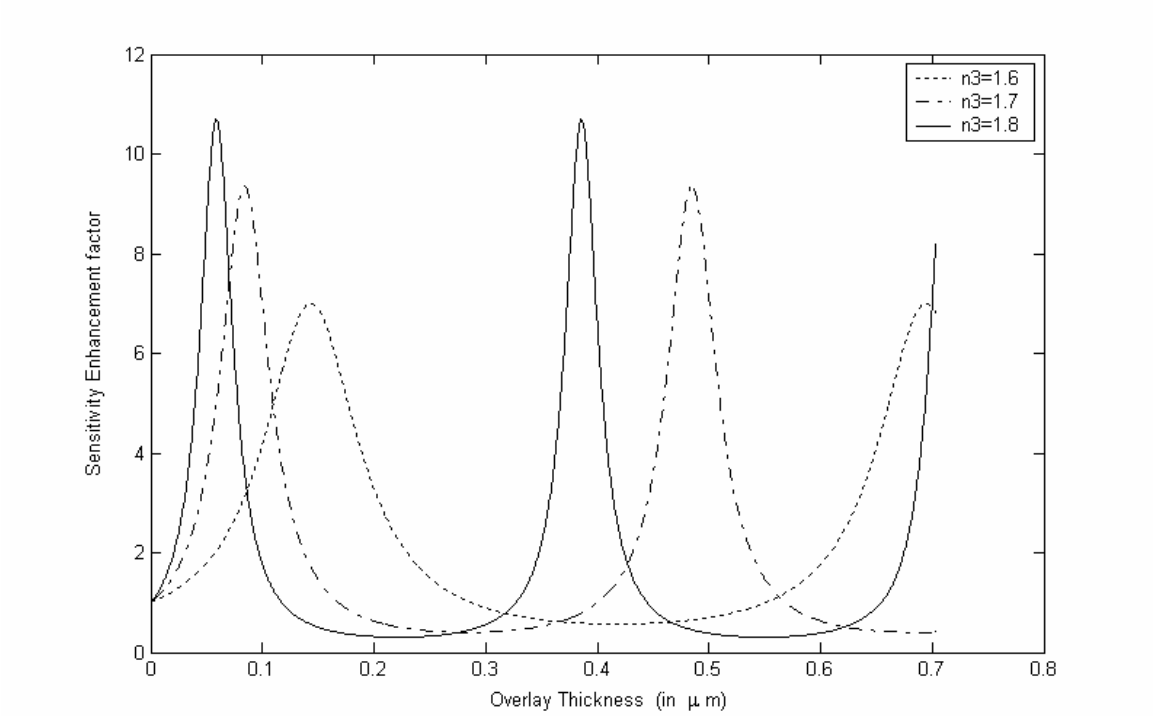

Fig 3.8 Overlay thickness vs sensitivity enhancement factor plots for different overlay refractive indices, at launching angle 10^0

The periodicity of the plots arise from the properties of thin film reflection [27]. We see that sensitivity enhancement could be achieved only by proper selection of the thickness of the overlay.

3.7 Fibre optic sensor for chemical reaction kinetics

In the previous sections, we have discussed the effect of coating the unclad fibre with a high refractive index overlay on the evanescent wave absorption. It has been inferred from the theoretical modeling that the sensitivity gets increased

when coated with a high index material. We now apply this to a sensor designed for chemical reaction kinetics study.

Kinetic studies provide very valuable information about reaction mechanisms. The conventional methods of studying rate coefficients are volumetric analysis [28] and optical transmission [29]. A simple optical sensing means for the determination of rates of time-dependent chemical reactions is based on the principle of fibre optic evanescent wave absorption. There are not many reported works on the study of chemical reaction kinetics using fibre optic sensors except a few [30,31].

The reaction rate of a chemical reaction is a quantity that defines how the concentration of a reactant or product changes with time. Consider a simple time-dependent chemical reaction ,

$$R_1 + R_2 = P$$

Where R_1 and R_2 are the two reactants and P is the product evolved during the reaction. The amount of P increases with time. If this product is an absorbing one, then the evanescent absorption will definitely increase as the concentration of P increases with time. As a result, the light at the output end of the fibre will decrease with time. The rate of decrease of the output power will be directly proportional to the rate of evolution of the product P. In other words, the variation of output power is a measure of the reaction rate.

3.7.1 Working principle

For a step index multimode optical fibre whose cladding has been replaced by an absorbing fluid sample, the power transmitted is written as,

$$P = P_0 \exp(-\gamma L) \qquad \ldots\ldots(3.23)$$

where $\gamma = \eta\alpha$, in which η is the average evanescent ratio and α is the bulk absorption coefficient, which is directly proportional to concentration of

the absorbing species. For a time dependent chemical reaction, the concentration of the absorbing fluid (ie., the concentration of the product of the chemical reaction) increases with time. Therefore we can rewrite equation (3.23) as

$$P(t) = P(0)\ \exp(-\gamma(t)L) \qquad \ldots\ldots(3.24)$$

and

$$\gamma(t) = \frac{2.303}{L}\log_{10}\frac{P(0)}{P(t)} \qquad \ldots\ldots(3.25)$$

The sensitivity of the sensor is generally determined by the rate of change of transmitted power with concentration. The higher the value of γ, the greater will be the sensitivity of the sensor. For a given length of the sensing region, the sensitivity of the evanescent wave absorption primarily depends on the amplitude of the evanescent field in the sensing medium and the number of reflections per unit length within the sensing region. Higher values of these two factors will essentially increase the sensitivity of the sensor.

3.7.2 Experiment and Discussions

The sensor head fabrication was done according to the procedure discussed in Chapter 2. The length of the unclad region was 2.5 cm. To give high refractive index coating over the polished core, Polystyrene with refractive index 1.59 was chosen as the overlay material . Sensor heads with overlay thicknesses 1.2 μm and 2 μm were prepared by dip coating.

An intensity stabilized diode laser giving peak emission at 670 nm was used as the source. The output was coupled to a Si detector (New Port 818-SL) which was interfaced with PC with Labview 7.0. Fig 3.9 shows the schematic of the experimental set up.

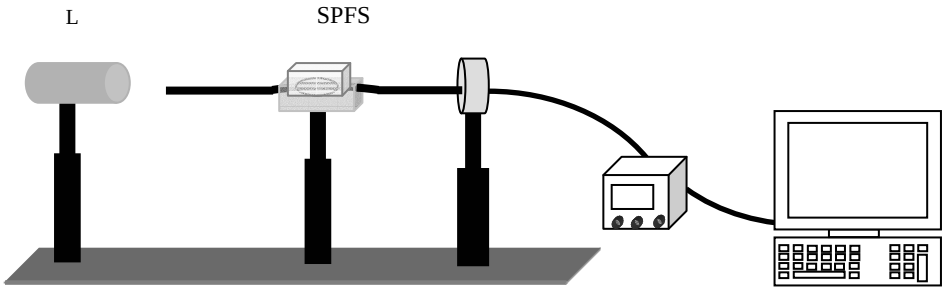

Fig 3.9 Experimental setup for time-dependent reaction kinetics study
L – Diode Laser(670 nm), SPFS- side polished fibre sensor,
D-detector (Newport -818-SL)

Experiments were conducted with bare fibre as well as with coated fibres.

A standard chemical reaction namely, the reaction between potassium iodide (KI) and potassium peroxdisulphate ($K_2S_2O_8$) was chosen for study. Equimolar solutions (7mM) of both these reagents were prepared in distilled water. The reaction resulted in the evolution of iodine according to the equation,

$$2KI + K_2S_2O_8 \rightarrow I_2 + 2K_2SO_4$$

During the reaction, iodine was produced in the reaction cell. The amount of iodine liberated increases with time. Two drops of starch was added as indicator so as to enhance the absorption.

Figure 3.10 represents the variation of absorption coefficient plotted against time, corresponding to uncoated fibre, and coated fibres.

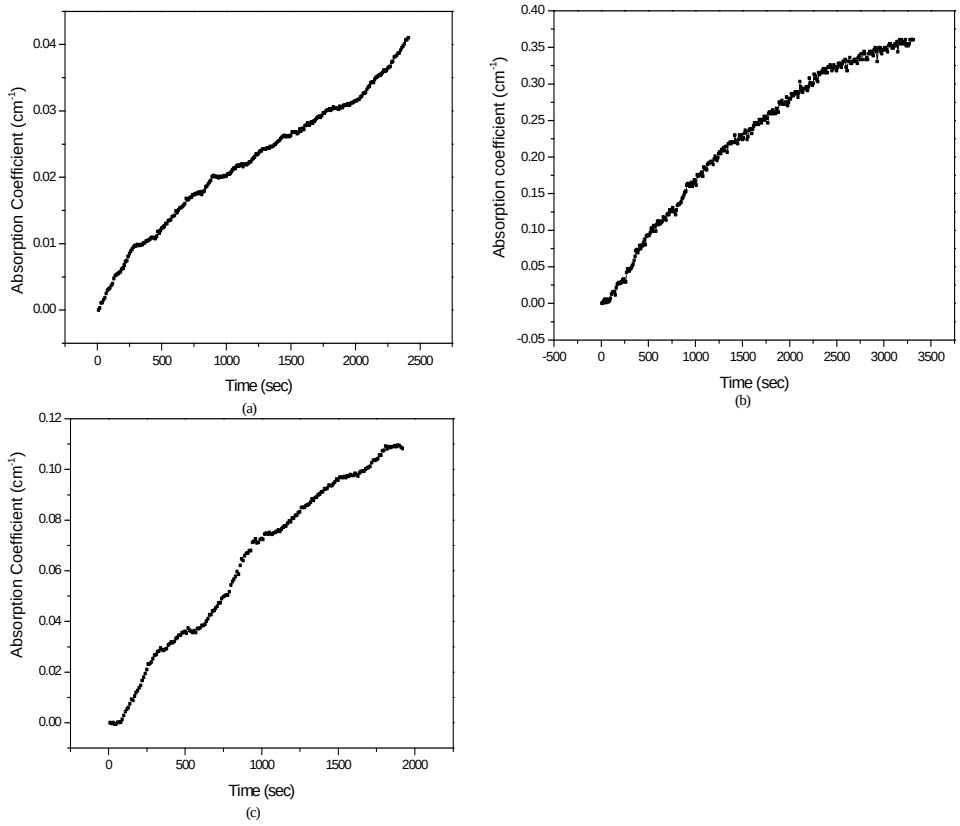

Fig 3.10 Variation of absorption coefficient with respect to time for (a) bare fibre (b) fibre with coating thickness 1.2 μm (c) fibre with coating thickness 2 μm

The absorption coefficients of the three sensor heads show different values and hence different sensitivities. Of the three, the uncoated fibre has got the smallest absorption coefficient. The sensor with a coating thickness 1.2 μm has got greater absorption coefficient than that of thickness 2 μm. We have already seen

that the evanescent wave absorption varies in a periodic fashion with overlay thickness.

There is a trend to show a linear variation of absorption with time during the initial phase. The time variation of the absorption coefficient is nonlinear with a tendency of saturation at longer duration. The initial slope of the graph was taken as the rate constant of the chemical reaction. The initial slopes obtained for the three cases are the following :

Bare fibre	:	$0.28 \times 10^{-4}\ sec^{-1}$
Coating thickness - 1.2 μm	:	$1.56 \times 10^{-4}\ sec^{-1}$
Coating thickness - 2 μm	:	$0.96 \times 10^{-4}\ sec^{-1}$

There is no given value in literature for the comparison of rate constant, which is essentially a function of reactant concentration. So in order to check the validity of the results obtained from the fibre measurements, we have to rely on the spectroscopic measurements.

The same reaction was studied using a spectrophotometer (JASCO UV/VIS/NIR V-570), operating in time scan mode, with wavelength fixed at 670 nm. The value of the rate constant obtained by this method was $1.87 \times 10^{-4}\ sec^{-1}$ which is close to that obtained using a fibre sensor head with overlay thickness 1.2 μm. The other two designs, fail to give correct values, most probably due to low sensitivity. The effect of the overlay coating is to enhance the sensitivity of the fibre sensor.

3.8 Conclusions

In this chapter we have discussed the effect of high refractive index overlay on the evanescent wave absorption . The effect of overlay thickness and refractive index on the sensitivity of the sensor has been numerically modeled. Details of the modeling related to the evanescent wave absorption for different overlay refractive indices and overlay thicknesses are also included in this chapter. It was observed that the evanescent wave absorption coefficient increased with increase in overlay refractive index and proper selection of overlay thickness. Experiments were also performed for studying the reaction kinetics of a standard chemical reaction. A side-polished polymer fibre sensor coated with a higher refractive index material was developed to study chemical reaction kinetics. The coated fibre showed enhancement in sensitivity as compared to bare fibre.

References

1. V. Ruddy, B. D. MacCraith, J.A. Murphy, *J. Appl. Physics* **67** (10), 6070-6074 (1990).
2. I. Schnitzer, A. Katzir, U. Schiessi, W. J. Riedel, M. Tacker, *J. Appl. Physics* **66** (11), 5667-5670 (1989).
3. Culshaw
4. S. Thomas Lee, P. Suresh Kumar, K. P. Unnikrishnan, V. P. N. Nampoori, C. P. G. Vallabhan, S. Sugunan, P. Radhakrishnan, *Meas. Sci. and Technol*. **14**, 858-861 (2003).
5. P. Suresh Kumar, S. Thomas Lee, C P G Vallabhan, V.P.N. Nampoori, P. Radhakrishnan, *Optics Commun*. **214**(1-6), 25-30 (2002).
6. Wolfgang Trettnak, Marc. J.P. Leiner, Otto S. Wolfbeis, *Analyst* **113**, 1519-1523(1988).
7. E. Toba, J. Kazama, H. Tanaka, T. Nishimatsu, H. Aizawa, H. Ishizawa, *IEICE Trans. Electron*. **E83-C**, 366-370 (2000).
8. Ainhoa Gaston, Ibon Lozano, Fatima Perez, Fernando Auza and Joaquin Sevilla, *IEEE Sensors Journal* **3**(6), 806-811 (2003)
9. Javier Senosiain, Idoya Diaz, Ainhoa Gaston and Joaquin Sevilla, *IEEE Trans. On Instrumentation and Measurement* **50**(6), 1656-1660(2001).

10. Joseba Zubia, German Garitaonaindia and Jon Arrue, *Appl. Optics* **39**(6), 941-946 (2000).
11. R.M. Ribeiro, João L.P. Canedo, Marcelo M. Werneck, Liliana R. Kawase, *Sensors and Actuators A* **101,** 69-76(2002)
12. Navneet K. Sharma, B.D. Gupta, *Optics Commun.* **216**, 299-303 (2003).
13. S. M. Tseng and C.L. Chen, *Appl. Opt.* **31**(18), 3438-47(1992).
14. N. Chen, S. Chi, and S. Tseng, *Opt. Lett.* **29**, 2219-2221 (2004).
15. G. Stewart, J. Norris, D. F. Clark, B. Culshaw, *Int. J. Optoelectron.* **6**(3), 227-238 (1991).
16. Richard Syms, John Cozens, Optical Guided Waves and Devices, McGraw-Hill Book Company Europe, England (1992)
17. G. Stewart, B. Culshaw, *Opt. And Quantum Electron*. **26**, S249-S259 (1994).
18. N.S. Kapany, Fibre Optics – Principles and Applications, Academic Press, NewYork (1967)
19. P.M. Shankar, L.C. Bobb, H.D. Krumboltz, *J. Light. Technol.* **9**(7), 832-837(1991).
20. F. J. Arregui, I.R. Matias, M. L. Amo, *Sens. Actuat A* **79**, 90-96 (2000).
21. S. K. Khijwania, B.D. Gupta, *Opt. Quantum Electron.* **31**, 625-636 (1999).
22. F.A. Muhammad, G. Stewart, W. Jin, *IEE Proceedings-J* **140**(2), 115-118(1993).
23. A.K. Ghatak, K. Thyagarajan, M.R. Shenoy, *J. Light. Technol.* **5**(5), 660-667(1987).
24. F.A. Muhammad, G. Stewart, *Electron. Lett.* **28**(13), 1205-1206(1992).
25. De-Kui Qing, Xiao-Min Chen, Kiminori Itoh, Masayuki Murabayashi, *J. Light. Technol*. **14**(8), 1907-1917(1996).
26. Yi-Zhen Lin, Jing-Hong Zhan, Shiao-Min Tseng, *IEEE Photonics Tech. Lett.* **9**(9), 1241-1243 (1997)
27. Max Born and Emil Wolf, Principles of Optics 7th Edn , Cambridge University Press (1999).
28. D.P. Shoemaker and C.W. Garland, Experiments in Physical Chemistry, McGraw-Hill, Tokyo (1967).
29. W.D. Prudy, F. Tarczynski, *Proc. SPIE* **3537**, 26-33 (1998).
30. P. Radhakrishnan, V.P.N. Nampoori, C.P.G. Vallabhan, *Opt. Engg*. **32**(4), 692-694 (1993).
31. P.K. Choudhury, Toshihiko Yoshino, *Meas. Sci. Technol.* **13**, 1793-1797(2002).

4

Dye doped polymer planar waveguides : Fabrication and characterization

Dye doped polymer waveguides are potential materials as optical gain media. This chapter deals with the fabrication and characterization of rhodamine 6G doped poly (methyl methacrylate) film waveguides. Free standing film waveguides were fabricated by tape casting method. The loss characterization was done by a non-destructive side illumination fluorescence technique.

4.1 Introduction

Organic dye lasers have become a subject of intensive research ever since Sorokin and Lankard reported the stimulated emission from an organic dye solution [1]. The use of solid matrix for dye lasers gets rid of many of the common problems associated with liquid systems like concentration variation due to evaporation of solvents. Solid state dye lasers offer added technical advantages such as compactness, manageability and versatility. The first attempt to develop solid-state dye lasers were reported in the late 1960's [2,3]. Ever since there have been intensive efforts to achieve the incorporation of organic dyes in solid matrices that might replace conventional liquid dye lasers. Most of the recent works have been done using either polymers [4,5] or silica gels [6,7] as the host media. Polymeric materials in particular offer advantages such as ease of processing, which permits fabrication of devices of virtually any shape and potentially cost-effective. Organic polymers poly methyl methacrylate (PMMA) and co-polymers of MMA such as HEMA [8-11] have been widely used as host material for laser dyes. Other commonly used polymer hosts include poly acrylic acid (PA) [12] and poly vinyl alcohol (PVA) [13].

In the field of photonics, considerable attention is centering on the use of polymer waveguides and fibers as they have a great potential to create all-optical devices [14,15] and polymer optical integrated circuits. Polymers show better optical transparency, homogeneity of refractive index and good compatibility with organic dyes. Moreover, waveguide structure with its long interaction length of active material is attractive as it is effective for controlling optical signals with low input power. Polymer waveguides and fibres doped with organic dyes have proved to be potential candidates for fibre lasers and

amplifiers [16-19]. By choosing appropriate dyes, we can obtain laser emission from doped polymer waveguide in the entire visible region. The combination of signal processing in optically active organic materials along with a passive mode of signal transmission in transparent polymers has been used in the design of all-optical switches as well [20].

This chapter deals with the fabrication of dye doped polymer film waveguides as well as their characterization. The properties of dye-doped polymer waveguides should be clearly known before they are used for all-optical devices. Improvement in the performance of these devices requires a thorough knowledge of the optical absorption and emission characteristics. The loss characterization was done by a non-destructive side-illumination fluorescence [21,22] technique.

4.2 Materials

4.2.1 Host Material : *Poly (methyl methacrylate) (PMMA)*

Although, through the years, a number of different materials have been tested as solid hosts for laser dyes, polymeric matrices present some important advantages as they usually show good compatibility with organic dyes, have excellent optical homogeneity [8] and are amenable to inexpensive fabrication techniques which could facilitate both miniaturization and the design of integrated optical systems. The basic requirements imposed on a polymeric host for laser dyes are good optical transparency at both pump and lasing wavelengths, good solubility of the dye in the material and resistance to pump laser radiation against photochemical reaction and optical damages.

Due to its favourable properties we chose poly methyl methacrylate (PMMA) for the present studies. The molecular structure of PMMA is shown in fig 4.1. This polymer has been the most frequently used host for lasing dyes due to its excellent transparency (with refractive index ~ 1.49) in the visible region and its relatively high laser-damage threshold.

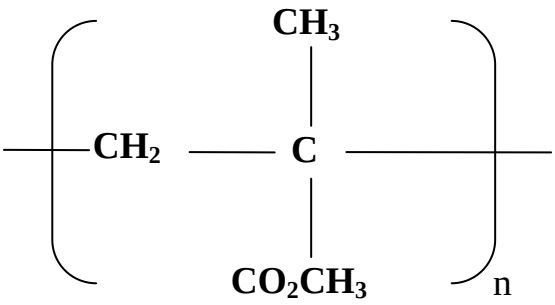

Fig 4.1 : Molecular structure of PMMA

4.2.2 Dye : *Rhodamine 6G*

Most of the dye lasers operate with the materials belonging to the xanthene family of dyes, which cover the wavelength region from 500-700nm and have generally very high quantum efficiency. The organic dye chosen for the present studies is the chloride of rhodamine 6G (Exciton), which belongs to the xanthene family of dyes. Fig 4.2 shows the molecular structure of the dye molecule. Rhodamine 6G has been frequently investigated in solid state dye lasers in a variety of solid hosts [8,10,23-26] on account of its high fluorescence

quantum yield, low intersystem crossing rate and low excited state absorption at both pump and lasing wavelengths.

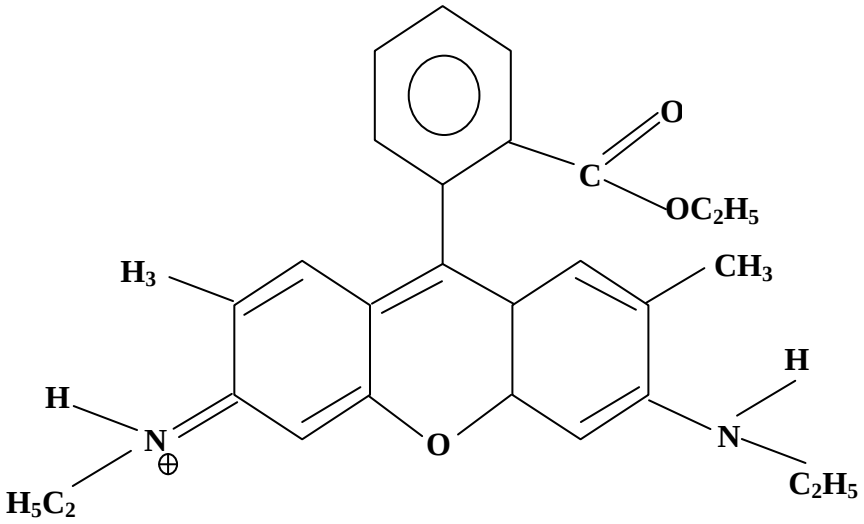

Fig 4.2 Structure of Rhodamine 6G

The absorption maximum of rhodamines is surprisingly dependent on the solvent, in particular with those dyes whose amino groups are not fully alkylated (eg. Rhodamine 110 and rhodamine 6G). The fluorescence spectra of these dyes closely resemble the mirror image of the long wavelength absorption band.

4. 3 Film Fabrication

Free standing films of Rhodamine 6G doped PMMA films were prepared through tape casting method. Weighed PMMA (HIMEDIA, MWAv-15000) granules were added to the pre-measured solvent- Methyl Ethyl Ketone

(MEK) (MERCK) in polypropylene jars (Tarson). Roll milling ensured complete dissolution of PMMA. Rhodamine 6G was then added to this prepared PMMA-MEK binder in desired concentration. Homogeneous mixing of the Rh6G in the matrix was ensured by roll milling.

The mix prepared as above was cast into thin sheets on a glass plate using double doctor blade tape casting technique (EPH Engineering, USA). This technique is useful for obtaining films of uniform thickness. The mix was poured through the gap between the blade and the glass plate. Desired thickness was maintained by controlling the blade to glass bed gap and the casting speed. After casting, the solvent evaporated leaving behind uniformly doped PMMA sheets. The cast tapes were removed from the glass bed to get uniform films of Rhodamine 6G doped PMMA. Films of various thicknesses and dye concentrations were prepared using this technique. The films were then cut into the size of 4cm x 2cm.

4.4 Absorption and emission spectra of the samples

The absorption spectra of the films were taken using a spectrophotometer (JASCO UV/VIS/NIR V-570). (see fig 4.3).

The absorption spectra showed the peak at 536 nm with a shoulder near 500nm. Spectral characteristics did not show any dependence on dye concentration except for the peak intensity which ensured the absence of any aggregation of dye molecules.

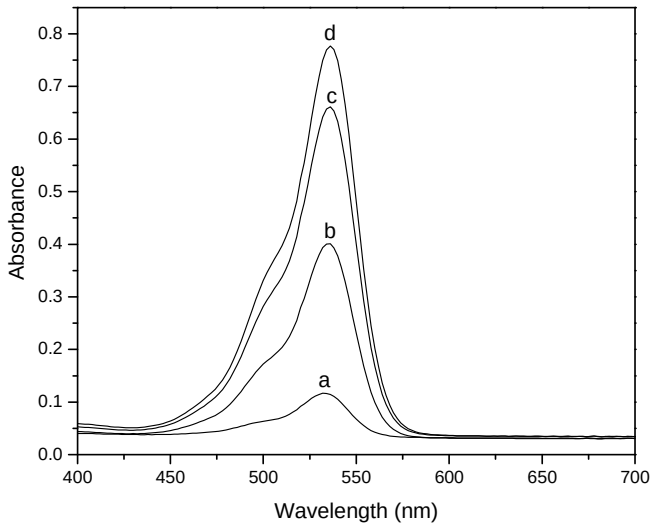

Fig 4.3. Absorption spectra of rhodamine 6G doped thin films (50 µm thick) for dye concentrations (a) 0.1mM (b) 0.5mM (c) 1mM (d) 1.5mM

Fluorescence emission from the dye doped polymer film waveguides were excited by the 532 nm (cw) from a diode pumped solid state (DPSS) laser ($Nd:YVO_4$). The front surface emission was focused to fall on the slit of a 0.2m grating-monochromator (Mc Pherson). The output from the monochromator-PMT assembly was given as input to a lock-in amplifier (SR-830) which was interfaced with PC using Labview 7.0.

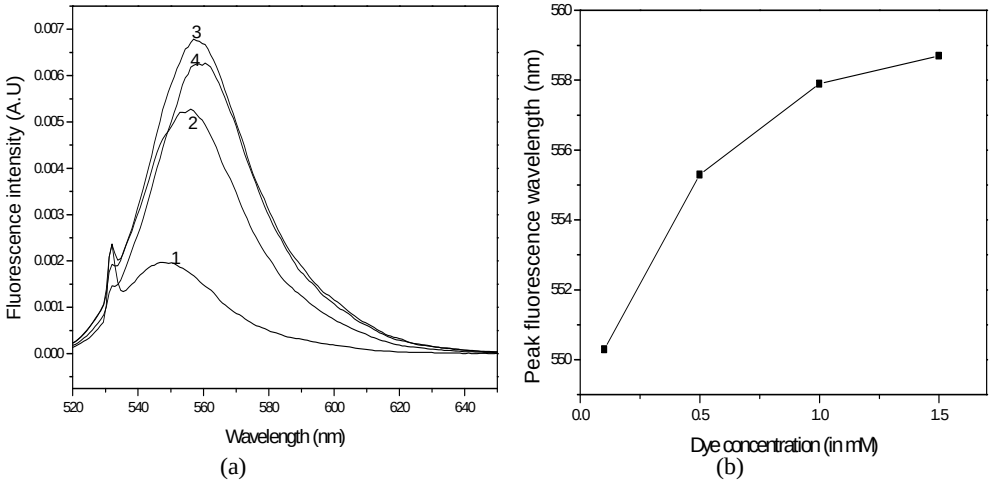

Fig 4.4. (a) Front surface fluorescence emission from Rh6G doped 50 µm thick PMMA films for dye concentrations (1) 0.1mM (2) 0.5mM (3) 1mM (4) 1.5mM. Sharp peak at low wavelength side is due to the pump radiation. (b) Variation of peak fluorescence wavelength with dye concentration

From figure 4.4, we observe that the peak of the fluorescence spectrum from the films gets shifted to longer wavelengths when the dye concentration is increased. This concentration dependent red shift was observed for dye solutions as well [27]. The red shift in peak fluorescence wavelength is a consequence of secondary absorption effects due to the overlap between the emission spectrum of the dye and the low energy tail of its absorption band [27].

A list of the environmental factors that affect fluorescence phenomena includes interaction with solvents and other dissolved compounds, temperature, pH and the concentration of the fluorescent species. Both the absorption and emission spectra as well as the quantum yields of the fluorescent molecules are

influenced by these parameters. The absorption spectra did not show any modifications with respect to dye concentration. This means that aggregate formation at high concentrations had a negligible effect on the observed fluorescence peak shift [28]. Hence the observed peak shift in the fluorescence spectra is a consequence of self absorption and reemission [29]. Since the emitted wavelength was longer than the absorbed one, self absorption of fluorescence radiation results in the fluorescence emission at longer wavelength. If the molecules have closely lying levels of different absorption cross section, absorption saturation to each level would also lead to a wavelength shift. However the red shift in the dyes is commonly attributed to the concentration effects resulting in self-absorption.

4.5 Loss characterization

As noted earlier, the properties of dye-doped polymer waveguides should be clearly known before they are used for all-optical devices. In order to optimize the performance of these devices, a thorough knowledge of the optical characteristics is essential. Optical attenuation in waveguides is one of such important parameter. There are different techniques for measuring the propagation losses in waveguide structures. Usually the propagation losses in fibres and planar waveguide structures are measured by the cut-back technique[30,31] which consists in comparing the transmittance of several guides with different lengths at a specific wavelength. The values of the loss parameter can also be extrapolated from a bulk measurement. The disadvantage of the cut-back technique is that it is a destructive method. Bulk measurements involve a broad band light source incident on a fixed length of the material and a

spectrometer to read the transmitted intensity. A non-destructive side-illumination fluorescence technique (SIF) is an alternative to the above mentioned techniques, for measuring the optical attenuation in dye-doped fibres as well as waveguides [22,32,33]. This measurement technique requires a monochromatic light source to illuminate the waveguide from the side. The fluorescence collected from one end of the waveguide is used as a light source to characterize the attenuation mechanisms in the planar waveguide structures. The excitation spot is shifted so as to collect fluorescence that propagated through various distances through the waveguide. Since the shorter wavelength light is more strongly absorbed, the SIF technique is ideal for measuring the attenuation coefficients at wavelengths in the tail of the absorption band of a dye molecule. This property is extremely useful because standard methods fail to take accurate measurements of attenuation coefficients in the tail region owing to the large absorption at resonance. (See the absorption spectrum in fig 4.3)

4.5.1 Experimental set up

The schematic diagram of the experimental set up is shown in figure 4.5. The film waveguide was mounted normally on a translation stage with respect to the incident radiation. The excitation source was 532 nm (cw) from a diode pumped Nd:YVO_4 laser. The side illumination of the dye doped waveguide generated fluorescence emission. The light emission from one end of the waveguide was collected by an optical fibre leading to a monochromator-photomultiplier tube assembly coupled with a lock-in amplifier (Stanford Research Systems SR830), which was interfaced to a PC by Labview 7.0.

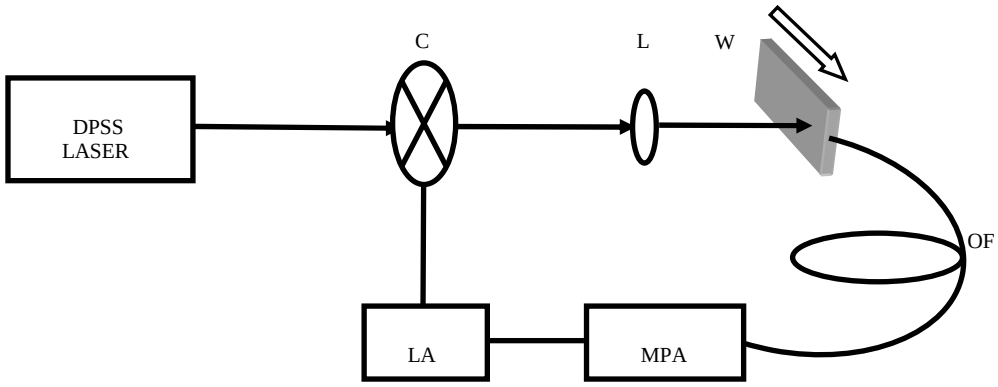

Fig 4.5 Experimental set up to record the fluorescence emitted from side-illuminated planar waveguide C – Chopper L – Focusing lens W – Waveguide OF – optical fibre LA – Lock-in-Amplifier MPA – Monochromator PMT assembly. Arrow shows the direction of translation of the waveguide.

To measure the transmitted fluorescence as a function of propagation distance through the waveguide, the illumination point on the waveguide was varied by translating the waveguide horizontally across the laser source. The direction of translation is indicated by an arrow mark in figure 4.5. The distance between the point of illumination and the waveguide edge from which light is collected is measured as 'z'. At each point of illumination, the fluorescence spectrum was charted. This was done for film waveguides with various dye concentrations and thicknesses.

4.5.2 Results and discussion

Experiments were conducted on film waveguides with varying dye concentrations (0.1mM, 0.5mM, 1mM and 1.5 mM). The side illumination fluorescence spectra were recorded for various propagation distances from one edge of the waveguide, for pump power 3mW. Figure 4.6.a shows the spectra of transmitted fluorescence light measured as a function of the propagation distance

(z) through the waveguide of thickness 50 microns and dye concentration 0.5 mM, for a pump power 3mW at 532 nm.

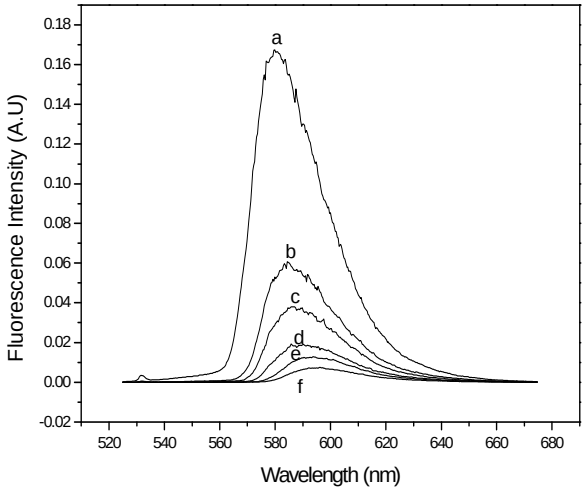

(a)

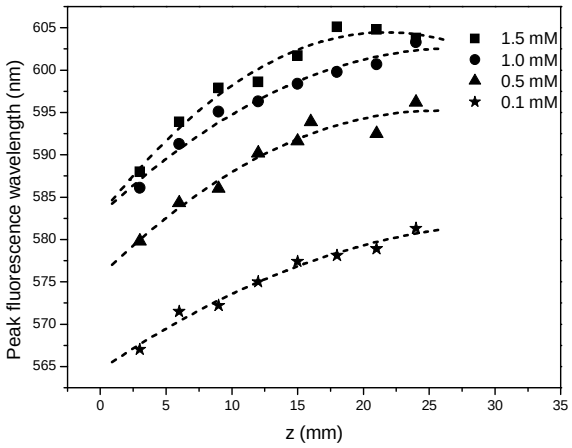

(b)

Fig 4.6. (a) Transmitted fluorescence as a function of propagation distance through the waveguide (*a*)z=3mm (*b*) z=6mm (*c*) z=9mm (*d*) z=12mm (*e*) z=18mm (*f*) z=24mm
(b) Variation of fluorescence peak with propagation distance (film thick ness = 50 µm)

As the propagation distance increases, the magnitude of the output intensity decreases due to various loss mechanisms such as absorption and scattering. In addition, there is a red-shift for the peak fluorescence emission as the illumination distance from one edge of the waveguide is increased. Similar redshift in the fluorescence emission from side-illuminated dye doped fibre has also been observed by other workers [32,33].

As indicated earlier, the redshift of the fluorescence signal is produced by the self-absorption of the dye due to the overlapping of the absorption and fluorescence spectra of Rh6G [27]. In the previous section we discussed the concentration dependent red shift of the fluorescence. We observe a similar behaviour on changing the distance of propagation through the waveguide. As the fluorescence light is guided through the dye doped waveguide, the effective pathlength is increased resulting in self-absorption and re-emission causing a redshift in the observed spectrum. Farther the point of illumination from the observation end, larger will be the effective path length which results in enhanced interaction between the dye molecules and the fluorescence emission generated. This results in an increased self absorption of the fluorescence and thereby shifting the emitted fluorescence peak towards the red side.

Figure 4.6.b shows the variation of fluorescence peak wavelength as a function of propagation distance through the waveguide. For shorter propagation distances in the waveguide, the redshift shows a linear behaviour whereas at longer distances, the shift tends to exhibit a saturation behaviour . This type of nonlinear behaviour of fluorescence peak with respect to z is predominant at higher dye concentrations as is clear from fig 4.6.b. This mechanism is similar to the concentration dependent redshift which is observed in dye solutions [27].

The fluorescence emission collected from the dye doped waveguide has got a spectral width of about 100nm and hence can be used as a broad wavelength light source for measuring the attenuation in the waveguide. The transmitted fluorescence was measured as a function of the propagation distance so as to characterize the attenuation in the waveguide.

From Beer-Lambert's law for linear optical attenuation in a medium,

$$I(\lambda, z) = I_0(\lambda)\exp(-\alpha(\lambda)z) \qquad \ldots (4.1)$$

where $I(\lambda,z)$ and $I_0(\lambda)$ represent the intensity of the transmitted light at wavelength λ at propagation distances z and z=0 respectively while $\alpha(\lambda)$ is the linear attenuation coefficient corresponding to wavelength λ .

We first applied the Beer-Lambert law in our data so as to characterize the optical loss in the waveguide. Figure 4.7 and 4.8 show plots of natural logarithm of transmitted fluorescence intensity versus propagation distance corresponding to various emission wavelengths, for film thickness 50 microns and 135 microns respectively.

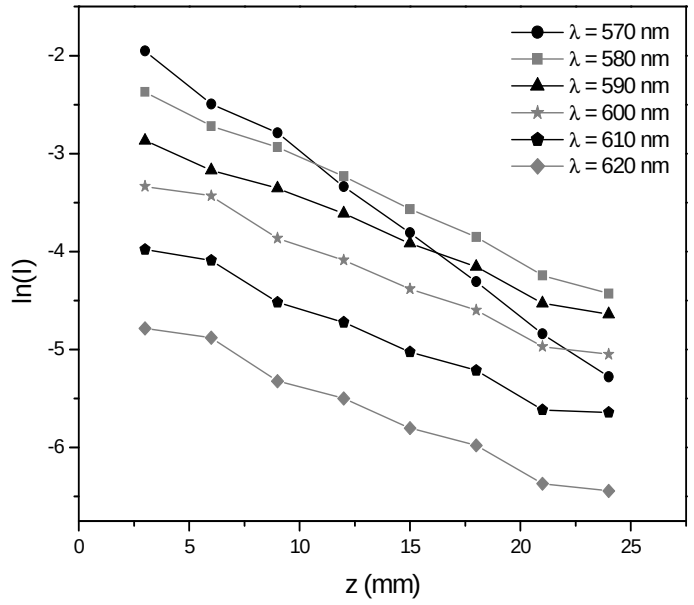

(a)

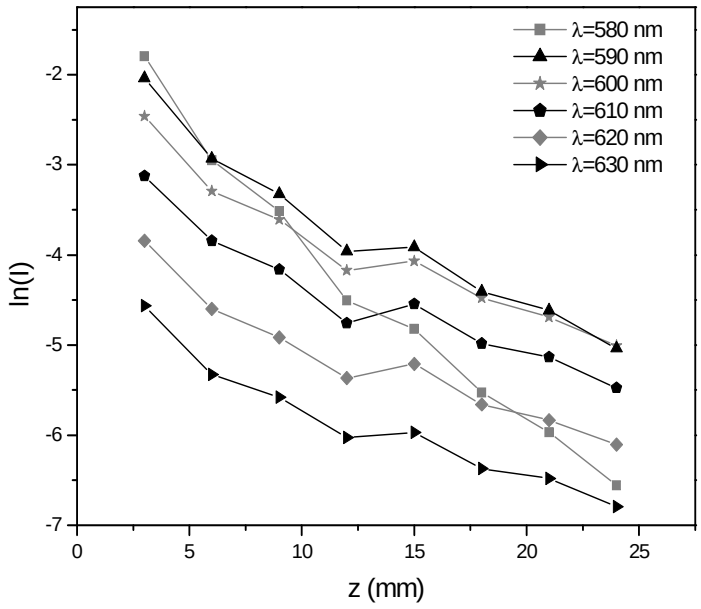

(b)

Fig 4.7 ln(I) vs z plots for film thickness 50 µm and dye concentrations
(a) 0.1 mM (b) 0.5 mM

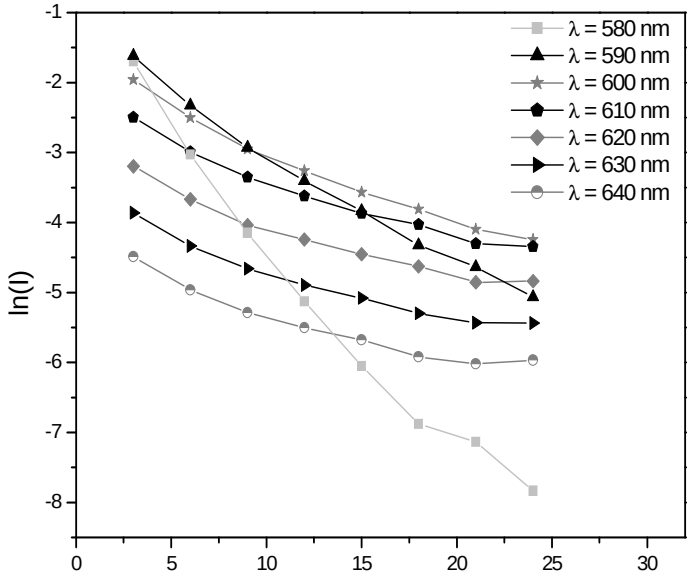

(c)

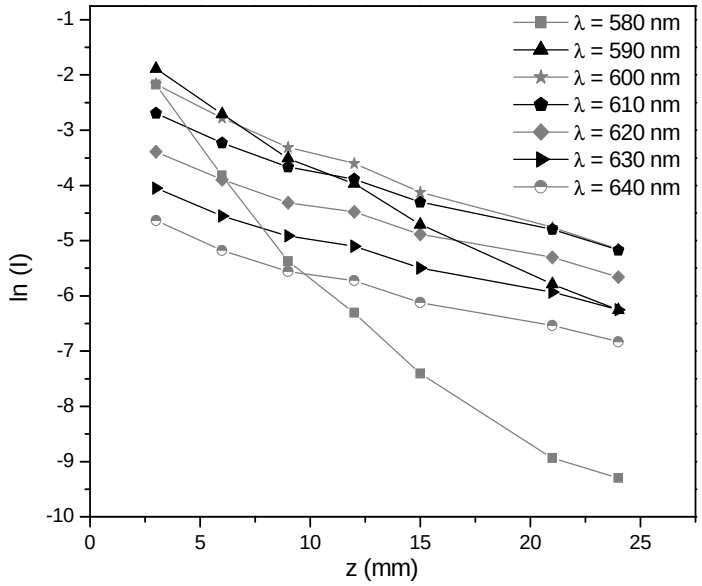

(d)

Fig 4.7 ln(I) vs z plots for film thickness 50 µm and dye concentrations (c) 1 mM (d) 1.5mM

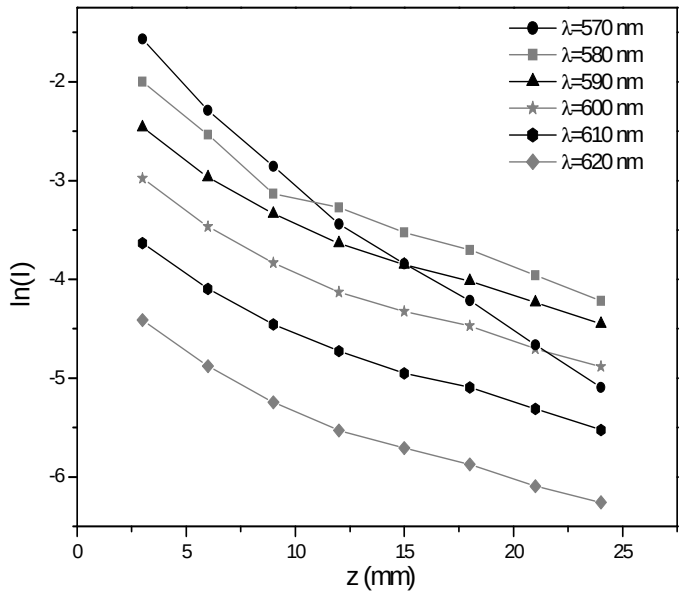

(a)

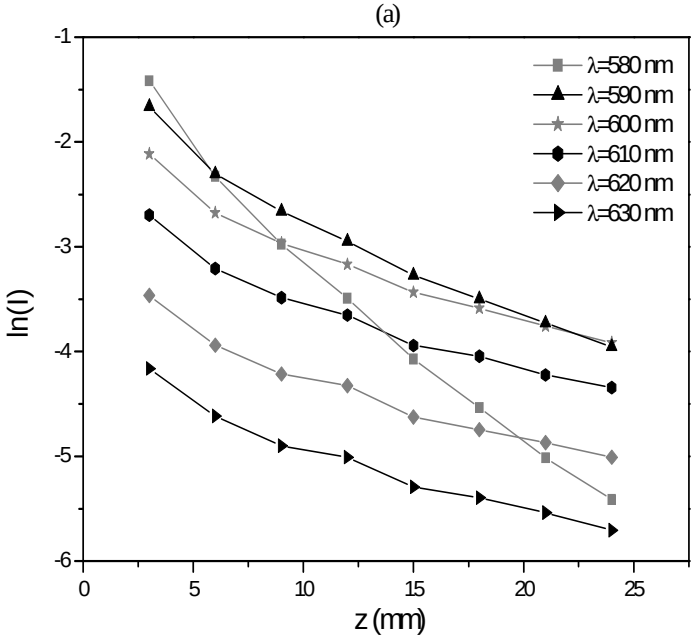

(b)

Fig 4.8 ln(I) vs z plots for film thickness 135 µm and dye concentrations (a) 0.1 mM (b) 0.5mM

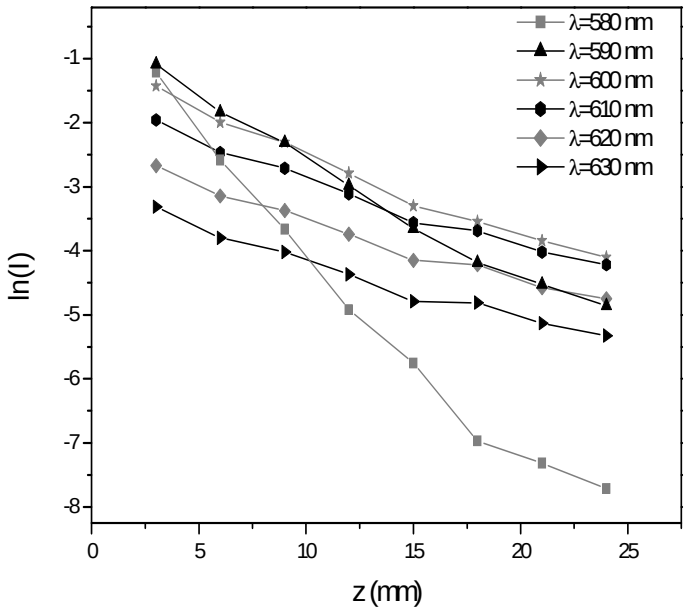

(c)

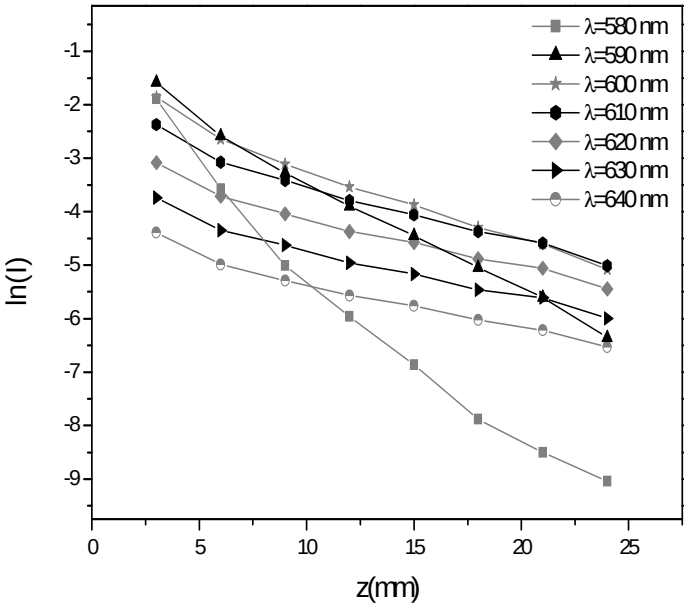

(d)

Fig 4.8 Ln(I) vs z plots for film thickness 135 µm and dye concentrations (c) 1 mM (d) 1.5m M

For samples with thickness 50µm and a low dye concentration (0.1 mM), the ln(I) vs z plots are linear. The observed linearity suggests that the attenuation mechanisms in the waveguide is linear and hence could be explained by the Beer-Lambert's law. For dye concentrations above 0.1 mM it is observed that the nonlinear behaviour of the ln(I) vs z plots is pronounced. The plots cannot be fitted to a single straight line. Each plot can be peeled off to different straight lines with different slopes.

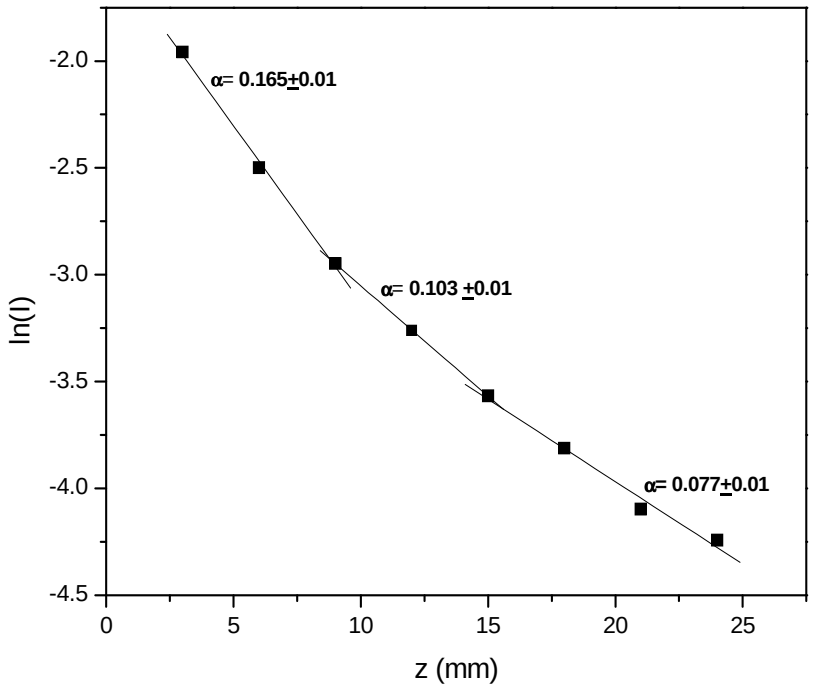

Fig 4.9 'Peeling of curve' method applied to ln(I) vs z plot at λ=600 nm. Figure clearly indicates different values of α at three regions of propagation distance.

Figure 4.9 shows the ln(I) vs z plot peeled into 3 straight lines , for waveguide with dye concentration 1 mM and thickness 50 microns giving attenuation coefficients of 0.165 mm^{-1}, 0.103 mm^{-1} and 0.077 mm^{-1} respectively at short, medium and long propagation distances..

At a higher thickness (135 µm), the sample with dye concentration 0.1 mM also exhibits this nonlinear behaviour. This means that for the same dye concentration, with an increased film thickness, a behaviour similar to that observed in films with higher dye concentration is observed. This can be justified as follows. By increasing the film thickness, the number of interacting dye molecules gets increased, and in effect is similar to the case of increasing dye concentration. For higher dye concentrations, irrespective of film thickness, the plots show non linearity which indicates more complex attenuation mechanisms. In other words, the nature of the attenuation coefficient α in these samples is determined by various parameters such as dye concentration, waveguide thickness and length of propagation through the waveguide. The exact nature of α cannot be fully known from our observations

The optical attenuation in dye doped PMMA waveguides can be due to several factors such as absorption by the dye, absorption by the host material and scattering. Out of these, the main factor contributing to the attenuation is the absorption due to dye molecules. The attenuation of PMMA in the visible wavelength region is very low [34,35] and hence we do not consider the contribution from the host material to the optical attenuation. For rhodamine dyes, the absorption and emission bands overlap, and hence a part of the emitted light is reabsorbed, which gets reemitted at a longer wavelength. As the fluorescence propagates through the sample, the intensity of the peak emission decreases with increasing length. In addition, a red shift in the peak wavelength

is also observed, due to self absorption and reemission as described above. While studying the attenuation mechanisms inside a dye doped waveguide, all these effects should be considered. In such a case, the attenuation coefficient for a particular wavelength $\alpha(\lambda)$ does not remain the same throughout the entire length of propagation – as inferred from our observations – but will be a function of propagation distance z so that ,

$$\alpha = \alpha(z) \qquad \ldots\ldots (4.2)$$

We distinguish the following two cases for optical attenuation coefficient in the waveguide.

Case (i) Only absorption of the pump beam is present inside the waveguide

Light at wavelength λ with initial intensity I_0, will decrease in its intensity with the propagation distance z. Let I be the intensity at any length z. The rate (spatial) at which the intensity decreases due to absorption is,

$$\frac{dI}{dz} = -\alpha_1 I \qquad \ldots\ldots .(4.3)$$

On integrating eqn (4.3), we get the Beer-Lambert's law

$$I = I_0 \exp(-\alpha_1 z) \qquad \ldots\ldots(4.4)$$

where α_1 is the linear absorption coefficient .

From eqn (4.4), we get,

$$\ln I = \ln I_0 - \alpha_1 z \qquad \ldots\ldots(4.5)$$

This provides linear relationship between $\ln I$ and propagation distance z.

Case (ii) Self-absorption and re-emission at λ are present

When there is reemission at λ by the dye molecules due to self-absorption of fluorescence at short wavelength side of the emission spectra, the

expression for $\frac{dI}{dz}$ should be modified. The rate (spatial) at which the intensity decreases due to absorption is $\alpha_1 I$ and the rate (spatial) at which the intensity increases due to reemission is $\alpha_1^{'} I$. Unlike the case of α_1, $\alpha_1^{'}$ is a function of z. i.e., $\alpha_1^{'} = \alpha_1^{'}(z)$.

Taking first order approximation, we write, $\alpha_1^{'} = \alpha_1^{"} z$, so that the "rate equation" can be written as,

$$\frac{dI}{dz} = -\alpha_1 I + \alpha_1^{'} I = \left(-\alpha_1 + \alpha_1^{"} z\right) I \qquad \text{.....(4.6)}$$

On integration we can write , $I = I_0 \exp(-\alpha_1 z + \alpha_2 z^2) = I_0 \exp(-\alpha z)$

where $\alpha = \alpha_1 - \alpha_2 z$ ……(4.7)

From eqn (4.6),

$$\ln I = \ln I_0 - (\alpha_1 - \alpha_2 z) z = \ln I_0 - \alpha_1 z + \alpha_2 z^2 \qquad \text{……(4.8)}$$

The observed nature of ln(I) vs z plots can now be explained on the basis of eqns (4.5) and (4.8). Consider the ln(I) vs z plots for a low dye concentration 0.1 mM (Fig 4.11). For a lower thickness 50µm, the experimental data shows good fit with eqn (4.5). For films with low dye concentration and lower thickness, the effect of re-emission processes on the absorption coefficient is negligible and α is independent of z. (see Fig 4.11a). For the same dye concentration, with increased film thickness, the data could be fitted with 2nd degree polynomial given by eqn (4.8) (fig 4.11b). As the film thickness is increased, the number of interacting dye molecules also got increased, and now the contribution from the re-emission processes becomes pronounced.

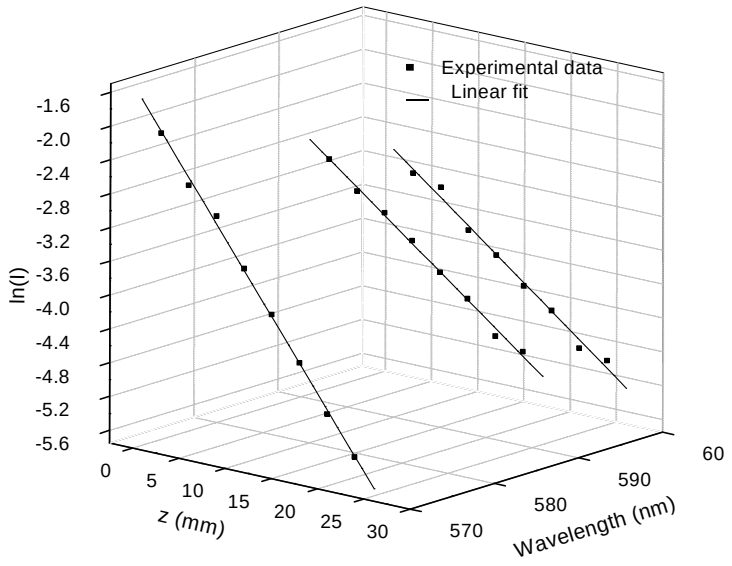

(a)

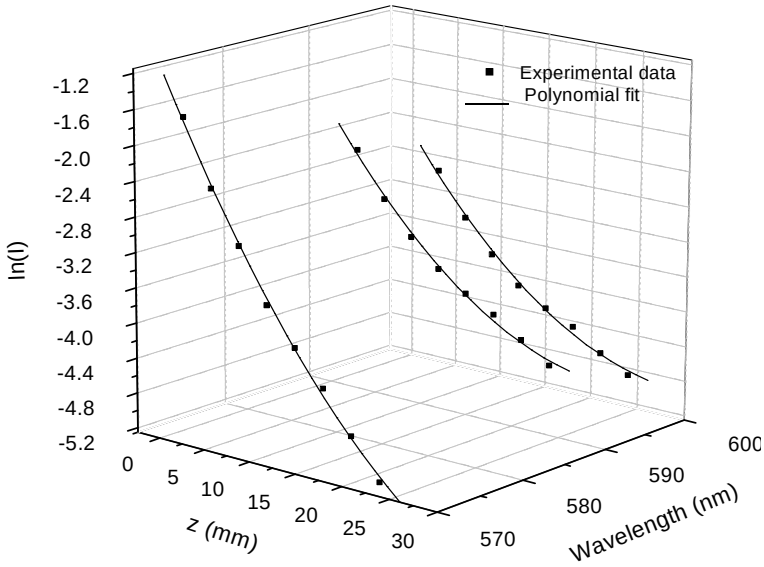

(b)

Fig 4.11 ln(I) vs z plots with linear fits and polynomial fits respectively for film thickness 50 μm (4.11a) and 135 μm(4.11b) for dye concentration 0.1 mM

For higher dye concentrations, irrespective of film thickness, the observed data on fluorescence emission as a function of z shows a good match with equation (4.8), supporting the existence of a space dependent attenuation coefficient. Fig 4.10 shows the experimental data fitted with a 2nd degree polynomial in z for wavelengths 590nm, 600nm and 610 nm for waveguide thickness 50 microns and at a dye concentration 1mM .

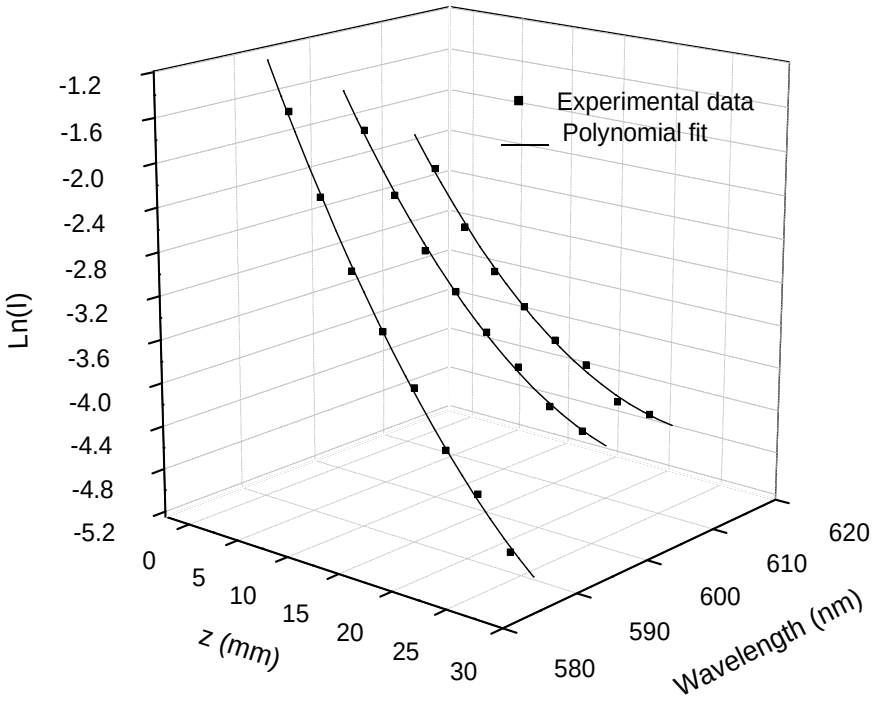

Fig 4.10 Polynomial fit for ln(I) vs z plots for 50 μm thick waveguide with dye concentration 1mM

Fig 4.12 shows the values of α_1 at various wavelelengths for the samples with different dye concentrations and thickness

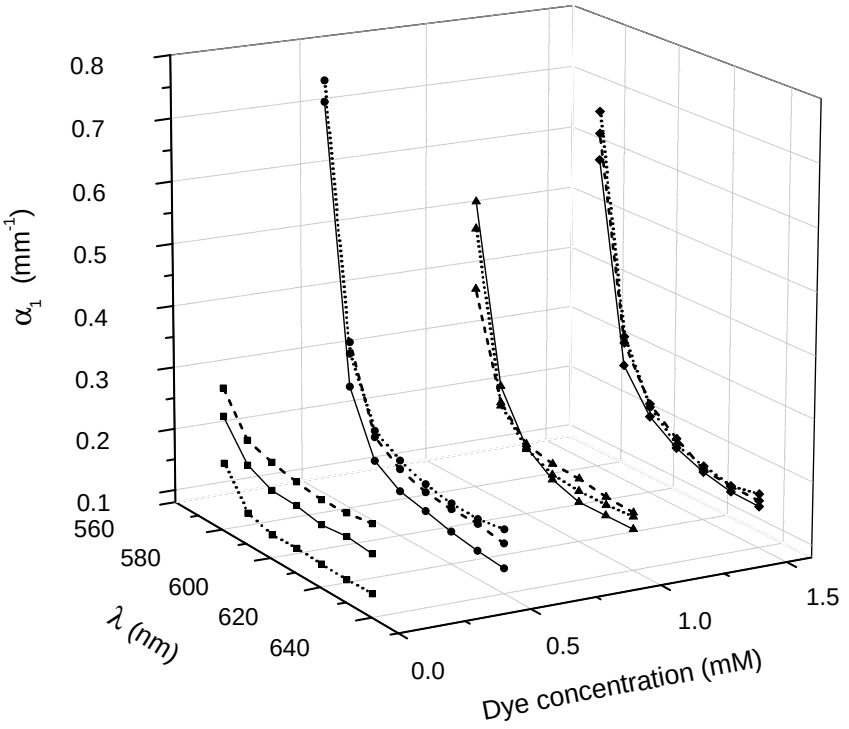

Fig 4.12 Absorption coefficient α_1 as a function of wavelength for various dye concentrations and thickness . ….. 50 μ ------ 115 μ ——— 135 μ

In the case of films with lowest dye concentration, the coefficient α_1 shows variation with film thickness. For higher dye concentrations we note that the film thickness has got negligible effect on α_1 as observed by other workers in dye doped fibres with different core diameters [36].

Fig 4.13 shows the variation of α_2 with wavelength for various dye concentrations and thickness . Note that for film with dye concentration 0.1 mM and thickness 50 μ m, $\alpha \cong \alpha_1$.

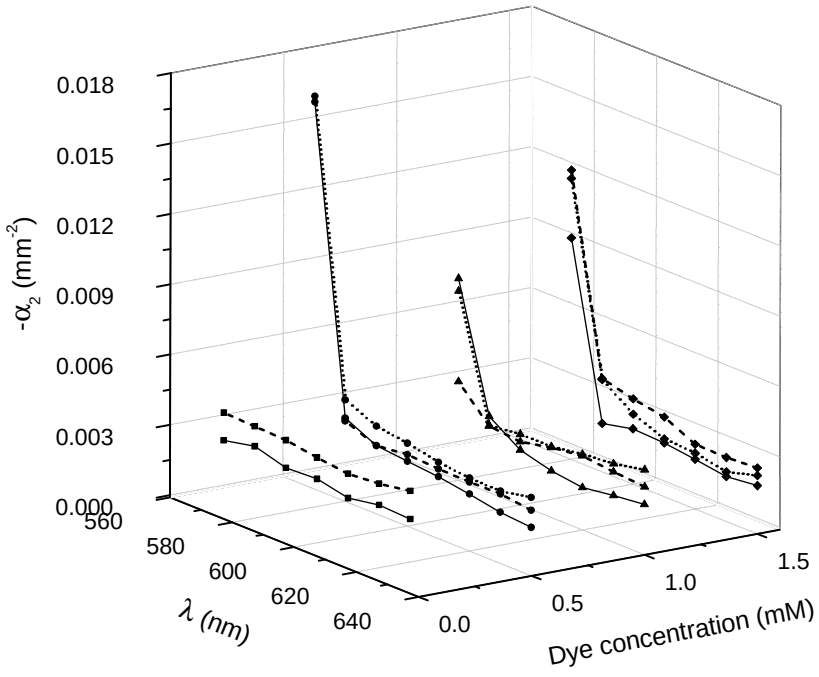

Fig 4.13 Space dependent term of absorption coefficient α_2 as a function of wavelength for various dye concentrations and thickness
. ….. 50 μ ------ 115 μ ——— 135 μ

Thus we see that, for dye doped waveguides – especially when there is an overlap between the absorption and emission bands – the attenuation cannot be fully defined by the usual Beer-Lambert's law. Due to several complex

interactions between the dye molecules and the propagating light, the attenuation coefficient gets modified with propagation distance and hence can be expressed as a function of propagation distance. In such waveguides, a space dependent attenuation coefficient will explain the observed attenuation mechanisms especially at higher dye concentrations.

4.6 Conclusions

In this chapter, we have discussed the fabrication and characterization of rhodamine 6G doped polymethyl methacrylate film waveguides. The absorption and front surface fluorescence emission of the fabricated films were recorded. The attenuation in the waveguides was characterized by a non-destructive side illumination fluorescence technique. We observed that the attenuation mechanisms in a dye doped waveguide – especially for the dyes having an overlap between the absorption and emission spectra – can be explained only with a space dependent attenuation coefficient. In such cases, the transmitted light will not strictly obey the conventional Beer-Lambert's law.

References

1. P.P. Sorokin and J.R. Lankard, *IBM J. Res Develop* **10**, 162-163 (1966).
2. B.H. Soffer, B.B. Mc Farland, *Appl. Phys. Lett* **10**, 266-267 (1967).
3. O.G. Peterson, B.B. Snavely, *Appl. Phys. Lett* **12** (7), 238-240(1968).
4. A. Costela, I. Garcia-Moreno, J. M. Figuera, F. Amat-Gueria and R. Sastre, *Laser Chem.* **18**, 63-84 (1998).
5. A. Costela, I. Garcia-Moreno, C. Gomez, O. Garcia and R. Sastre, *J. of Appl. Phys* **90**(7), 3159-3166 (2001).
6. D. Lo, J.E. Parris, J.L. Lawless, *Appl. Phys. B* **55**, 365-367 (1992).
7. Y. Sorek, R. Reisfeld, I. Finkelstein and S. Ruschin, *Appl. Phys. Lett.* **66**(10), 1169-1171 (1995).

8. A. Costela, F. Florido, I. Garcia-Moreno, F. Amat-Guerri, J.M. Figuera and R. Sastre, *Appl. Phys. B* **60**, 383-389 (1995).
9. F. Lopez Arbeloa, T. Lopez Arbeloa, I. Lopez Arbeloa, A. Costela, F. Florido, I. Garcia-Moreno, J.M. Figuera, F. Amat-Guerri and R. Sastre, *Appl. Phys. B* **64**, 651-657 (1997).
10. A. Costela, I. Garcia-Moreno, J.M. Figuera, F. Amat-Guerri, R. Mallavia, M. D. Santa-Maria and R. Sastre, *J. of Appl. Phys* **80**(6), 3167-3173 (1996).
11. Kwong-Cheong Yee, Teck-Yong Tou, Seik-Weng Ng, *Appl. Opt* **37**(27), 6381-6385 (1998).
12. A.V. Deshpande and E.B. Namdas, *Appl. Phys. B* **64**, 419-421 (1997).
13. Seong-Shan Yap, Wee-Ong Siew, Teck-Yong Tou and Seik-Weng Ng, *Appl. Opt* **41**(9), 1725-1728 (2002).
14. M.G. Kuzyk, D.W. Garvey, S.R. Vigil, D.J. Welker, *Chemical Physics* **245**,. 533-544 (1999).
15. Mark G. Kuzyk, Dennis W. Garvey, Brian K. Canfield, Steven R. Vigil, David J. Welker, Jeff Tostenrude, Chris Breckon, *Chemical Physics* **245**, 327-340 (1999).
16. G. D. Peng, P.L. Chu, Z Xiong, T.W. Whitbread, R.P. Chaplin, *J.Lightwave Technology* **14**(10), 2215-2223 (1996).
17. A. Tagaya, S. Teramoto, T. Yamamoto,K. Fujii, E. Nihei, Y. Koike, K. Sasaki, *IEEE J.of Quantum Electronics*, **31**(12), 2215-2220 (1995).
18. Akihiro Tagaya, Shigehiro Teramoto, Eisuke Nihei, Keisuke Sasaki, Yasuhiro Koike, *Appl. Optics* **36**(3), 572-578 (1997).
19. Vincent Dumarcher, Licinio Rocha, Christine Denis, Celine Fiorini, Jean-Michel Nunzi, Frank Sobel, Bouchta Sahraoui, Denis Gindre, *J.Opt. A: Pure Appl. Opt* **2,** 279-283 (2000).
20. D.J. Welker, M.G. Kuzyk, *Appl. Phys .Lett* **69**(13), 1835-36(1996).
21. R. J. Kruhlak, M.G. Kuzyk, *J. Opt. Soc. Am. B* **16**(10), 1749-1755(1999).
22. K Geetha , M Rajesh, V P N Nampoori, C P G Vallabhan and P Radhakrishnan, *J. Opt. A: Pure Appl. Opt.* 6 , 379–383 (2004).
23. Akihiro Tagaya, Shigehiro Teramoto, Elsuke Nihei, Keisuke Sasaki, Yasuhiro Koike, *Appl. Optics* **36**(3), 572-578(1997).
24. Ken Kuriki, Takeyuki Kobayashi, Nana Imai, Toshihiko Tamura, Susumu Nishihara, Yukihisa Nishizawa, Akihiro Tagaya, Yasuhiro Koike, Yoshi Okamoto, *Appl. Phys. Lett.*, **77**(3), 331-333 (2000).
25. Xiao-lei Zhu, Dennis Lo, *Appl. Phys. Lett,* **80** (6) , 917-919 (2002).
26. Alexander Argyros, Martijn A. van Eijkelenborg, Stuart D. Jackson, Richard P. Mildren, *Opt. Lett* **29**(16) , 1882-1884 (2004).
27. F.P. Shäfer (Ed.), Dye Lasers, Topics in Applied Physics Volume 1, Springer-Verlag, Berlin Heidelberg, 1990
28. F.L. Arbeloa, P.R. Ojeda, I.L. Arbeloa, *J. Photochem. Photobio A* **45**, 313 (1988).
29. I.L. Arbeloa, *J. Chem. Soc. Faraday Trans II* **78**, 989 (1982).

30. D.W. Garwey, K. Zimmerman, P. Young, J. Tostenrude, J.S. Townsend, Z. Zhou, M. Lobel, M. Dayton, R. Wittorf and M.G. Kuzyk , *J.Opt.Soc.Am.B* **13**(9), 2017-2023 (1996).
31. Toshikuni Kaino, *J.Opt.A:ure Appl.Opt* **2** ,R1-R7 (2000).
32. R.J. Kruhlak, M.G. Kuzyk, *J.Opt.Soc.Am. B* **16**(10), 1756-1767 (1999).
33. E. De La Rosa-Cruz, C.W. Dirk, O. Rodriguez and V.M. Castano, Fiber and Integrated Opt. **20**(5), 457-464 (2001).
34. C. Koeppen, R.F. Shi, W.D. Chen, A.F. Garito, *J. Opt. Soc. Am. B* **15**(2), 727-739 (1998).
35. G. D. Peng, P.L. Chu, SMIREE, X. Lou, R.A. Chaplin, *J. Electrical and Electron. Engg, Australia-IE Aust & The IREE Society* **15**(3), 289-296 (1995).
36. Robert J. Kruhlak, Characterization of molecular excited states for nonlinear optics , PhD Thesis, Washington State University (2000).

5

Amplified spontaneous emission in dye doped planar waveguides

The observation of Amplified Spontaneous Emission (ASE) from dye doped planar waveguides of various thicknesses and dye concentrations is discussed in this chapter. Optical gain characterization was done by a variable stripe length method widely used for both organic and inorganic materials prepared in a slab geometry. The propagation characteristics of ASE through the waveguide and tunability of ASE are also discussed.

5.1 Introduction

One of the fundamental quantities of importance for a laser medium is its optical gain. Simple measurements of emission in highly excited systems with gain are difficult to interpret since emission is geometry dependent and not directly related to fundamental parameters. Under lasing conditions, further complications are introduced by the coupling of molecular emission to optical cavity modes. A useful and convenient method of measuring gain is based on measurements of amplified spontaneous emission (ASE). This technique was first demonstrated in 1970 by Silfvast and Deech [1] for high gain pulsed metal vapour lasers. Shank ***et al*** modified this for pulsed dye lasers [2]. ASE is a phenomenon where the spontaneously emitted light gets amplified as it propagates along the gain medium and even without the feedback of the emitted radiation.

In this chapter, we discuss our observation of ASE from dye doped planar waveguide strucutures of various thicknesses and dye concentrations. Gain characterization was done by a variable stripe length method widely used for both organic and inorganic materials prepared in a slab geometry [3,4]. The cross section of the pump beam was in the form of a stripe. The optical gain in each sample is studied by the relation between the pump length and ASE intensity. We also discuss the propagation characteristics of ASE through the waveguide. This was done by shifting the position of the excitation stripe in such a way that the ASE from the end of the pump stripe is guided along different lengths of the waveguide.

For most dyes, the absorption and emission bands overlap and the short wavelength fluorescence is reabsorbed. For such dyes the observed fluorescence peak is shifted to longer wavelengths at higher concentrations. Thus, wavelength tuning can be achieved by changing the dye concentration [5]. Similar red-shift was observed for the spectra taken from transversely

pumped dye-doped fibres and waveguides when the excitation spot position was shifted along the length of the fibre/waveguide by translating either the source or the waveguide [6-8]. Using a similar technique, we investigated the wavelength tuning in a transversely pumped Rh6G doped PMMA film waveguide by observing the wavelength changes of ASE.

5.2 Amplified Spontaneous Emission

Any gain medium can amplify not only the input field from a laser oscillator or any other source, but also the spontaneous radiation emitted by the excited molecules of the amplifier itself. The ASE cascade of emission from dye molecules in the excited state is stimulated by the spontaneous emission from other molecules' decay from an excited state. ASE is not, then, a purely spontaneous phenomenon, but spontaneously emitted photons that are amplified by further coherent stimulated emission. The emitted photons will be of the same frequency centred around the wavelength of maximum gain. In materials with high gain, the laser- like amplified spontaneous emission (ASE) occurs without the aid of multiple pass gain build up in a cavity with mirrors. It requires relatively high pump powers in the single pass gain geometry. A signature of amplified spontaneous emission is gain narrowing of the fluorescence spectrum. As the pump intensity increases the spectrum changes from a normal fluorescence to pure ASE. The direction of ASE is perpendicular to the direction of polarization of the incident intensity.

5.3 Gain measurement

The ASE theory starts with a one dimensional approximation [3], describing the rate of change of fluorescence intensity with length of the pumped region as,

$$\frac{dI}{dz} = AP_0 + gI \qquad \text{……(5.1)}$$

where I - Fluorescence intensity propagating along the Z-axis.

AP_0 - Spontaneous emission proportional to pump intensity

g - net gain given by $g' - \alpha$ where g' is the gain due to stimulated emission and α is the optical loss

l - length of the pumped region

The solution of eqn. (5.1) with respect to pump length is

$$I_l = \frac{AP_0}{g}\left[\exp(gl) - 1\right] \qquad \text{……(5.2)}$$

Shank et al [2] measured the single pass gain of dye laser by comparing the intensities of ASE in single and double cell lengths. By writing an equation similar to that of eqn. (5.2) for a pump stripe of length $l/2$, we get

$$I_{l/2} = \frac{AP_0}{g}\left[\exp(g\,l/2) - 1\right] \qquad \text{……(5.3)}$$

From equations (5.2) and (5.3), the net gain can be obtained as,

$$g = \frac{2}{l}\ln\left[\frac{I_l}{I_{l/2}} - 1\right] \qquad \text{… ..(5.4)}$$

5.4 Experiment

Experiments were conducted on free standing thin films of poly methyl methacrylate (PMMA) doped with Rhodamine 6G. Details of sample

preparation are given in Chapter IV. We conducted experiments on films with dye concentrations, 0.5 mM, 1mM and 1.5 mM. Experimental results presented here are for samples with $50\,\mu$m thickness, unless otherwise specified. The samples were transversely pumped using 10ns pulses from a frequency doubled Nd:YAG laser (532 nm, 10Hz). A set of calibrated neutral density filters were used for varying the pump energy. The beam was focused into a narrow stripe of approximately 50 microns width. The stripe length was varied using an adjustable slit.

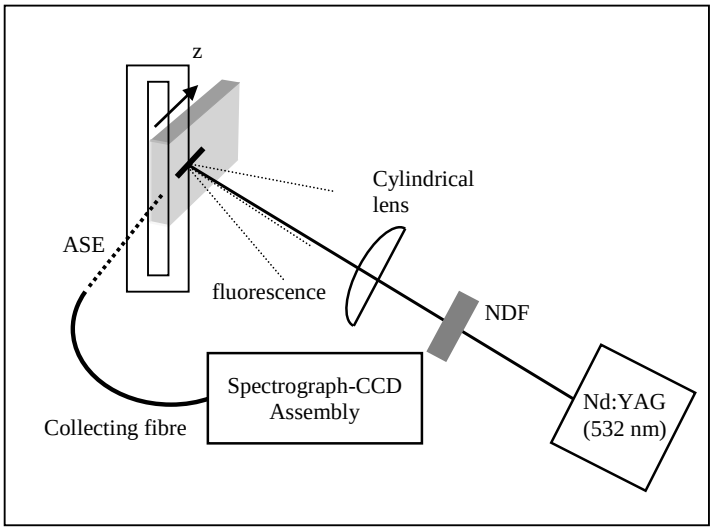

Fig 5. 1 Excitation and light collecting schemes

When ASE occurs in a long narrow stripe, most of the light is emitted at the ends of the stripe. The emission from the sample was collected by a fibre and directed to a 0.5 m spectrograph (SpectraPro-500i) coupled with a cooled CCD array. The distance between the collecting fibre and the waveguide edge was 1cm. A slit was kept infront of the fibre so that only the axially confined modes are collected. The sample was kept on a translator so

as to enable horizontal shifting of the excitation stripe along the length of the waveguide. We first placed the pump stripe right upto the edge of the film (z=0) and recorded the emission spectra for various pump energies. Then the stripe position was shifted, thereby varying z - the distance between one end of the pump stripe and the observation edge of the film. (Fig 5.1) Observations were made with excitation stripe lengths 2mm, 4mm and 6mm.

5.5 Results and Discussions

5.5.1 Observation of ASE

First we recorded the emission spectra for z=0, at various pump intensities with a constant pump stripe of length 2mm. (fig 5.2).

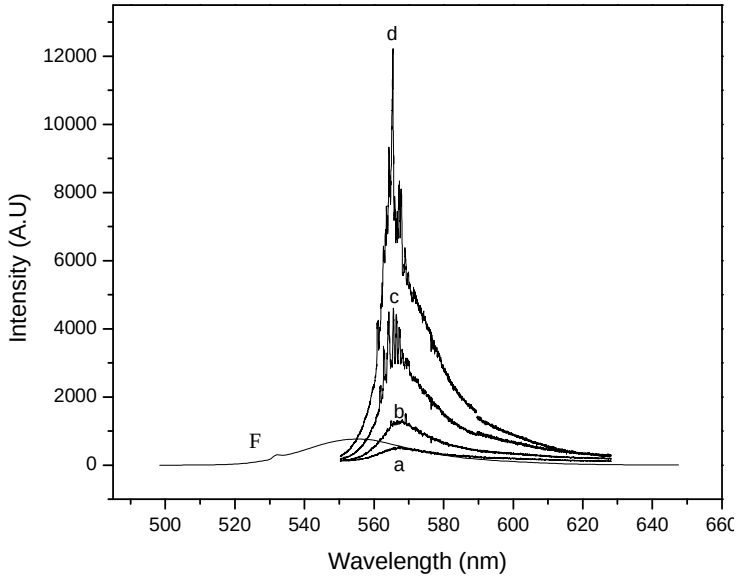

Fig 5.2a : Emission from the waveguide edge for stripe length 2mm at various pump energies for a dye concentration 0.5 mM (a) 0.10 mJ/pulse (b) 0.31 mJ/pulse (c) 1 mJ/pulse (d) 9.1 mJ/pulse

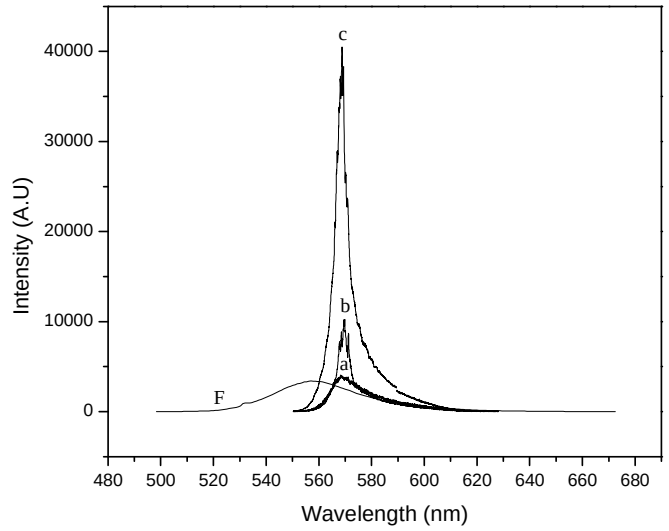

Fig 5.2b : Emission from the waveguide edge for stripe length 2mm at various pump energies for a dye concentration 1 mM (a) 0.7 mJ/pulse (b) 2.2 mJ/pulse (c) 6.4 mJ/pulse In the case of (a) the Y-axis is scaled by multiplying with 5

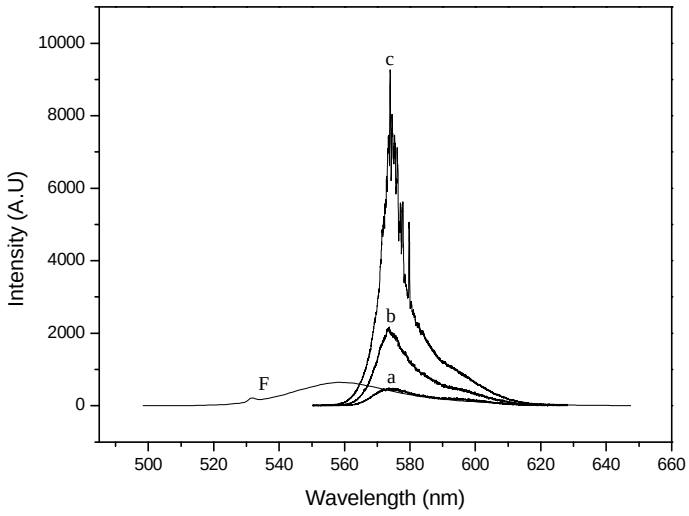

Fig 5.2c : Emission from the waveguide edge for stripe length 2mm at various pump energies for a dye concentration 1.5 mM (a) 0.126mJ/pulse (b) 0.4mJ/pulse (c) 1.26mJ/pulse

In all the above figures 'F' represent the front surface fluorescence emission. As observed from figures 5.2a, 5.2b and 5.2c, at low pump energies, the emission spectrum is broad. But above the pump energy 0.31mJ/pulse, the peak of the spectrum at around 565 nm grew strongly for the sample with dye concentration 0.5 mM. At E=9.1 mJ/pulse, a narrow spectrum centered at 565.4 nm with a FWHM of only ~ 5 nm was obtained. For the sample with dye concentration 1mM, a narrow peak at 569.8 nm with FWHM 4.8nm was obtained with pump energy 2.2 mJ/pulse. When the pump energy was further increased to 6.4 mJ/pulse, the peak intensity increased by nearly 4 times that of the former case. But there was a slight increase in the FWHM. The enhancement in the linewidth at higher pump energies is due to the enhancement in gain at larger wavelengths . The peak was obtained at 568.8 nm. For dye concentration 1.5 mM, we got a narrow spectrum with linewidth 5.2 nm at pump energy 1.26 mJ/pulse. The peak emission wavelength was observed to be at 573.9 nm. Details are given in table 5.1.

Dye concentration : 0.5 mM		*Dye concentration : 1.0 mM*		*Dye concentration : 1.5 mM*	
Pump Energy mJ/pulse	FWHM (nm)	Pump Energy mJ/pulse	FWHM (nm)	Pump Energy mJ/pulse	FWHM (nm)
0.03	>50	0.07	21.5	0.04	31
0.10	24.1	0.22	18.8	0.126	17
0.31	18.7	0.7	14.7	0.4	11.9
1.0	10.7	2.2	4.8	1.26	5.2
3.1	8.1	6.4	5.1		
9.1	5.1				

Table 5.1 Spectral widths at various pump energies for pump stripe length 2mm

Spectral narrowing of the emitted radiation can be due to several reasons. A variable stripe length method was used to confirm whether the phenomenon responsible for spectral narrowing is ASE. If ASE occurs, spectra should be broad at short stripe lengths and should narrow as the excitation length increases [4,9].

For all the 3 dye concentrations specified above, we recorded the spectra for stripe lengths 2mm, 4mm and 6mm at various pump powers . Figure 5.3 shows a representative plot for the dye concentration 0.5 mM.

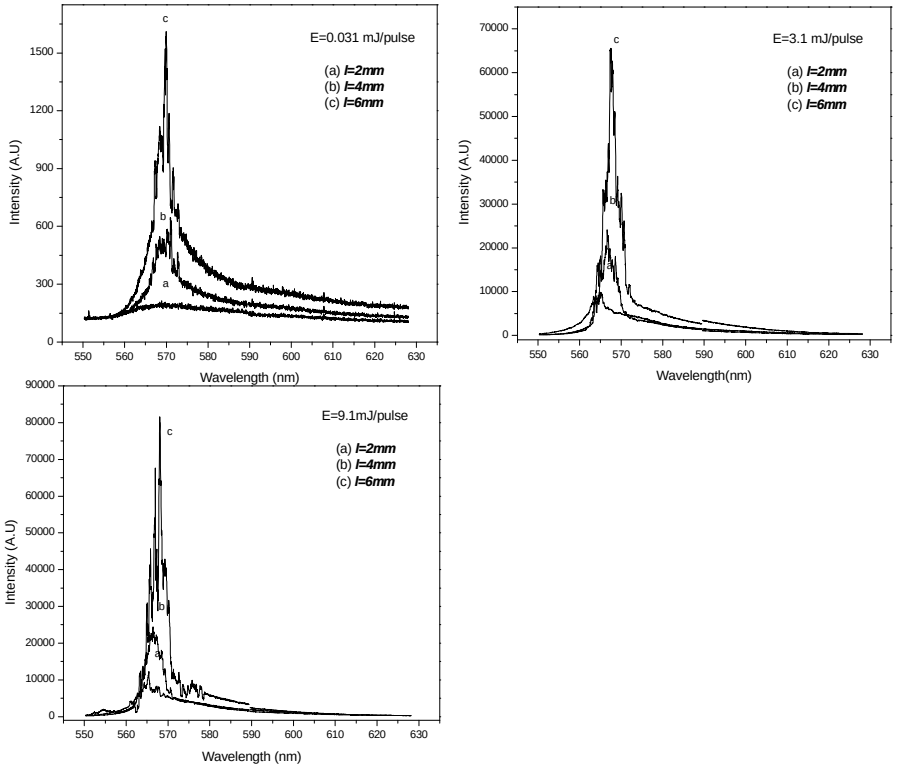

Fig 5. 3. Spectral narrowing with increase in stripe length for various pump Energies (Dye concentration : 0.5 mM)

As the pump stripe length increased, the threshold moved to lower energies. Also, for a given pump energy, the FWHM reduced when stripe length increased from 2mm to 4mm. (see Table 5.2), with a slight shift in the peak wavelength. We also see a slight increase in the linewidth with further increase in stripe length, due to enhanced gain at longer wavelengths too. Enhanced stripe length increases number of molecules interacting with the pump beam. At higher stripe lengths, additional emission like T→T (triplet-triplet) or between states of weakly fluorescing dimers may result into enhanced FWHM.

Dye concentra-tion (mM)	Pump Energy (mJ/pulse)	FWHM (nm)		
		$l = 2mm$	$l = 4mm$	$l = 6mm$
0.5	3.1	8.1	5. 6	2.5
1	0.22	18.8	3.6	6.2
1.5	0.4	11.9	5.4	6.1

Table 5.2. FWHM of spectral emission for various pump energies and beam stripe lengths

5.5.2 Gain measurement from ASE spectra

For g proportional to pump power, then for pump power such that $g > l^{-1}$, eqn. (5.2) indicates that the stimulated emission intensity will increase exponentially. Below this input power, the intensity variation will be less than exponential. This change in power dependence gives rise to a characteristic break point in the output intensity as a function of input power [3]. At the highest input powers, saturation occurs, since the amplified light is large enough to deplete a significant fraction of excited states.

Figure 5.4 gives a typical plot showing the dependence of the light intensity emitted from the edge, integrated over all wavelengths, on the pump energy. The sample dye concentration was 1 mM .

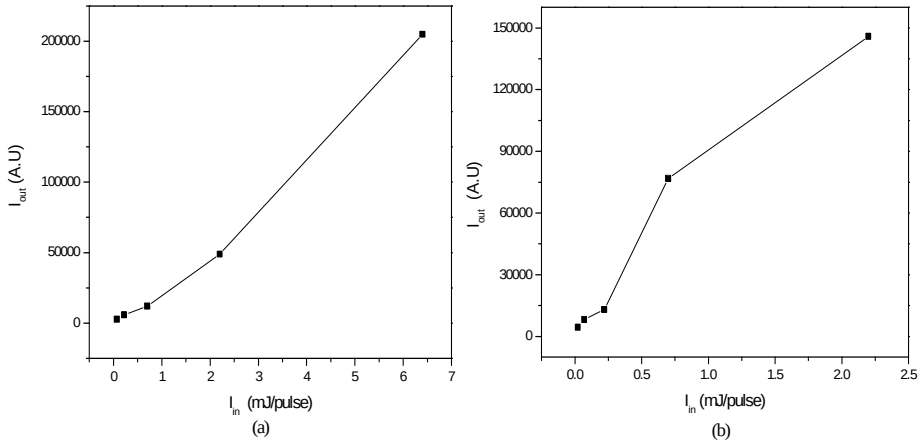

Fig 5.4 . Total emission intensity integrated over all wavelengths vs pump energy for pump stripe lengths (a) 2mm (b) 4mm

Equation (5.4) applies only for pump powers upto the onset of saturation. The gain was calculated for pump energies 0.31 mJ/pulse, 0.7 mJ/pulse and 0.4 mJ/pulse respectively for the samples with dye concentrations, 0.5 mM, 1.0 mM and 1.5 mM. Figure 5.5 shows the wavelength versus gain plots for 50 μm thick waveguides with various dye concentrations. The wavelength for maximum gain shifted to red as dye concentration was increased. We also observe a wider gain band width for higher dye concentration.

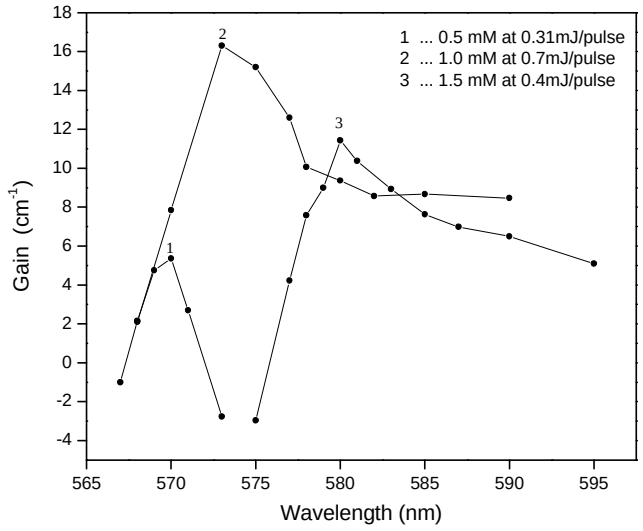

Fig 5.5 Wavelength vs gain plots for various dye concentratins

.

We also studied the thickness dependence on the gain. (figure 5.6)

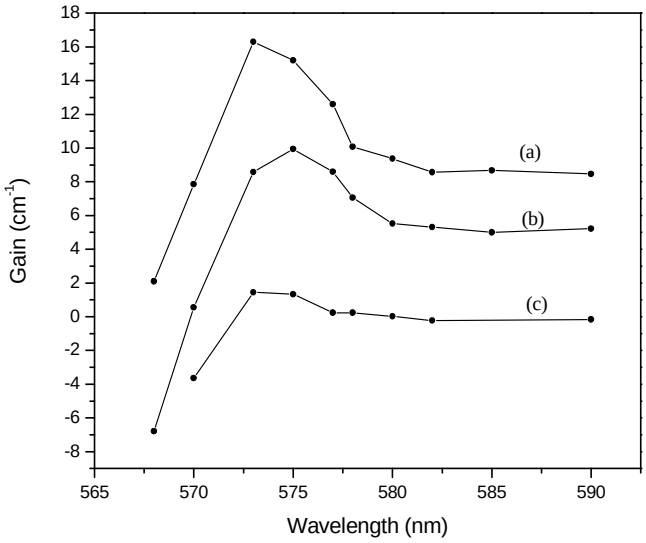

Fig 5.6 Wavelength vs gain plots for dye concentration 1mM at pump power 0.7mJ/pulse , for film thickness (a) 50 μ m (b) 115 μ m(c) 135 μ m

The maximum gain was obtained for the smallest thickness 50 μm. At higher thickness, the planar structure of the waveguide will be nearer to that of bulk medium which will reduce the gain with respect to that of thin film structure.

5.5.3 ASE propagation through the waveguide and wavelength tunability

It is well-known that by varying dye concentration, wavelength tuning can be attained in dye lasers [5]. For rhodamine 6G, there is a spectral region of overlap between the absorption and emission bands. As a result, the short wavelength emission from the dye molecules gets absorbed by themselves and is re-emitted at a longer wavelength. Due to this self-absorption and re-emission process, the peak emission wavelength shows a red-shift with increase in concentration [5]. This property is utilized in the concentration dependent tuning of the emitted wavelength. Increasing the pathlength through the dye doped sample is somewhat similar to an increment in dye concentration. A similar redshift was observed when the pathlength through the waveguide/fibre was increased [6-8].

When irradiated with a narrow stripe, the ASE will be maximum at the stripe ends, along a transverse direction. We changed the position of the excitation stripe by translating the waveguide horizontally across the exciting beam. Now, the ASE emitted at the end of the stripe was made to traverse through the sample. By shifting the position of the exciting stripe, we varied the propagation length of the emission through the waveguide. Emitted light was collected exactly in a similar manner for the case z=0. Fig 5.7 shows the spectra obtained for various z values at a pump energy 9.1mJ/pulse for various stripe lengths for a sample with dye concentration 0.5 mM.

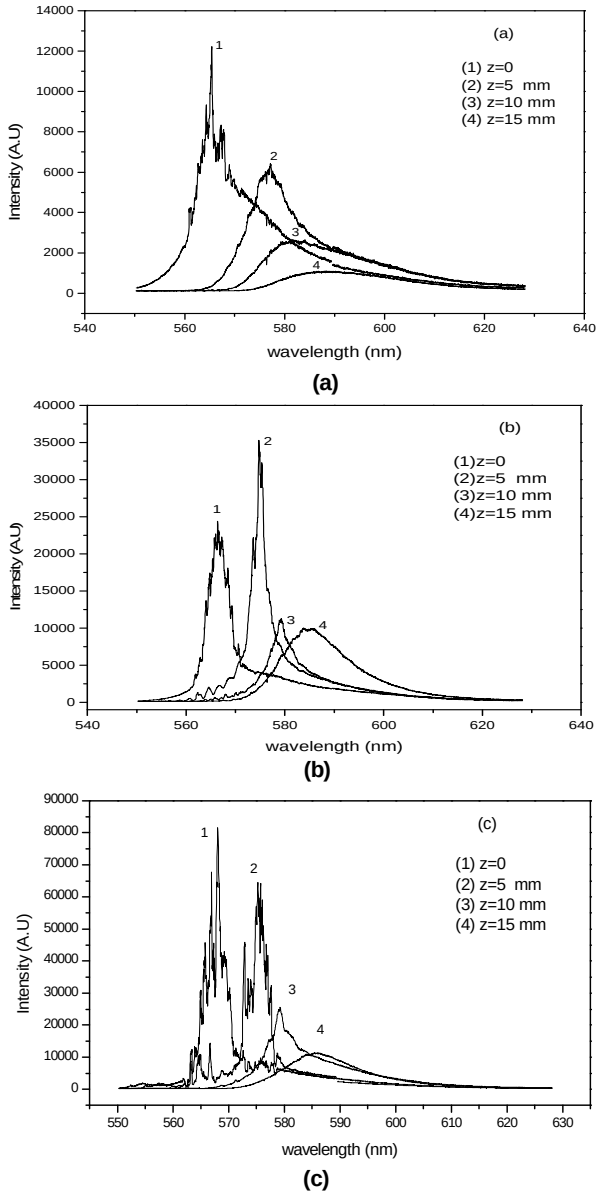

Fig 5. 7 Evolution of ASE as it is guided through various lengths through the waveguide for stripe lengths (a) $l = 2mm$ (b) $l = 4mm$ (c) $l = 6mm$ for pump energy 9.1 mJ/pulse (Dye concentration : 0.5 mM).

We observed a red-shift of the emission peak with increase in length of propagation. Even after propagation through the sample, we got a narrow emission spectrum, especially for longer stripe lengths.

For a stripe length of 2mm, we got narrow emission peaked at 565.4 for propagation distances z=0 and at 577.2 nm for z=5mm. Thus the peak wavelength could be tuned over 12 nm . The spectral width increased from 5nm to 11nm when z changed from 0 to 5mm. For further propagation lengths, the emission became broad and ASE character of the emission was lost. With longer pump stripe lengths, we got narrow emission even for z=15mm. ASE could be tuned from 566.6 to 585.4 and 568.1 to 586.1 for stripe lengths 4mm and 6mm respectively. The tunability range thus got enhanced. A tunability of around 19 nm was obtained for stripe length of 4mm as z varied from 0 to 15mm. It should also be noted that during the tuning the spectral width generally increased upto 16 nm. Table 5.3 shows the details of wavelength tuning for a pump stripe of length 4mm, for 3 different dye concentrations.

Dye concentration (mM)	Pump Energy (mJ/pulse)	Variation in *z* (mm)	Variation in *FWHM* (nm)	Tuning range (nm)	Tunability (nm)
0.5	9.1	0-15	4.6 - 15.8	566.6 - 585.4	18.8
1	2.2	0-15	4.6 - 13.4	571.5 - 590.8	19.3
1.5	1.26	0-15	5.4 - 15.8	579.3 - 592.9	13.6

Table 5.3 FWHM and peak wavelength for different ‘z’ values for a pump stripe length 4 mm

We note that maximum gain and tunability is obtained with dye concentration 1mM. For an increased dye concentration (1.5 mM), the gain as well as the tunability gets reduced. This can be attributed to the well-known concentration quenching of fluorescence emission for dyes. From the fluorescence emission spectra of these samples, we have observed quenching of fluorescence emission from the film with dye concentration 1.5 mM. (see fig 4.4a in Chapter 4). For the same sample we also observed that the saturation behaviour of the redshift with propagation distance is pronounced. (see fig 4.6b in Chapter 4).

Conventionally, wavelength tuning is achieved by the use of distributed Bragg reflectors as coupling mirrors in resonant cavities [10]. In external cavity solid state lasers, wide-range wavelength tuning has been achieved by the use of grating as the dispersion element. A tunability of around 53 nm was obtained with a multiple prism-grating solid state dye laser where the gain medium was a rhodamine 6G (Rh6G) doped modified PMMA with trapezoidal geometry [11]. Multimode lasing and wide band tuning in sol-gel distributed feed back waveguide lasers have also been reported [12-14]. In these lasers tuning was achieved either by varying the period of gain modulation [12,13] or by varying the temperature of the gain medium, thereby varying its refractive index [14]. By the first method, a tunability of more than 30 nm was achieved. By the latter method, with a Rh6G doped sol-gel silica waveguide, 17nm tunability was obtained by varying the temperature from 21^0C to 58^0C while with Rh6G doped PMMA waveguide, 6nm tunability was obtained by varying temperature from 22^0C to 98^0C.

A technique for tuning the ASE wavelength by controlling the waveguide thickness has been reported for conjugated polymer films [15] as well as for dye-doped solid state waveguide[16]. A wide range tunability of around 30 nm was observed in these two cases.

The main advantage of the present technique is that no bulk optics are used for tuning. By simultaneous spectral measurement from both ends of the pumped waveguide for different positions of the pump stripe along the waveguide, simultaneous tuning of dual wavelength emission can also be achieved.

One of the important points to be noted is that the intensity at longer wavelengths of the ASE got amplified on traversing through the waveguide. Output intensity at shorter wavelengths showed the usual exponential decrease. Fig 5.8 shows the variation of output intensity at different wavelengths with propagation length through the waveguide.

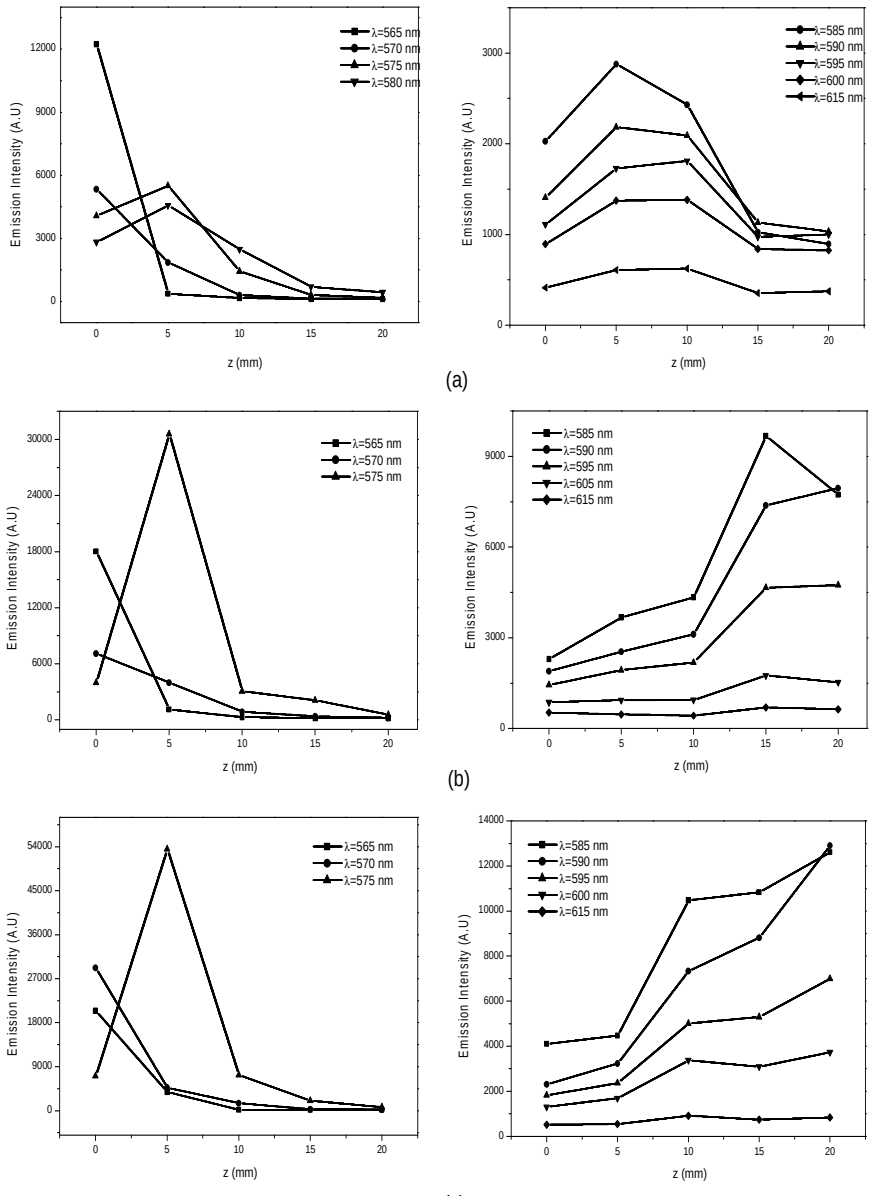

Fig. 5.8 Emitted power at various wavelengths vs propagation length through the waveguide for stripe lengths (a) $l = 2mm$ (b) $l = 4mm$ (c) $l = 6mm$ for pump energy 9.1 mJ/pulse

As can be clearly seen from the figure, as the propagation distance z increases, emission intensity showed enhancement in intensity in the long wavelength region. This is due to the gain in the long wavelength region due to reemission as well as due to gain achieved as the radiation is propagated through the amplifying medium. Such emission enhancement became prominent as the stripe length of the pump beam was increased. Increase in the stripe length enhances the interaction length between the pump radiation and the dye molecules. This will result in gain in the spectral emission in addition to the gain due to reemission in the long wavelength region. Propagation characteristics of emitted radiation through the waveguide cannot be described by the usual Lambert-Beer law with single attenuation or gain coefficient. Due to complex interactions between the radiation and dye molecules in the gain media, one has to describe a space dependent attenuation and gain coefficient.

5.5.4 Photostability

The analysis of the changes in the emission spectrum as a function of irradiation time, gives information regarding the photostability of the samples. The intensity of the ASE from the samples decreased with the number of pump pulses in a far from linear fashion (see fig 5.9). The solid lines are the best fits for the nonlinear curves. This type of behaviour was explained to be due to complex photothermal mechanisms of dye degradation [17,18].

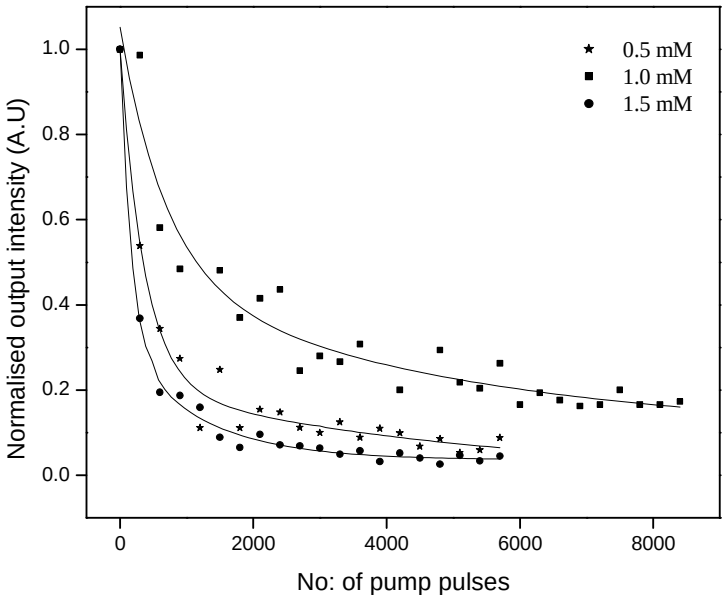

Fig 5.9 Emitted intensity as a function of the number of pump pulses for Rh6G doped 50 µm thick PMMA film waveguides with various dye concentrations. Laser pump energy and repetition rate : 3.6 mJ/pulse and 10 Hz respectively

Number of pulses that produce a 30% drop in the output intensity are 670, 2900 and 380 for dye concentrations 0.5mM, 1mM and 1.5 mM respectively as obtained from the fitted curves. Out of the three dye concentrations under study, highest photostability was obtained for the sample with 1mM dye concentration. The highest optical gain was also achieved with this dye concentration. Several previously reported works discuss the apparent direct relationship between lasing efficiency and photostability [17-21]. The higher the efficiency, the lower the rate of degradation. The gain enhances with concentration (due to increase in the number of molecules taking part in the interaction). However there is a competing phenomena with increase in concentration due to collisional energy exchange causing enhancement in

bleaching. This results into possible optimum concentration at which gain and stability is maximum. In the present case, it is about 1mM.

5.7 Conclusions

We have characterized the gain in the dye doped planar waveguide structures by ASE measurement technique. Measurements were done for samples with dye concentrations 0.5mM, 1mM and 1.5 mM. Maximum gain (16.8 cm^{-1} at 573 nm) was obtained for a 50 μm thick waveguide with dye concentration 1mM. We have studied the propagation characteristics of amplified spontaneous emission through the transversely pumped films. With increase in propagation length through the waveguide, the emission peak showed a red-shift due to self-absorption and re-emission by the dye molecules. As the radiation propagated through the amplifying medium, spectrally narrow output at longer wavelengths was obtained due to the gain achieved at these wavelengths. Thus we could tune the ASE wavelength. The maximum tunability obtained by this method was ~19 nm .

References

1. W.T. Silfvast, J.S. Deech, *Appl. Phys. Lett* **17**, 97-99 (1970).
2. C. V. Shank, A. Dienes, W.T. Silfvast, *Appl. Phys. Lett* **17**, 307-309 (1970).
3. K.L. Shaklee, R.F. Leheny, *Appl. Phys. Lett* **18** (11), 475-477 (1971).
4. Michael D. McGehee, Rahul Gupta, Siegfried Veenstra, E. Kirk Miller, Maria A. Diaz-Garcia, Alan J. Heeger, *Phys. Rev. B* **58** (11), 7035-7039 (1998).
5. F.P. Shäfer (Ed.), Dye Lasers, Topics in Applied Physics Volume 1, Springer-Verlag, Berlin Heidelberg (1990).
6. R.J. Kruhlak, M.G. Kuzyk, *Linear Optical Properties of Waveguides and Fibers*, Proc. SPIE **3799**, 312-319 (1999).
7. E. De La Rosa-Cruz, C.W. Dirk, O. Rodriguez and V.M. Castano, *Fiber and Integrated Opt.* **20**(5), 457-464 (2001).
8. K. Geetha, M. Rajesh, C.P.G. Vallabhan, V. P.N. Nampoori and P. Radhakrishnan, *J. Opt. A: Pure Appl. Opt*. **6,** 379-383 (2004).

9. Maria A. Diaz-Garcia, Susana Fernandez De Avila, Mark G. Kuzyk, *Appl. Phys. Lett* **80**(24), 4486-4488 (2002).
10. J.E. Roman, K. A.Winick, *Appl. Phys. Lett* **61**(23), 2744-2746 (1992).
11. Francisco. J. Duarte, *Appl. Opt* **38**(30), 6347-6349 (1999).
12. Xiao-lei Zhu, Dennis Lo, *Appl. Phys. Lett*, **80**(6) , 917-919 (2002).
13. Dennis Lo, Lei Shi, Jun Wang and Guo-Xuan Zhang, *Appl. Phys. Lett* **81**(15), 2707-2709 (2002).
14. Xiao-lei Zhu, Dennis Lo, *J.Opt. A: Pure Appl. Opt*. **3**, 225-228 (2001).
15. A. K. Sheridan, G.A. Turnbull, A.N. Safonov, I.D.W. Samuel, *Phys. Rev. B* **62**(18), R11 929-R11 932 (2000).
16. Xiang Peng, Liying Liu, Jianfeng Wu, Yigang Li, Zhanjia Hou, Lei Xu, Wencheng Wang, Fuming Li, Mingxin Ye, *Opt. Lett* **25**(5), 314-316 (2000).
17. M.L. Ferrer, A.U. Acuna, F. Amat-Guerri, A. Costela, J.M. Figuera, F. Florido, R. Sastre, *Appl. Optics* **33**, 2266 (1994).
18. A. Costela, I. Garcia-Moreno, J.M. Figuera, F. Amat-Guerri, J. Barroso, R. Sastre, *Optics Commun.* **130**, 44-50 (1996).
19. F. Amat-Guerri, A. Costela, J.M. Figuera, F. Florido, R. Sastre, *Chem. Phys. Lett*. 2**09**, 352 (1993).
20. A. Costela, F. Florido, I. Garcia-Moreno, R. Duchowicz, F. Amat-Guerri, J.M. Figuera, R. Sastre, *Appl. Phys.B* 6**0**, 383 (1995).
21. A. Costela, I. Garcia-Moreno, J.M. Figuera, F. Amat-Guerri, R. Sastre, *Appl. Phys.Lett.* 68, 593-595 (1996).

6

Multimode emission from dye doped polymer planar waveguides

Multimode laser emission from transversely pumped polymer film waveguides doped with rhodamine 6G is presented. The edge emitted spectrum clearly indicated the existence of periodic resonant modes. The reflections from the lateral faces of the free standing film provided the optical feedback thus giving rise to a Fabry-Perot like optical cavity. This together with the guidance through the gain medium gave rise to intense narrow emission lines. Selective mode excitation with pump energy is also discussed .

6.1 Introduction

Organic solid state lasers are attractive because of their wide wavelength tunability and processing flexibility. There have been a lot of investigations on organic polymer lasers with various organic material systems such as dye-doped polymers [1-4] and conjugated polymers [5-9]. Laser emission from dye doped dendrimer and dendrimer doped polymers has also been reported during the past few years [10-11]. Polymeric materials in particular offer advantages such as ease of processing, which permits fabrication of devices of virtually any shape and potentially very low cost. Hence, dye doped polymers continue to attract researchers as promising gain media for solid state lasers. The combination of the tunability and high efficiency of laser dyes with the high power density that can be easily achieved in waveguide structures make devices based on dye doped polymer waveguides and fibres very promising [12-16]. Wide range tunable laser emission have been reported from polymer thin films in optically pumped distributed feedback scheme [12,17]. There have been numerous investigations on laser emission from polymer planar microcavities [18,19] and polymer micro-ring lasers as well [20-21].

This chapter describes the details of our work on multimode laser emission from a transversely pumped free standing polymer film of polymethyl methacrylate(PMMA) doped with the laser dye rhodamine 6G. Since the film was freestanding – surrounded by air on both sides – the reflections from the lateral faces of the sample provided the optical feedback for laser action. This was evident from the lasing mode-spacing dependence on the film thickness. The leaky mode emission from the film waveguide showed a planar microcavity like behaviour due to Fabry-Perot effects. Selective mode excitation was also observed with an increase in pump power.

6.2 Energy level structure of dye molecule

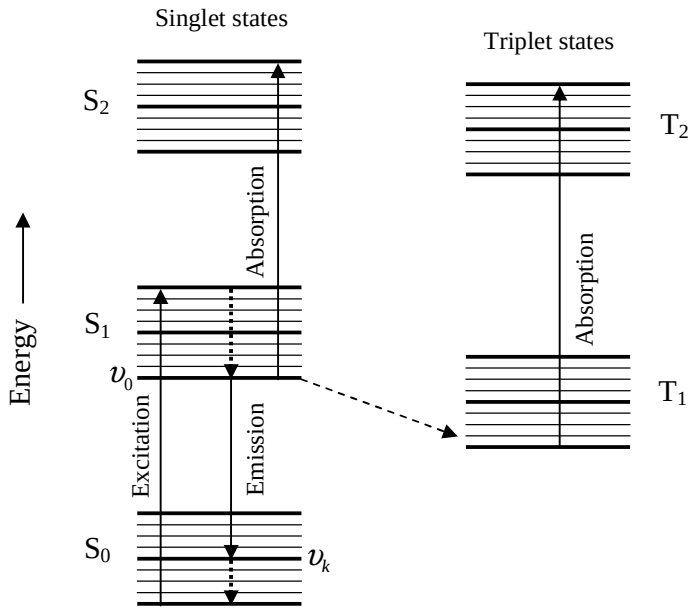

Fig 6.1 Schematic representation of energy levels of an organic dye molecule

Figure 6.1 shows the relevant energy levels of an organic dye molecule such as Rhodamine 6G [22,23]. State S_0 is the ground state. S_1 , S_2 (Singlet) and T_1 ,T_2 (Triplet) are excited electronic states. Singlet $\rightarrow$Triplet or Triplet $\rightarrow$ Singlet transitions involve a spin flip and are far less likely to occur than the transitions between two singlet or between two triplet states. Transitions between two singlet states or between two triplet states which are spin allowed, give rise to intense absorption and fluorescence. The characteristic colour of organic dyes is due to $S_0 - S_1$ absorption and fluorescence emission is due to $S_1 - S_0$ transition.

The typical energy separation such as $S_0 - S_1$ is about 20,000 cm^{-1}. The singlet and triplet states in turn are split further into vibrational levels. Typical energy separation between two adjacent vibrational levels (shown as dark horizontal lines in fig 6.1) within a given singlet or triplet state is about 1500cm^{-1}. The fine splitting shown in the figure as lighter lines corresponds to rotational levels, whose spacing is a few cm^{-1}.

The pumping cycle of a dye laser can be described by a 4-level system. At sufficiently high pump intensity, population inversion may be achieved between the level υ_0 in S_1 and higher rovibronic levels υ_k in S_0, which have a negligible population at room temperature due to small Boltzmann factor $\exp(-E(\upsilon_k)/kT)$. As soon as the gain on the transition $\upsilon_0(S_1) \rightarrow \upsilon_k(S_0)$ exceeds the total losses, laser oscillation starts. The lower level $\upsilon_k(S_0)$ which now becomes populated by stimulated emission from $\upsilon_0(S_1)$ is depleted very rapidly by collisional de-excitation to the lowest level in S_0.

Intersystem crossings between S_1 and T_1 levels will reduce the fluorescence quantum efficiency of the laser dye. Presence of heavy metals like Fe or groups like halides enhance such intersystem crossing and hence will act as "killers" of fluorescence emission. Molecules such as oxygen or cyclo-octotetraene (OCT) are often added to the dye solutions to quench the triplet population.

6.3 Fabry-Perot Cavities

Fabry-Perot (F-P) cavity is an optical resonator formed by two partially reflecting mirrors separated by a distance d and is the most commonly used cavity for optical feedback in a laser device.

The transmission spectrum of F-P cavity is the axial mode pattern which contain peaks of equispaced frequency interval $\frac{c}{2d}$. A free standing thin film can be modelled as a number of F-P cavities which are optically coupled in series (fig 6.2). One can think of the higher modes as those leaking out of the F-P structures.

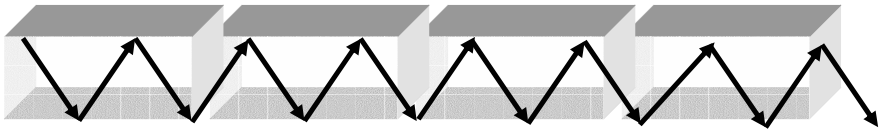

Fig 6.2 Light propagation in planar waveguide represented by serially connected F-P etalons

6.4 Experimental setup

The experimental setup was the same as the one described in Chapter V except for the difference in the light collecting scheme. Here no slit was placed in between the film and the collecting fibre, so as to allow the collection of the leaky rays from the surfaces of the waveguide (see fig 6.3).

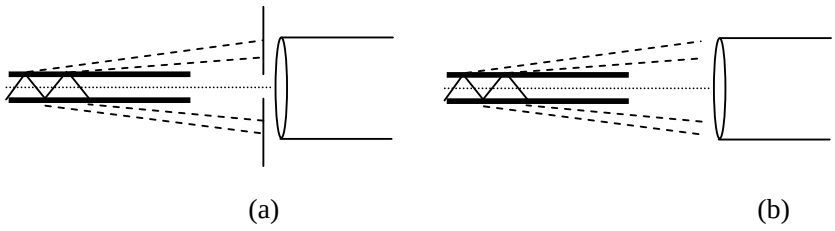

Fig 6.3 Diagrammatic representation of recording the leaky modes from planar waveguide using optical fibre (a) with slit to record the lower propagating modes only (b) without slit to record the complete mode pattern

The amplified spontaneous emission(ASE) threshold for the sample with 1.5 mM dye concentration was found to be 0.126 mJ/pulse for a pump stripe of length 2mm. The threshold decreased for increased stripe lengths. The emission from a 50 μm thick sample having a dye concentration of 1.5 mM was collected by varying the pump energy from 0.02 mJ/pulse to 1.82 mJ/pulse. The pump beam was focused into a narrow stripe of length 6mm and approximately 50 microns width.

6.5 Results and Discussions

6.5.1 Observation of multimode emission

Figure 6.4 shows the emission spectra recorded for different points of transverse excitation (z) at a pump energy 0.2mJ/pulse for a 50 μm thick film of dye concentration 1.5 mM pumped with a stripe of length 6 mm. The distance between one end of the pump stripe and the observation edge of the film was measured as 'z'.

The spectrum shown in fig 6.4(b) clearly indicates the existence of resonant modes. The average mode spacing is ~2.3 nm which agrees with the axial mode spacing of F-P etalon of thickness 50 μm . The strongest emission lines at 576.5 nm and 578.8 nm had a FWHM ~ 0.6 nm. Such a spectral narrowing is characteristic of laser emission.

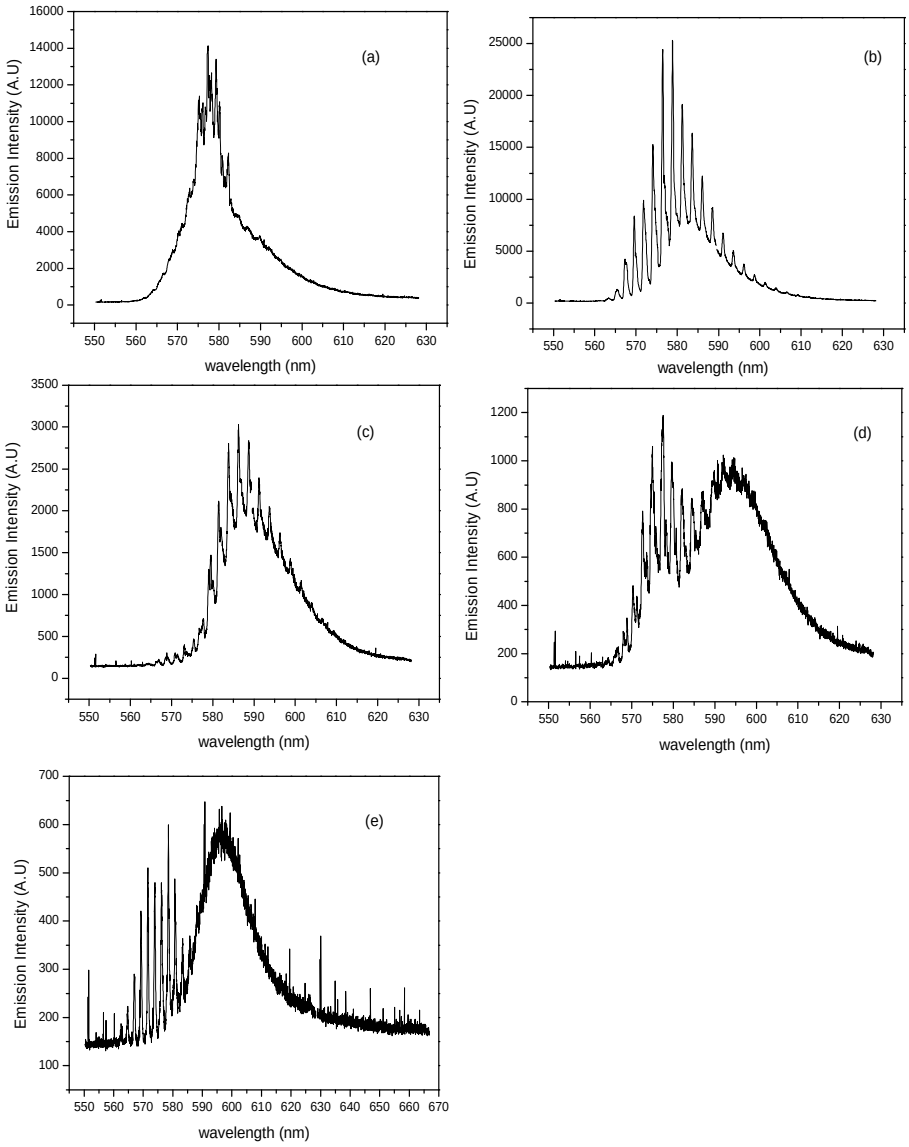

Fig 6.4. Emission spectra from a 50 μm thick film at pump energy 0.2 mJ/pulse for (a) z=0 (b) z=5 mm (c) z=10 mm (d) z=15mm (e) z=20mm

Laser emission requires an external feedback. In our case, there were no external mirrors to provide the feedback. Since the pumped polymer film was a free standing one, the lateral faces of the film acted as mirrors giving rise to a Fabry-Perot type optical cavity whose length corresponds to the film thickness. Owing to the sample geometry and pumping scheme, the longitudinal modes of this cavity form the transverse modes of the waveguide. The axis of the F-P etalon is normal to the guiding direction of light through the film. In the case of a thin stripe excitation, the stimulated emission occurs in a direction along the stripe [6]. Both the stimulated emission along with the propagation in the guiding gain medium and the feedback at the lateral faces induce high gain for laser action, though reflections at the lateral faces are much smaller than that of conventional cavity mirrors. The fine structure pattern in the spectra shown in fig 2 can be attributed to the axial modes of the Fabry Perot formed by two surfaces of the planar waveguide. These modes are guided through the planar waveguide. In other words the planar waveguide can be thought of as formed by a number of serially connected F-P etalons. This can be verified from the mode spacing.

The mode spacing at λ can be calculated using the equation which describes Fabry-Perot cavities viz.,

$$\Delta\lambda = \frac{\lambda^2}{2nL} \qquad \ldots\ldots(6.1)$$

where λ is the wavelength of the strongest emission line, n is the refractive index and L is the length of the resonator cavity.

In the present case, the length of the Fabry Perot cavity corresponds to the thickness of the film. Putting the values for λ, n and L as 576 nm, 1.49 and 50 μm respectively, we get the mode spacing as 2.23 nm which is the same as the observed value 2.3 nm within experimental error.

The emission spectra for a film with same dye concentration, but different thicknesses 115 μm and 130 μm taken for z=10mm are shown in figure 6.5.

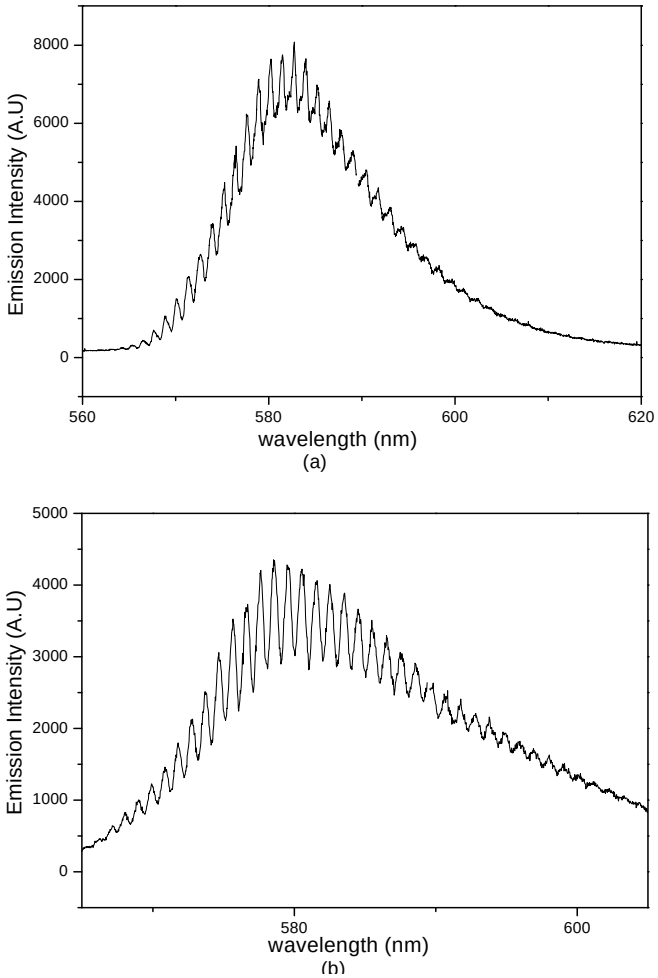

Fig 6.5. Emission from (a) 115 μm (b) 130 μm thick samples at pump energy 0.2 mJ/pulse and z=10 mm

As expected, the line spacing for the 2 cases were smaller than the one for sample thickness 50 μm. For the 115 μm thick sample the obtained mode spacing is 1.25 nm and the calculated value was 0.99 nm. For the 130 μm thick sample, we got the mode spacing as 0.9 nm which is close to the calculated value 0.86 nm. Thus the observed mode spacing agrees with the calculated values. These observations confirm that the observed equally spaced fine structures in the emission spectra are F-P type modes of the optical cavity formed by the film thickness, which gets guided through the film.

Similar phenomenon was observed by Yokoyama et al [11] in laser dye doped dendrimer solution. The observed results can also be compared with typical emission from Fabry-Perot micro-cavity lasers [24]. The F-P like behaviour of asymmetric thin-film waveguide was explained to be quite similar to that of thin-film microcavities [25] . The present case can be considered as the F-P behaviour of a thick symmetric waveguide . The reflections at film-air interface serve the purpose of metallic mirrors or Bragg reflectors used in microcavity thin film lasers [18].

If we collect light by keeping a narrow slit in between the fibre and the waveguide edge, these structures vanish. On placing a narrow slit, we restrict the collection of light emission along the waveguide axis. In the absence of slit, light emitted at different angles from the waveguide surface can also be collected . Note that used a polymer optical fibre with 0.98 mm core diameter and N.A 0.5 for collecting the emitted light. Hence the observed emission can be considered as the leaky modes of the film waveguide.

Leaky mode emission and microcavity like behaviour due to F-P effect from asymmetric luminescent film waveguides has been studied earlier [25]. The corresponding emission was tilted towards the substrate side of the sample. The free standing polymer film in the present experiment was

a symmetric waveguide, and the higher order transverse modes of the waveguide leaked into air at different angles. The dependence of the peak intensity and spectral width of the leaky mode self trapped exciton emission on the observation direction has been studied in anatase thin films [26]. We have also noticed that the intensity of the peaks depended on the collecting angle.

The mode patterns were observed only when there was a separation between one end of the pump stripe and the waveguide edge from which emission was collected . As seen from fig 6.4, the emission spectra comprises of equally spaced mode structures, superposed over the amplified spontaneous emission (ASE). For z=0, when the pump stripe was placed right upto the edge of the film, the mode structures were not prominent, except for some weak structures superposed over the ASE. When z was increased from 0, the emitted light was allowed to guide through the film so that the effect of the F-P modes became predominant. Modes acquired sufficient gain so that the mode structures became prominent. Now the emission spectrum got broader and we get prominent mode structures over the spectral range 560-600 nm(fig 6.4 b). Since the length of the unpumped region increased with increasing z, eventually the intensity of the whole emission together with the mode structures diminished. The propagation of fluorescence as well as ASE in similar sample geometry and pumping scheme has already been described in the previous chapters.

The collected spectrum contained both the stimulated emission and ASE. We have noticed that the observed modes are the higher order transverse modes (leaky modes) of the waveguide. For larger z, these modes instead of propagating through the sample, leak out through the waveguide surface. The modes which get propagated through the whole length of the unpumped region undergo self-absorption and remission. Hence there is a red-shift for the emitted light and for larger z, the ASE gets separated out of

the laser emission as is clear from fig 6.4(d) and fig 6.4(e). At higher pump powers this is more evident.(Fig 6.6 and 6.7)

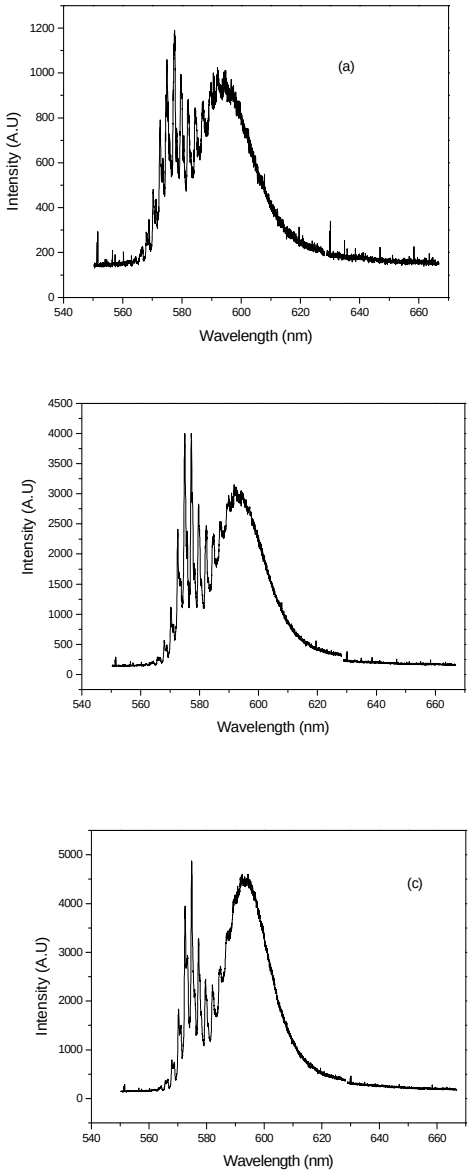

Fig 6.6. Emission from 50 μm thick film for z=15mm at pump energy (a) E=0.2 mJ/pulse (b) E=0.63 mJ/pulse (c) E=1.82 mJ/pulse.

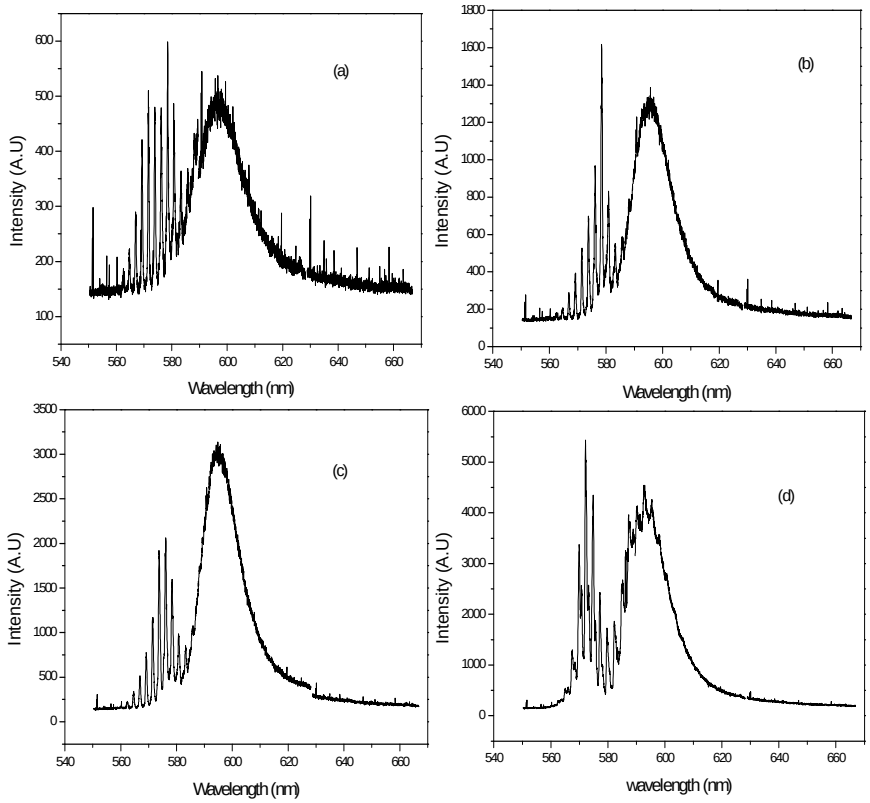

Fig 6.7. Emission from 50 μm thick film for z=20mm at pump energy (a) E=0.02 mJ/pulse (b) E=0.2 mJ/pulse (c) E=0.63 mJ/pulse (d) E=1.82 mJ/pulse.

Thus by the horizontal translation of the excitation stripe, thereby varying z, we can separate out the laser emission and ASE. We also noticed the emergence of mode strucutres over the redshifted ASE spectrum at pump power 1.82 mJ/pulse for z=15mm and z=20mm(fig 6.6.c and 6.7 d). This suggests that further increase in pump power could lead to prominent mode structures over the redshifted ASE spectrum.

6.5.2 Selective mode excitation

On increasing the pump energy, a selective excitation of laser mode was observed. Figure 6.8 shows the emission spectrum at z=5mm recorded for various pump powers. We observed that as the pump power was increased, the centre lines of the spectrum gained more energy. Though there was an increase in intensity for the whole emission, it is clear from the figures that energy from other modes got coupled to the high gain mode at 576.5 nm as the pump power was increased.

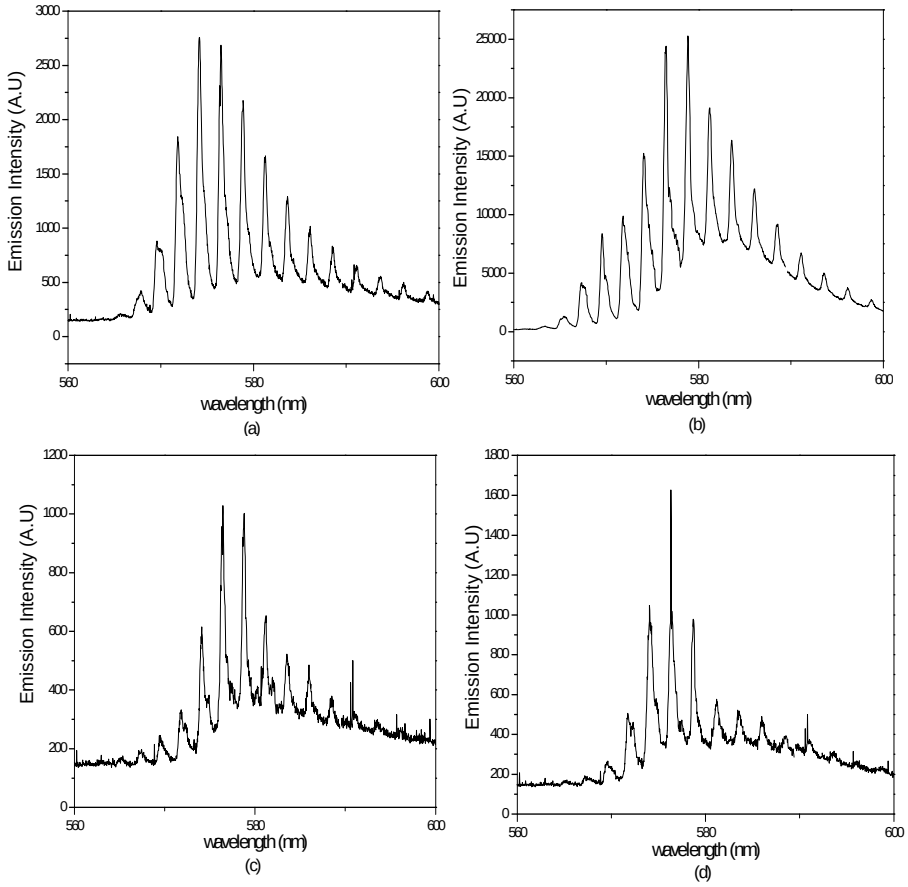

Fig 6.8 Emission from 50 μm thick film for z=5mm at pump energy
(a) E=0.02 mJ/pulse (b) E=0.2 mJ/pulse (c) E=0.63 mJ/pulse (d) E=1.82 mJ/pulse.
For (c) and (d) the Y-axis values should be multiplied by a factor of 10^2

The output intensity was very high for pump energies 0.63 mJ/pulse and 1.82 mJ/pulse. To avoid the saturation of the CCD sensor, we placed neutral density filter (with OD =2) just infront of the slit of the CCD. The intensity of the mode at 571.5 nm shoots up when the pump energy reaches 1.82 mJ/pulse and the line width is reduced to ~0.4 nm.

Fig 6.9 shows a similar behaviour observed in the case of spectra recorded for a film with dye concentration 1 mM and thickness 50 μm excited with a pump stripe of length 2mm and z=10mm.

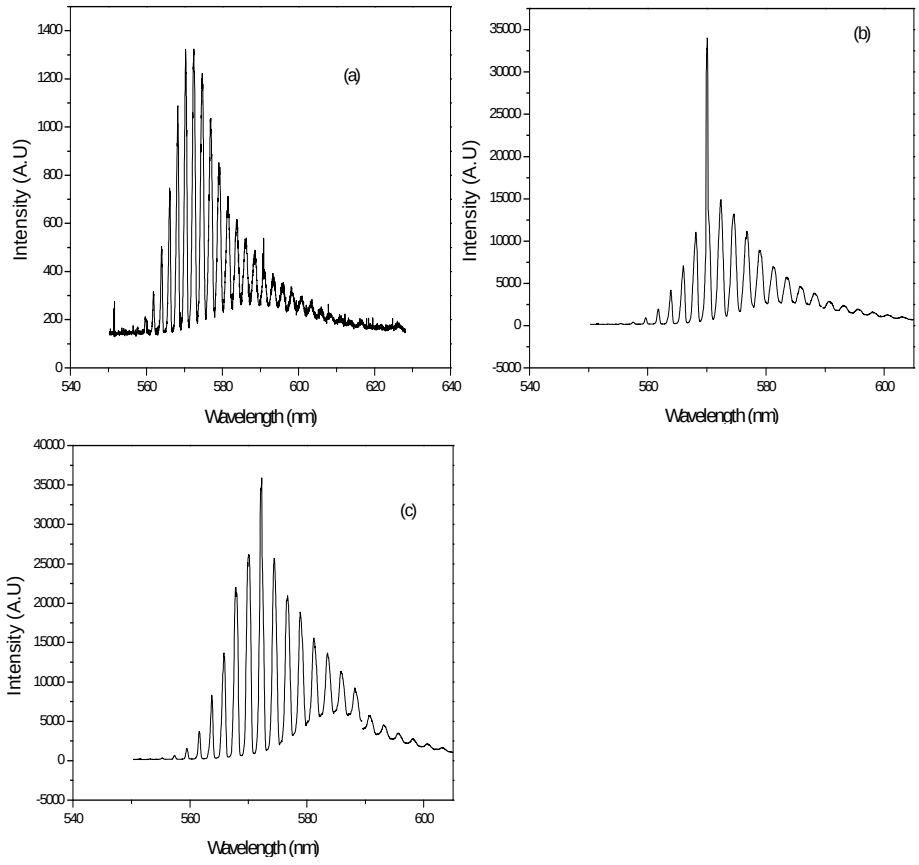

Fig 6.9 Emission from 50 μm thick film with dye concentration 1 mM for z=10mm at pump energy (a) E=0.07 mJ/pulse (b) E=0.7 mJ/pulse (c) E=2.2 mJ/pulse

We observe that the ASE background is negligibly small. The mode at 570.1nm shoots up for the pump energy 0.7mJ/pulse with FWHM as small as 0.3 nm.

The mode competition can be clearly seen from fig 6.10.

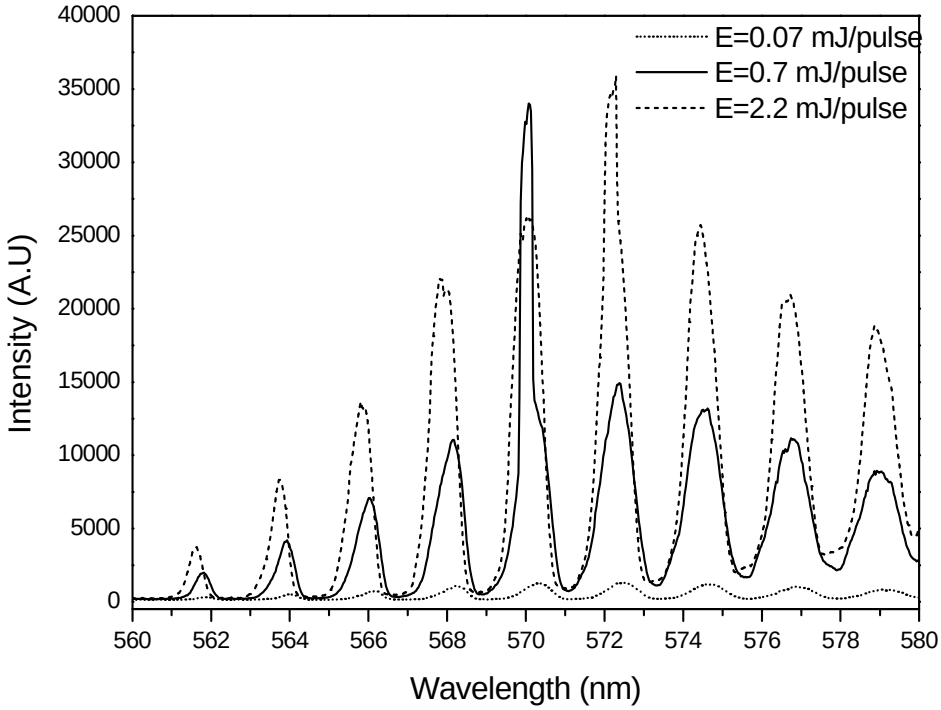

Fig 6.10 Mode competition at various pump energies

6.6 Conclusions

A compact solid state laser based on dye doped polymer is demonstrated . Laser emission was observed from a transversely pumped free standing poly methyl methacrylate film doped with rhodamine 6G . The film was 50 μm

thick with dimension 4cm x 2 cm. Reflections from the lateral faces provided the optical feedback. This together with the guidance through the gain medium gave rise to intense narrow emission lines. For the waveguide with dye concentration 1.5 mM, an intense line with FWHM ~ 0.4 nm was observed at 576.5 nm due to energy transfer from other modes. For dye concentration 1mM, narrow emission at 570.1nm was observed with linewidth 0.3 nm. The ASE was easily tuned by changing the point of pumping on the waveguide structure thereby separating the lasing modes from the ASE.

References

1. B.H. Soffer, B.B. Mc Farland, *Appl.Phys.Lett* **10**, 266-267 (1967).
2. O.G. Peterson, B.B. Snavely, *Appl. Phys. Lett* **12** (7), 238-240(1968).
3. A. Costela, I. Garcia-Moreno, J.M.Figuera, F. Amat-Gueria and R. Sastre, *Laser Chem*. **18**, 63-84 (1998).
4. A. Costela, I. Garcia-Moreno, C.Gomez, O. Garcia and R. Sastre, *J. of Appl. Phys*,**90**(7), 3159-3166 (2001).
5. Michael D. McGehee, Rahul Gupta, Siegfried Veenstra, E. Kirk Miller, Maria A. Diaz-Garcia, Alan J. Heeger, *Phys. Rev. B* **58** (11), 7035-7039 (1998).
6. S.V. Frolov, Z.V. Vardeny, K. Yoshino, A. Zakhidov, R.H. Baughman, *Phys. Rev. B* **59** (8), R5284-R5287 (1999).
7. George Heliotis, Donal D.C. Bradley, Graham A. Turnbull, Ifor D.W. Samuel, *Appl. Phys. Lett* **81** (3) , 415-417 (2002).
8. M. Fakis, I. Polyzos, G. Tsigaridas, V. Giannetas , P. Persephonis, I. Spiliopoulos, J. Mikroyannidis, *Phys. Rev. B* **65** (19), 195203-1 – 195203-7 (2002).
9. Fumitome Hide, Maria A. Diaz-Garcia, Benjamin J. Schwartz, Mats R. Andersson, Qibing Pei, Alan J. Heeger, *Science* **273**, 1833-1836 (1996).
10. Akira Otomo, Shiyoshi Yokoyama, Tatsuo Nakahama, Shinro Mashiko, *Appl. Phys. Lett* **77** (24), 3881-3883 (2000).
11. Shiyoshi Yokoyama, Akiro Otamo, Shinro Mashiko, *Appl. Phys. Lett* **80**(1), 7-9(2002).
12. Vincent Dumarcher, Licinio Rocha, Christine Denis, Celine Fiorini, Jean-Michel Nunzi, Frank Sobel, Bouchta Sahraoui, Denis Gindre, *J.Opt. A: Pure Appl. Opt* **2,** 279-283 (2000).
13. G. D. Peng, P.L. Chu, Z Xiong, T.W. Whitbread, R.P. Chaplin, *J.Lightwave Technology* **14**(10), 2215-2223(1996).

14. Akihiro Tagaya, Shigehiro Teramoto, Eisuke Nihei, Keisuke Sasaki, Yasuhiro Koike, *Applied Optics* **36**(3), 572-578 (1997).
15. Takeyuki Kobayashi, Werner J. Blau, *Opt. Lett* **26** (24), 1952-1954 (2001).
16. M. Karimi, N. Granpayeh, M.K. Morraveg Farshi, *Appl. Phys B* **78** , 387-396 (2004).
17. F. Sobel, D. Gindre, J.M. Nunzi, C. Denis, V. Dumarcher, C. Fiorini-Debuisschert, K.P. Kretsch, L. Rocha, *Opt. Mat* **27**, 199-201(2004).
18. N. Tessler, G.J. Denton, R.H. Friend, *Nature* **382**(22), 695-697(1996).
19. H. Becker, R.H. Friend, T. D. Wilkinson, *Appl. Phys. Lett* **72**(11), 1266-1268(1998).
20. M. Kuwata-Gonokami, R.H. Jordan, A. Dobalapur, H.E. Katz, M.L.Schilling and R.E. Slusher, *Opt. Lett* **20**(20), 2093-2095(1995).
21. S.V. Frolov, Z.V. Vardeny, K. Yoshino, *Appl. Phys. Lett* **72**(15), 1802-1804, 1998.
22. A. Yariv, Optical Electronics 4th Edn., Saunders College Publishing, USA (1991).
23. W. Demtröder, Laser Spectroscopy 3rd Edn., Springer Veralg, Berlin (1996).
24. R.C. Polson, G. Levina, Z.V. Vardeny, *Appl. Phys. Lett* **76**(26),3858-3860(2000).
25. A. Penzkofer, W. holzer, H. Tillmann, H.H. Horhold, *Optics Communications* **229**, 279-290(2004).
26. V. Kiisk, I. Sildos, A. Suisalu, J. Aarik, *Thin Solid films* **400**, 130-133(2001).

7

Summary and future prospects

General conclusions of the present work and future prospects are discussed in this chapter.

7.1 General Conclusions

The previous six chapters in this thesis present the design and fabrication of photonic devices using polymer optical fibres and polymer waveguides.

Polymer optical fibres owing to their large diameter, large numerical aperture, flexibility and geometrical versatility have attracted much research interest in the field of optical sensing. One of the new techniques in the design of fibre optic sensors is the usage of side polished fibres. Side polished polymer optical fibres have been successfully employed for the fabrication of compact sensors for measuring refractive index and absorption. The sensor performance and methods for the enhancement in the performance were studied numerically and accordingly the experiments were designed. A refractometer with wide dynamic range and a sensor for measuring chemical reaction kinetics were fabricated and characterized.

Dye doped polymer waveguides and fibres are potential candidates for solid state gain media. High power and high gain optical amplification in organic dye-doped polymer waveguides is possible due to extremely large emission cross sections of dyes. We have fabricated free standing film waveguides of rhodamine 6G doped poly methylmethacrylate, by double doctor blade tape casting technique. Optical loss characterization for films with various thickness and dye concentration was done by a non-destructive side illumination fluorescence technique. The experimental observations clearly indicated a space dependent attenuation coefficient.

The observation of amplified spontaneous emission (ASE) from these samples and the characterization of optical gain are also discussed. The

propagation characteristics of ASE through the films were studied. A new method for tuning the ASE wavelength was demonstrated by which a maximum tunability of 19 nm was achieved.

Multimode laser emission based on leaky mode propagation from these free standing film waveguide was one important study. The edge emitted spectrum clearly indicated the existence of periodic resonant modes. The reflections from the lateral faces of the free standing film provided the optical feedback thus giving rise to a Fabry-Perot like optical cavity. This together with the guidance through the gain medium gave rise to intense narrow emission lines with line width ~0.3 nm .

7.2 Looking Forward

Though fibre optic sensors have many advantages over their conventional bulk counterparts, from the applicability viewpoint, more attention should be paid over certain key parameters such as cost, size and sensitivity. Novel fabrication techniques, well suited for industrialization, have to be developed. Numerical methods need to be used for designing and optimizing these devices. Single mode side polished fibre components with metallic coatings can be designed for sensors, couplers, filters and polarisers. Sensors and optical amplifiers based on dye doped polymer fibres could be developed. Work in this direction has already started in our lab.

Studies using picosecond pump source will be useful to understand fast optical processes taking place in the dye doped media especially due to intersystem and intrasystem crossings.

The demand for photonic devices that meet both performance criteria and economic requirements has opened the door for novel technologies such as polymer photonics. Development of novel solid-state lasing media such as highly luminescent conjugated polymers opens up new possibilities for applications and technologies. In contrast to other organic chromophores, they suffer little concentration quenching.

New designs of compact laser sources could be taken up. Microcavity lasers is a novel approach to lasing action in optically pumped organic solids.